PRACTICAL ENVIRONMENTAL SENSING ON OPTICAL COMMUNICATION INFRASTRUCTURE

by

Joseph W. Catudal

A dissertation submitted in partial fulfillment of
the requirements for the degree of

Doctor of Philosophy

(Computer Sciences)

at the

UNIVERSITY OF WISCONSIN–MADISON

2024

Date of final oral examination: August 13, 2024

The dissertation is approved by the following members of the Final Oral Committee:

Paul Barford, Professor, Computer Sciences
Suman Banerjee, Professor, Computer Sciences
Dante Fratta, Associate Professor, Civil Engineering
Ming Liu, Assistant Professor, Computer Sciences

All Rights Reserved

© Copyright by Joseph W. Catudal 2024

Dedicated to my children and great explorers Sophie, Everett, Camille, and Ada;
and to my wife and dearest friend, my fellow adventurer Danielle.

ACKNOWLEDGMENTS

I would like to express my deepest and heartfelt gratitude to all those who supported me throughout the journey to complete this body of work.

First, I am extremely grateful to my advisor, Dr. Paul Barford. One of the most crucial skills I have learned is to evaluate problem sets differently, to think more about exploring and expanding than simply about accomplishing. Thank you for the motivation and latitude to expand my technical understanding far beyond my comfort zone. You taught me how rewarding this research and discovery process can be, especially when done well. I am honored to have worked with you and appreciate all the encouragement and insightful feedback along the way.

I would also like to thank the members of my dissertation committee, Dr. Banerjee, Dr. Liu, and Dr. Fratta, for their thoughtful consideration of this work, constructive criticism, and support throughout this process. Thank you also to Dr. Herb Wang, Neal Lord, Dr. Cliff Thurber, Dr. Matt Sinclair, and Dr. Mohit Gupta for your expertise, experience, and collaboration in this process over the years. Your wealth of knowledge was instrumental in bringing many distinct bodies of knowledge together.

I want to extend special thanks to Bill, Paul, and Tom from the University of Wisconsin-Madison DoIT. Your kindness, patience, and willingness to let me try strange things with your equipment made all of this research possible, and kept me encouraged to never stop trying new things.

Thank you to my colleagues Tyler, Weijun, Jason, Arjav, Akshay, Dante, Bhavya, Keith, and Kalpit. Your camaraderie, stimulating discussions, and commitment to this research made this journey possible, and I could not have done it without your assistance. I also am deeply indebted to Buff for his technical support and assistance with the experimentation construction. Your expertise and positive attitude for every construction and equipment request was most welcome, and provided significant contributions to this research.

Thank you also to my fellow academics and friends Todd, Karl, Josh, Will, Drew, Erin, Scott, David, and Olivia. You provided the encouragement I needed in tough

spots and were always quick to share your experiences in your own journeys. You reminded me that a surge of hard work does not always yield a commensurate result, yet this process indeed bears fruit.

I would like to extend profound thanks to all my Linthicum colleagues. My time with you was compelling and rewarding. You taught me to think and observe differently, and to always find a way. It has changed how I see the world.

Lastly, I owe my deepest gratitude to my parents, my family, and my friends for their unwavering support and encouragement. Much like this dissertation, the path in life that led me to Wisconsin was much more nuanced than I expected, with many twists and turns, and plenty of surprises. Your belief in me at every step of the way has been my greatest source of strength and motivation in this endeavor.

Thank you all for your invaluable contributions.

CONTENTS

LIST OF TABLES

LIST OF FIGURES

ABSTRACT

Optical networks are an essential component of today's communications infrastructure, providing connectivity across the globe at trillions of bits per second on a single optical fiber. Significant advances in monitoring environmental effects through the use of dedicated fiber optic sensors has also provided a wealth of information about the world around us. However, fiber optic sensing on communications infrastructure is largely limited due to diverging requirements between the two applications.

In this thesis, we explore the potential of using fiber optic network communications infrastructure as a sensing platform in a metro environment. Our overall approach to this research is to examine the potential for widespread environmental sensing on optical communications infrastructure through empirical study. We identify several approaches for measuring characteristics of light in fiber and develop laboratory-based experiments to further develop these designs, and then validate their effectiveness at detecting physical events on optical fiber. We provide insight into the characteristics that make a fiber optic route a potential candidate for environmental sensing, and for limiting factors that may not be initially considered when selecting routes for monitoring.

We first leverage the functions of a commodity optical transceiver to measure environmental effects on optical fiber to understand the existing capabilities of monitoring via the use of optical communications infrastructure. We conducted laboratory experiments to observe polarization changes under repeated bending strain and vibration. In addition, we monitor a 4-kilometer fiber path in an urban setting, examining the result of specific events along its indoor and outdoor routes, including opening fiber trays and truck-mounted tap testing. We also installed a specially designed 100-meter fiber route and observed polarization transience, correlating external factors such as diurnal patterns, temperature changes, precipitation, and passing freight trains to evaluate the sensing potential of these devices. While the optical transceiver is capable of detecting small polarization transients, low sampling rate and weak coupling to vibration sources limit the effectiveness of

detecting some anthropological activity, such as passing freight trains.

We then explore environmental sensing on optical communication fiber through polarimetry-based measurements to improve our environmental sensing capabilities. We construct a low-cost polarimeter with a sampling rate capable of detecting vibrations of interest. We then design and build our own polarimeter to increase sensitivity to polarization transients and evaluate various metrics to characterize environmental effects. We examine the outcomes of different levels of coupling of a fiber to a vibration-resonant medium to detect freight trains. Finally, we compare these findings with the monitoring of the same railway route using a campus network optical fiber and assess the response strength to passing trains. Our findings show that sensor accuracy is strongly influenced by the level of coupling between a sensing fiber and a vibrating medium.

After exploring the use of polarimetry for inferring environmental effects, we created a low-cost, easy-to-implement fiber specklegram sensor capable of detecting physical effects on optical fiber. We construct a prototype sensor and establish metrics for evaluating environmental changes that affect the fiber. Subsequently, we enhance the design to increase its stability and portability, and examine the results of strong coupling with a vibrating medium in a laboratory setting with fiber lengths up to 1 km. We then deploy our sensor in situ and analyze its performance in measuring cultural events in a metro environment. Our device shows high sensitivity to train traffic, but accuracy can be impacted due to ambient effects or events that overstimulate the sensor and fiber.

The research presented in this thesis demonstrates a practical approach to using sensing capabilities in network infrastructure. This work provides a foundation for numerous opportunities for research, public safety, and smart city applications that can complement traditional sensing methods.

1 INTRODUCTION

The Internet has revolutionized the way we send and receive information, particularly when it comes to safety information about significant events. In the past, people relied on traditional media outlets such as television, radio, and newspapers to receive updates about events such as natural disasters, terrorist attacks, or other emergencies. However, with the ubiquity of Internet connectivity, information can be disseminated and shared in near-real-time, allowing for faster and more efficient communication.

Emergency services, government agencies, and news organizations can quickly provide alerts, updates, and safety instructions about predicted or ongoing situations. This information can be crucial for people who may be in the affected area or have loved ones who are affected.

The Internet has also enabled the development of innovative new systems and frameworks that can provide even more accurate and timely information during significant events. For example, some cities and towns have implemented emergency alert systems that can send text messages or push notifications directly to residents' smartphones in the event of an emergency [4]. These systems can provide important information about evacuation orders, shelter locations, and other critical information. The alerts are driven by data processed through detection or prediction systems designed to provide early warning to protect the safety and welfare of the people involved. One prominent method that can provide data for indicators of threats to public safety is *ground motion sensing*.

Ground motion sensing is a crucial technology for early detection of significant events. Sensing networks are designed to detect the occurrence of an earthquake through strategic placement and integration of different types of collection devices[4, 5]. This information can be used to issue early warnings and inform emergency response efforts, potentially saving lives. Ground motion sensing is also important for assessing the structural integrity of buildings and infrastructure. Vibrations caused by ground motion can have a significant impact on the integrity of structures. Ground motion sensors can be used to monitor the behavior of struc-

tures during earthquakes or over time, providing data that can be used to improve building design and safety features, ensuring structures are resilient and safe for use [6, 7]. Ground motion sensors can help identify areas that are at high risk of seismic activity and can be used to issue early warnings to miners. This information can be critical to ensuring the safety of workers and preventing accidents [8]. Lastly, sensing equipment can also be used to detect explosions [9]. This information can be used to alert authorities and emergency responders, enabling them to respond quickly and efficiently to address the situation.

In modern urban areas, even with the advent of wireless networking, the Internet still relies on physical components to function. Data centers, servers, and fiber optic transponders and cables are essential components of network infrastructure that allow the quick transfer of massive amounts of data between clients and the rest of the global network. These physical components, specifically fiber optic cables, can be subject to the same environmental effects that ground motion sensors are designed to detect [10, 11, 12]. Given the nearly ubiquitous land-based optical network communications in metro areas, this raises an interesting question. Can we opportunistically measure environmental effects with optical communications infrastructure to improve environmental sensing capabilities?

One of the more novel and successful methods of ground motion sensing is through the use of optical fiber cables as a sensing medium. Distributed Acoustic Sensing (DAS) sends pulses of light down a dedicated fiber and determines precise locations and amount of strain changes on the fiber, which can be used to locate disturbances from tens of kilometers away [13, 14, 15, 16]. Although these systems are very effective and precise, they are still expensive to deploy, require large amounts of storage and processing to deliver results, and require dedicated infrastructure to perform operations.

In recent years, there has been increasing interest in using optical fiber infrastructure in communication networks for environmental monitoring [17, 18, 19, 10, 20, 21]. The broad deployment of optical fiber in terrestrial and submarine environments presents a wide range of possibilities for research, public safety, and smart city applications that would not be possible with traditional geophone arrays and

other fiber-based sensing methods. The main challenge is to find ways to modify existing network communication systems for use in sensing applications.

Unlike sensing fiber, which is specifically deployed to detect environmental effects, optical transport equipment and infrastructure engineering is designed to eliminate ground motion as sources of noise. Several studies have been conducted using commodity optical transport equipment for sensing capabilities. Due to the high coupling and quiet seismic conditions on the sea floor, some promising work has been done capitalizing on these optimal conditions for sensing. The presence of sea swells and earthquakes can be detected on the basis of polarization and phase changes by accessing the internal values of optical transport receivers [19, 10].

While previous studies have shown the potential for physical sensing through optical communications infrastructure in specific settings with low noise and/or dramatic signatures, our goal is to test and develop capabilities in more complex and constrained environments to determine its potential in general applications. The combination of fiber optic communications and environmental sensing within the same infrastructure has substantial potential for both domains. The possibility of improved monitoring and real-time data collection in various sensing applications emphasizes the need for continued research and innovation. By exploring this space, we aim to identify practical solutions that utilize existing communication networks as a sensing platform, creating a more intelligent infrastructure which benefits both the capabilities and societal benefits of optical network communications infrastructure.

1.1 Our Approach

1.1.1 Research Questions

Our overall approach to this research is to examine the potential for widespread environmental sensing on optical networked communications infrastructure. Given the complexities that exist in using this infrastructure for an unintended purpose, our research questions focused on three distinct dimensions:

- What are the capabilities and limitations for using optical communications infrastructure for environmental sensing in metro and urban areas?
- How can we integrate sensing capabilities onto optical communications infrastructure effectively?
- How can we expand sensing through optical communications infrastructure with minimal impact to its primary function?

1.1.2 Description of Approach

Throughout our research, our unifying analytic technique is the empirical evaluation of sensor designs installed on optical communications fiber. In our analysis, we identify several approaches that can measure characteristics of light and develop laboratory-based experiments to further develop these designs, and then validate their effectiveness at detecting events of interest in a metro environment. Measurement of environmental effects on optical fiber in ideal situations has been conducted in prior studies. These results inform our work. However, our research is focused on sensing applied to a more complex environment, with high levels of ambient vibration, on infrastructure optimized for use in communication networks. We identify and evaluate methods to leverage existing designs and for opportunistic means of measurement, which do not often align for ideal measurement conditions for environmental effects.

In pursuit of our research objectives, in each study we evaluate and give understanding into the environmental effects to which metro fiber links are subjected, how these effects might be measured, and highlight opportunities and challenges with regard to sensing applications. We employ multiple approaches to optical measurement to determine viable alternative sensing methods for sensing applications in metro environments. In addition, to provide practical solutions for sensing through communication infrastructure, we describe designs that can be constructed at low cost and with minimal modifications to the infrastructure in order to limit disruption to the primary application of networked communications. With our

findings, we present a cohesive, well-developed study of the hidden world of environmental signals that can be found on our communication networks and practical means of how they can be revealed.

1.1.3 Transceivers: Efficacy of Using Commodity Optical Equipment for Environmental Sensing

Modern optical transceivers routinely recover incoming light signals billions of times a second, adapting to changes in polarization and phase state that can occur as a result of birefringence while traveling through the fiber. However, the operational design focus for these devices is strictly for network communications performance, not for reporting state change information. We opportunistically leverage this equipment using custom firmware and software that integrates adjustments from the adaptive equalizer into quantifiable measurements. This allows us to measure polarization state as it changes when the fiber under test is subjected to environmental effects. Using existing installations of optical communications infrastructure and equipment is the first and most direct approach to environmental sensing with minimal modifications [22].

1.1.4 Homebrew: Low-Cost Polarimetry Based Environmental Sensing on Optical Fiber

We further investigate by employing and developing equipment designed to detect polarization transience. Our initial study on commodity hardware was able to measure polarization state, but its sensing capability was limited by *sampling frequency*. Polarimeters are purpose-built to report detailed polarization information at high rates, but can be prohibitively expensive to use at scale. A previously designed low-cost polarimeter has been shown to detect polarization changes from environmental effects [23, 24, 21]. After evaluating this design, we develop our own to expand sensitivity to minor vibrations at a wider range of polarization states and conduct a lab-based evaluation. We measure polarization transience as a

response to passing trains from a nearby building and evaluate the significance of coupling to vibration-resonant mediums. Our design offers a low-cost alternative to traditional polarimeters with increased sensitivity for the use of sensing on optical communications fiber [25].

1.1.5 Seismospeckle: Practical Specklegram Sensing on Optical Communications Fiber

Lastly, we explore alternative methods of measurement beyond polarization state and transience. Fiber specklegram sensing is a type of optical fiber sensor that measures an interference pattern generated by multiple modes of light that change paths when a fiber is disturbed. However, optical communication infrastructure often employs singlemode fiber, designed to restrict light to a single mode during transport. We consider the use of visible light through singlemode fiber, which resides underneath the fiber's cutoff wavelength, thereby creating modal dispersion of the emitted light. Exploiting this distortion effect allows for the measurement of the projected modes, which we monitor for physical changes to the fiber's geometry. Although this sensor is subject to more disturbance from ambient sources and provides a reduced sensing range compared to our previous designs, its equipment cost is significantly lower and offers improved portability for easier installation.

1.2 Contributions of this Thesis

Each contribution of this thesis demonstrates how we developed and evaluated original designs to monitor the changing characteristics of light in optical fiber to improve our understanding of sensing on communications infrastructure in a general case. The major contributions from each study include:

- **Optical transceiver analysis for sensing.** We conducted a thorough analysis of an widely-used Acacia AC1200 model DWDM transceiver [26] for its capability to be used as an environmental sensor with customized software

and settings. Although optical communications equipment has been used in other works for sensing, we provide a detailed explanation of available sources of information and their suitability to be used for environmental sensing applications. We also highlight our process of selecting settings that would amplify measurement of polarization transience. We provide laboratory results for bending and vibration strain on varying lengths of fiber, and in situ evaluations to demonstrate specific polarization transient signatures that can be characterized for specific effects that affect the fiber. We conduct and report on a detailed characterization of a 4-km campus route with indoor and outdoor portions that include segments that run underneath freight railways and city street intersections. Lastly, we explain our process for installing a custom 100-meter fiber route for sensing and identify several different environmental effects that generate distinct polarization transient results. We learn through our investigation that while many environmental effects can be observed through monitoring polarization change with a commodity transceiver on optical communications infrastructure, obtaining this data at a sufficient sampling rate is difficult and will impact sensing capability. By using this equipment, we establish a baseline in answering our research questions and open additional avenues of study to improve sensing capabilities and reveal nuances in using communications infrastructure for an alternative function.

- **Novel low-cost polarimeter.** We evaluate an existing low-cost polarimeter design and report on our initial findings with regard to sensitivity and suitability of polarization rotation rate metrics. We then improve upon this design and evaluate its effectiveness compared to a commercial polarimeter through the use of laboratory experiments and in-situ deployments. We show that our polarimeter can optimally increase overall responsiveness and improve the optimal minimum sensitivity by at least 29% over the original design. We additionally compare train-event monitoring results on a series of routes with different levels of coupling and highlight its importance when selecting routes

for environmental sensing applications. Our work shows the capabilities of using optical fiber communication infrastructure for more robust sensing methods, which provides an example of what sensing can be possible with modifications to the coupling of a fiber route.

- **Low-cost specklegram sensor.** We design and develop a short-range sensor capable of monitoring disturbances on OS2 fiber optic cable using visible light and inexpensive components to develop a sensor for at a fraction of the cost of other sensors. While not as precise as other methods, this sensor offers improved deployability over larger, more cumbersome designs, and can be deployed in short- and long-term capture modes. We show its effectiveness in laboratory and real-world environments and highlight future use cases for this design to provide advantages over other methods of fiber optic sensing on communications infrastructure.

- **Observations for sensing on fiber optic communications infrastructure.** Fiber installations for communications are engineered much differently than routes designed for environmental sensing. We provide insight into the characteristics that make a fiber optic route a potential candidate for environmental sensing, and for limiting factors that may not be initially considered when selecting routes for monitoring. We also analyze the effect of coupling of a fiber to a medium that transfers vibrations of interest. Lastly, we show that small portions of fiber subjected to building noise or ambient air flow may occlude transient effects and must be limited in order to improve sensing capabilities.

1.3 Dissertation Outline

The remaining chapters of this manuscript are organized as follows. In Chapter 2, we provide background information on the characteristics of light as it pertains to the transmission of data through optical fiber, the technology and infrastructure regarding optical communication networks, and methods and technologies for

ground motion sensing. In Chapter 3, we present our methodology and results for our research and experiments for the use of commodity optical transport equipment for environmental sensing. In Chapter 4, we explore the design of a novel, improved, low-cost polarimeter and polarization transience measurements. In Chapter 5, we describe our work in fiber specklegram sensing using an ultra-low-cost sensor suitable for measuring effects on shorter fiber spans. Finally, we provide a summary of our research in these areas and highlight avenues for future work in Chapter 6.

2 RELATED WORK

This dissertation is informed by the disciplines in the areas of photonics, fiber optic communications and networks, ground motion sensing, and fiber optic sensing. Having a detailed understanding of each of these domains is essential in conducting our research to utilize optical communications infrastructure for a sensing system.

2.1 Light Characteristics for Data Transmission and Sensing through Optical Fiber

In this section, we describe the characteristics of light and their importance in fiber optics applications. As our research goal is to detect environmental effects imposed on deployed fiber, understanding the physical nature of the communications infrastructure and transport medium is essential to enable its use as a sensing system. Although the field of study of photonics spans numerous applications, we focus here on four fundamental characteristics that specifically pertain to communications and sensing using light through the waveguided medium of optical fiber: Amplitude, phase, polarization, and wavelength [27, 28]. After a description of each of these characteristics, we explain their relevance to both sensing and communication applications.

2.1.1 Amplitude

The amplitude of light describes the maximum oscillation of the electric or magnetic field component of an electromagnetic light wave. The electric field component's amplitude directly relates to the light's intensity. Intensity describes the amount of energy carried by a light wave in a unit area, proportional to the squared amplitude of the electric field component [29]. A common way to express optical power is in dBm, the ratio of optical power in relation to 1 milliwatt [30].

The earliest optical networked communication devices modulated the intensity of light through pulses. This is described as On-Off Keying (OOK) modulation, a simple form of Amplitude-Shift Keying (ASK). Although OOK modulation is inexpensive to implement, one of its main limitations is its limited bandwidth efficiency, as only one level of amplitude is used to represent the data [31]. Although more advanced versions of OOK are still being developed for specific applications [32], simple OOK modulation is less effective in high-speed systems that require high bandwidth and efficient use of available spectrum [27, 33]. Today, coherent optical transport schemes incorporate modulation of amplitude as an element to encode information [1].

Early optical fiber sensors also measured the intensity of light to determine environmental changes around a fiber under test. Using the property of total internal reflection (discussed later in Section 2.2.1), light guided by a fiber will leak out of the core if the refractive index of the surrounding medium is similar to that of the fiber, which may detect the presence of liquid, or if an extreme bend radius is inflicted upon the fiber, such as in applications of pressure sensors [34, 35].

2.1.2 Phase

The phase of light describes the specific point of oscillation in a wavelength that a light wave occupies at a given point in time [36]. Phase modulation is used to encode data onto a light wave that can more efficiently capitalize on bandwidth and provide higher data rates compared to simpler modulation techniques. Modern coherent optical transport systems modulate both amplitude and phase, resulting in a more complex constellation of symbols that supports a more efficient bandwidth [37, 27, 38].

As intensity is proportional to the amplitude of the wave, coherent light waves that are out of phase with each other on the same optical path will cause destructive interference which reduces the intensity of the combined waves. Fiber specklegram sensors use this phenomenon as a key principle for measuring physical changes in a fiber [39].

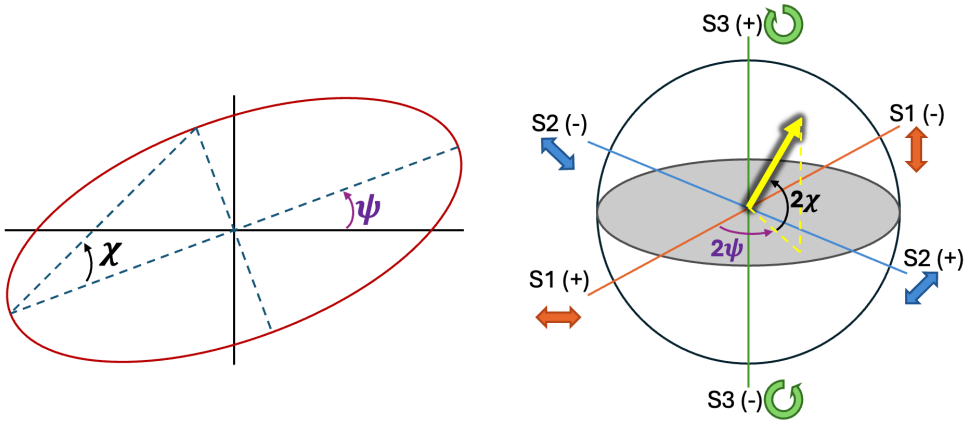

Figure 2.1: Diagram of Polarization Ellipse (left) and Poincaré Sphere (right), ellipticity and orientation angles and Stokes parameters shown.

2.1.3 Polarization

Light is a transverse wave that oscillates perpendicularly along its direction of travel. It is also an electromagnetic wave composed of both an electric wave and a magnetic wave that oscillate orthogonally in relation to each other. The orientation of the electric-wave oscillation is the polarization of light. Polarization can be decomposed into vertical and horizontal components, each with an independent amplitude and phase [40]. This characteristic plays a vital role in modern coherent optical communication, explained in further detail in Section 2.2.3.

These components are commonly expressed in two ways to describe the state of polarization. First, polarization can be described as an ellipse having two angles that correspond to the orientation (ψ) and the ellipticity (χ) of the polarization state. Second, they can be described as a Stokes vector consisting of four parameters, where S_0 describes the overall intensity of light (which is usually normalized), S_1 describes the linear vertical to horizontal polarization, S_2 describes the linear polarization from $+45°$ to $-45°$ and S_3 describes the circular polarization from right-hand to left-hand rotation [41]. Both the angles for the polarization ellipse and the Stokes parameters can be represented on a Poincaré sphere, shown in Figure 2.1. The Stokes parameters S_1 to S_3 are normalized from 1 to -1 [40].

To calculate the transience of polarized light through a given system, a Jones

matrix can be used to determine the result. Multiplying the complex amplitudes of the vertical and horizontal components of the polarization vector by the Jones matrix presents a theoretical transformation of an input polarization state into its output. However, it is important to note that light does not necessarily maintain a single polarization state and may become disordered, which is referred to as unpolarized. For example, a beam of sunlight is unpolarized such that it contains randomized states of polarization. The intensity of light that maintains a specific polarization divided by the total intensity of the light is expressed as the Degree of Polarization (DOP). Using a Muller calculus, one can mathematically model polarization through a complex optical system and determine the DOP [40].

As light propagates through an optical fiber, its polarization will change due to *birefringence*. This property causes different polarization components to travel at different velocities. Birefringence can be induced by several factors, such as imperfections in the fiber structure, temperature variation, and external stresses caused by ground motion. The complex integration of these factors can appear as a random change in polarization from the light source to the destination [42]. Digital communication devices must compensate for this effect through complex signal processing and therefore must track polarization to properly reconstruct the digital signal.

2.1.4 Wavelength

The wavelength of light refers to the distance over which a wave repeats itself. For visible light, different wavelengths correspond to different colors. Depending on the application, optical communication uses a wide range of wavelengths as seen in Table 2.1. Generally, shorter wavelengths are used in shorter distance and multimode applications, which benefit from equipment that is lower cost and requires less energy to operate. Longer wavelengths are used in single-mode configurations and long-haul applications.

The wavelength bands are selected because of the optimal performance between several fundamental sources of loss and dispersion in silica optical fiber. First,

Band	Wavelength	Purpose
850-Band	850 nm	Home/Enterprise Multimode
O-Band	1260-1360 nm	Original/Historical Use
E-Band	1360-1460 nm	Single + Multimode
S-Band	1460-1530 nm	Passive Optical Networks
C-Band	1530-1565 nm	DWDM + Long Distance
L-Band	1565-1625 nm	DWDM + Long Distance
U-Band	1625-1675 nm	Maintenance/Monitoring

Table 2.1: Optical communication bands and common usage.

Rayleigh scattering occurs because of microscopic irregularities in the fiber's material makeup. As wavelengths become shorter, these irregularities cause significant dispersion. Second, the material absorption of fused silica rises significantly after 1700 nm, and is no longer a suitable medium for such long wavelengths. Lastly, peaks in absorption exist at about 950, 1250, and 1400 nm because of molecular-level water vapor in the material. Modern day fabrication processes have significantly reduced these water peaks, but their presence still defines the communication bands used today [27, 43].

Although advancements in optical communication have enabled new technologies to transmit and receive encoded information, the wavelengths that find most common use in single-mode metro applications today are in the C-band, which ranges from 1530 to 1565 nm. The C band is preferred in these applications due to its low signal loss and the availability of optical amplifiers that can boost signal strength over long distances [44, 45].

2.2 Fiber Optic Communications Equipment and Networks

In addition to examining the fundamental properties of light, we explore the contemporary applications of fiber optic networks and infrastructure, as well as the integral components that facilitate and optimize this mode of communication.

2.2.1 Optical Fiber

Optical fiber is a waveguide medium, designed to direct and contain light that enters one end. This is achieved through total internal reflection; as the light traveling through the fiber encounters a change in medium with a lower refractive index at an angle larger than the critical angle, it is completely reflected back into the first medium. Fiber optic cables will generally have three or more layers, depending on the application. The center of the fiber is the *core*, intended for the fundamental mode of travel. Surrounding the fiber is the *cladding*, constructed with a lower refractive index in order to guide the light modes through the cable. The transition between the core and the cladding may be step-indexed, with a rapid change of refractive index, or graded-indexed, with many gradual changes of refractive index moving away from the center of the core. Outside of the cladding, a *buffer* layer physically protects the fiber. Strength members may be added, such as cables or synthetic fibers, to protect the fiber from tensile strain, before being enclosed in a jacket. Several fibers may be bundled into a larger cable, which may contain gel, powder, armor, additional strength members, and/or encapsulating jackets. A diagram of a fiber optic cable is shown in Figure 2.2.

There are two primary types of cable, either designed for single mode or multimode transmission. Multimode fiber will typically have a larger fiber core to allow several modes of light to travel through the medium, while single mode fiber has a small core that limits transmission to a single mode, drastically reducing attenuation and dispersion for extended distances [42, 46]. Multimode communications components are often more inexpensive to deploy than their single mode

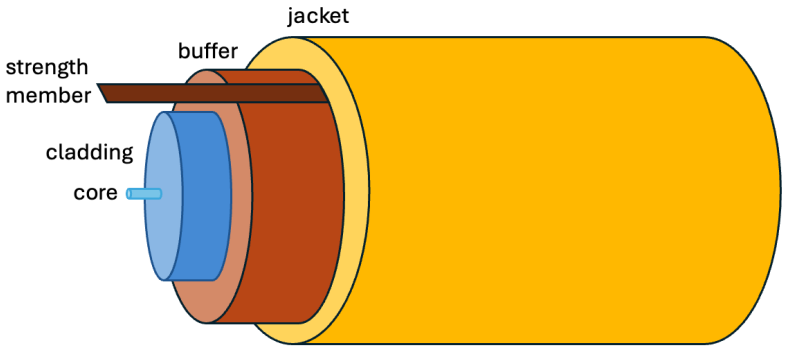

Figure 2.2: Cross-section of a fiber optic cable with components identified.

Recommendation	Title	Wavelength
G.651.1	50/125μm Graded-Index Multimode Fiber for FTTH Systems	850/1330 nm
G.652.C, G.652.D	Standard Single-Mode Fiber for CWDM Systems	1260-1675 nm
G.654.A-E	Cut-off Shifted Single-mode Fiber for Long Haul Networks	1550 nm
G.656	Non-zero Dispersion Fiber for CWDM and DWDM System	1460-1625 nm
G.657.A, G.657.B	Bend-insensitive Single-mode Fiber for FTTH Systems	1260-1625 nm

Table 2.2: Common ITU-T fiber optic specifications.

counterparts.

Because of the wide range of applications that optical fiber can support, it is specifically engineered for wavelength bands and the nature of the external environment. The International Telecommunication Union, Telecommunication Standardization Sector (ITU-T), governs the specifications of fiber types through official recommendations [46]. Some of the common-use recommendations can be seen in Table 2.2. Cables are created with specific cutoff wavelength ranges to maximize propagation and minimize intermodal dispersion.

2.2.2 Digital Signal Processors and Coherent Optical Transmission

Optical transport Digital Signal Processors (DSPs) correct for signal impairments, but are also responsible for performing several functions to efficiently transport data across an optical medium. Figure 2.3 shows a block diagram for the functions

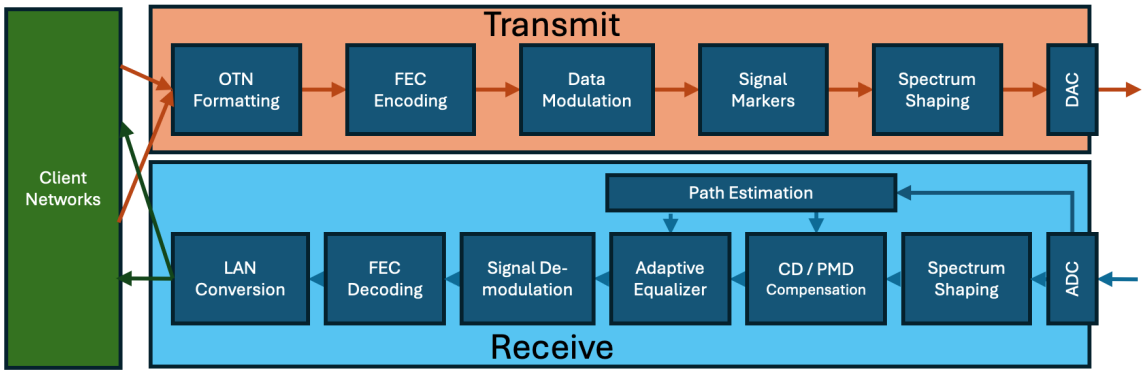

Figure 2.3: Block diagram of optical Digital Signal Processor functions [1, 2].

required to transmit and receive data in an optical link [1]. First, client-side data is aggregated according to the operator's configuration before sending to the DSP. DSPs then format the client data into the specified Optical Transport Network (OTN) wrapper, attach frame information, and conduct encoding for Forward Error Correction (FEC) [47]. The frame is then mapped to the different polarization waves, and a signal marker is added to assist the receiver with estimating the recovery of the frame. The data are then shaped to fit within the assigned transmission spectrum. Lastly, the packet is formatted and shaped for conversion to analog signal and transmitted using an optical transmitter. The receiving DSP follows a similar reconstruction, but in reverse, receiving the information and compensating for dispersion, evaluating the incoming signal marker and then applying adaptive equalization, demodulating the frame, performing FEC decoding, and distributing the data to the client Local Area Networks (LAN) according to the transport receiver's settings [1, 2].

The optical transmitter is responsible for transmitting the analog signal and encoding it onto the vertical and horizontal polarizations, modulating the orthogonal in-phase and quadrature phase components on the carrier light signal. These polarizations are combined and transmitted through the optical fiber medium to the receiving end. The receiver splits the received waves by polarization and uses a local oscillator to recover the phase component information through 90° hybrid

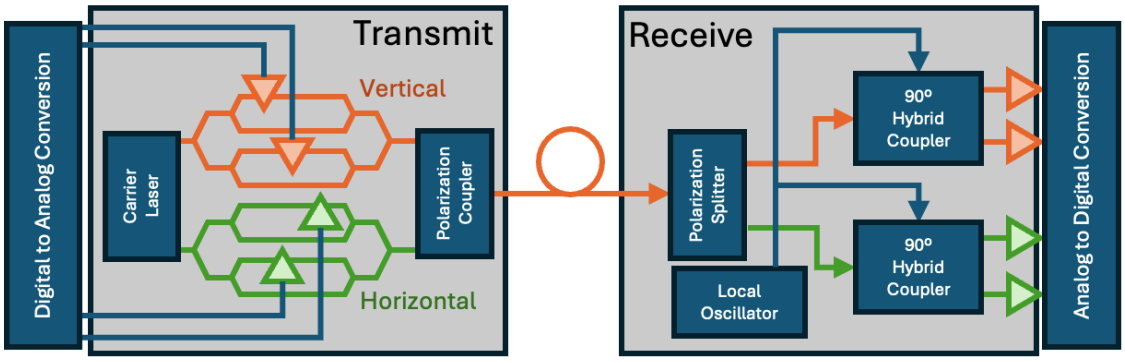

Figure 2.4: Diagram of coherent optical transmitter and receiver functions [1, 3].

couplers, before sending the signal to be digitally processed. A diagram of this process is shown in Figure 2.4 [1, 3].

2.2.3 High Bandwidth Solutions in Optical Networks

In the effort to increase the capability of optical-based networks, several different methods are used to increase the bandwidth of a given link. One method optical networks use is coherent optical communication, which encodes information on orthogonal polarizations on the same carrier [37]. The phase and quadrature components are modulated on each carrier wave in order to generate data symbols in Dual Polarization Quadrature Shift Keying (DP-QSK). As the requirement for more throughput increases and the signal is sufficiently above the noise floor, modulation schemes can be more complex, such as Polarization Division Multiplexing with 16-Quadrature Amplitude Modulation (PDM-16QAM) and Dual Polarization with 64-Quadrature Amplitude Modulation (DP-64QAM), with each symbol representing a higher order of bits (4 and 6 bits, respectively). Another way to increase data rates is by frequency multiplexing. For example, Dense Wave Division Multiplexing (DWDM) enables multiple channels that reside in wavelength bands (from 1530 to 1625 nm) of variable width to carry information in a single fiber. [48].

2.2.4 Fiber Optic Network Applications

Fiber optic communication has been widely adopted due to its capabilities and advantages over traditional copper medium. Datacenters can leverage optical switches and transport to meet requirements for low latency and high bandwidth, providing additional benefits of reduced power consumption and greater resistance to electromagnetic interference. Similarly, optical fibers used in LANs and last-mile installations for home and office networks bring higher bandwidth benefits to end users. Metro fiber and 5G applications require the bandwidth that can be provided through the efficient use of optical networks [38]. Optical transportation benefits from extremely low attenuation through the use of optical repeaters, forming the longest and highest throughput terrestrial-based networks, with endpoints being able to communicate quickly from more than thousands of kilometers away.

2.2.5 Optical Transport Signal Impairments

Due to the dispersion tendencies of an optical pulse to spread out in time, there are several impediments to achieving optimal bit rates that must be considered. Chromatic Dispersion (CD) is a temporal drift of wavelengths due to the index of refraction being a function of frequency [40, 49]. Similarly, Polarization Mode Dispersion (PMD) relates to the temporal drift between different polarizations that distorts the original signal [40, 27]. Differential Group Delay (DGD) describes the distance between the two signal components [50, 40]. Although earlier optical communication systems required specialized fiber in order to limit these errors, modern DSPs are capable of identifying the different components, maintaining a signal lock on transmission, and will routinely mitigate these effects [51].

2.2.6 Performance Metrics for Optical Communication

In order to monitor network performance, hundreds of metrics have been developed and are available for use on optical transport network devices. We list several commonly used metrics that can track efficiency and identify problematic situations

in these networks. Bit Error Rate (BER) expresses the frequency in which an error is identified in communications, typically given as a negative exponent. BER can be calculated both before and after Forward Error Correction (FEC), and is a good baseline measurement for the quality of a given optical link [52]. Optical Signal-to-Noise Ratio (OSNR) measures the ratio of optical signal power to noise in a given optical channel. A higher OSNR indicates a higher signal quality, which translates to better performance in terms of data transmission and error rates [53, 54]. With an expected bit rate, Q-factor can be used to find the ideal OSNR. Q-factor is a metric based on the understanding that data symbols are not evenly distributed between '0' and '1' signals during transmission, and take their distribution into account [55].

2.2.7 Network Monitoring

Given the requirements for optical transport networks, continuous monitoring and maintenance can become cumbersome. Over several years, life-cycle replacement of outdated components and additional expansion of the network often results in equipment sourced from different vendors. Different vendors and capabilities package proprietary monitoring tools to assist in collecting metrics and alerts via reporting utilities, such as Simple Network Management Protocol (SNMP), or via streaming telemetry utilities. This may result in monitoring segmentation and increased complexity as the network continues to mature and develop to meet requirements [56, 57]. Monitoring large optical networks is a significant area of research that requires innovation and adaptability to satisfy network operational requirements. We provide a few examples of solutions that address this problem in several different ways.

NetSage was developed to ingest metric data from multiple sources to support operators and managers who oversee the International Research Networks Connections (IRNC) backbones. This system also allows different operators to request metric visualizations with the context most appropriate for their task through the use of a simplified query interface to build a dashboard [58]. Netpaca was devised

as a monitoring dashboard using the Grafana visualization platform [59] by first identifying actionable metrics and alerts, then increasing the scale of the monitoring service to approach the problem from the ground up to overcome shortcomings in vendor specific products to form a holistic approach [60]. OpTel was designed to leverage purpose-built streaming telemetry focused on through a vendor-agnostic, scalable approach to monitor and manage optical backbone networks between cloud provider datacenters. Of particular interest relating to the development of reporting capabilities of optical transport devices, they found that 15 second reporting intervals were most efficient at detecting persistent events over transitory ones, and were able to predict future network-degrading events up to 15 minutes after early warning indicators [61].

During the development of this thesis, we recognized the need for a scalable and holistic monitoring solution that could ingest performance monitoring metrics and correlate network events to external environmental effects. To this end, we developed a prototype system, Optimon. A high-level overview of our system is shown in Figure 2.5. This system was designed with a centralized approach to monitoring, with distributed collection nodes residing on the transport management network capable of collecting and filtering specified metrics. Optimon is vendor-agnostic and performs data sanitization on the collection nodes before sending pertinent information to a library node. The library node retains the original data on long-term storage devices and also maintains recent data in a time-series database using the open-source Telegraf, Influx DB, Grafana (TIG) stack [62]. The user can build and apply transformations to the reported data to discover trends and anomalies. Lastly, the user interfaces with the command node on the internal management network to modify collection and storage settings from a single location. As a minor contribution, we have made the Optimon repository available for use and further development [63].

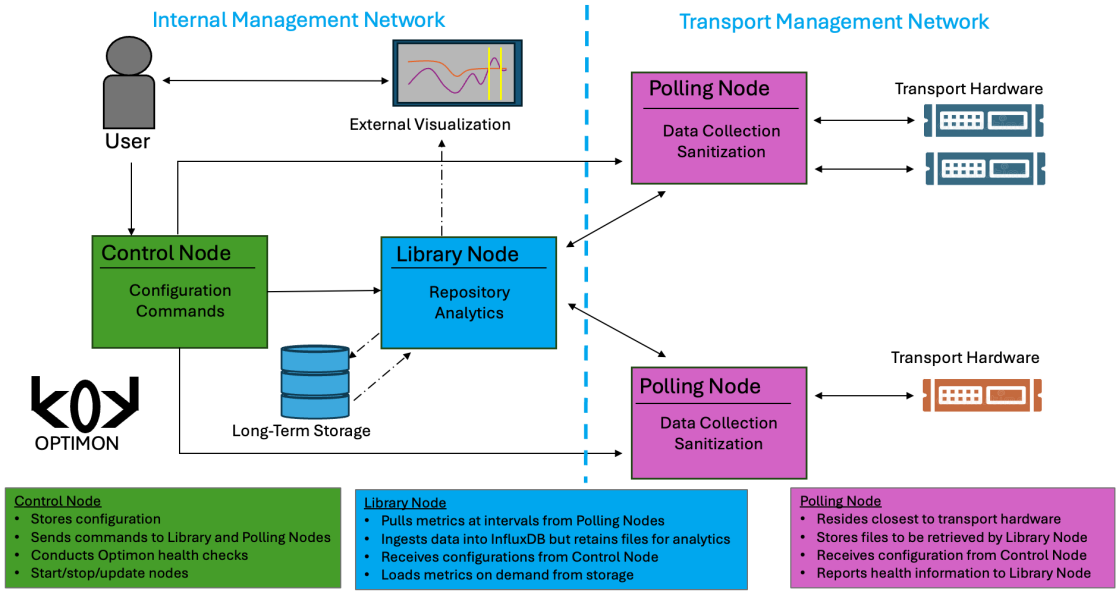

Figure 2.5: Diagram of Optimon, a prototype optical network monitor.

2.3 Ground Motion Sensing

Earthquakes are one of the most powerful and destructive forces on Earth, and their impacts can be catastrophic to our lives. In 1906, more than 3,000 people lost their lives in San Fransisco in the quake and the fires and destruction that followed [64]. One hundred years later, almost 1,150 residents of West Sumatra were killed in the earthquake and the region was crippled with the loss of infrastructure [65].

The ability to identify earthquakes in real time is crucial for protecting human lives and minimizing damage. Earthquakes are characterized by several waves of different intensities that can be detected and alerted to help minimize the loss of life. P-waves travel quickest from an earthquake's epicenter and are characterized by compression and expansion of the ground radiating in the direction of travel. These are commonly non-destructive and comparatively minor. S-waves follow after and are characterized by transverse vibration along the direction of travel and are more intense. Following the P- and S-waves, the most intense and damaging surface waves arrive [66, 67, 4, 68]. This pattern of propagation can be used to trigger early

warning systems, initiate emergency response efforts, and inform public safety officials and the general public.

2.3.1 Detection Technologies and Networks

Identification of early waves and coordinating arrival time between different seismic sensors allows for identifying the location, magnitude, and expected duration of seismic events [4]. Before the use of digital recording, sensing technology in the 1930s consisted of the recording the movement of a mass suspended on a spring on paper or film in strong-motion accelerographs [69]. The critical need for ground motion sensing capability has driven the advancement of these technologies to take many different forms today. Modern sensing networks require the use of different systems such as California's ShakeAlert system, consist of a range of sensors that include broadband seismometers that are capable of recording a wide range of frequencies [70], short-period sensors that are more sensitive but limited in frequency range [9], and strong-motion sensors that can monitor higher magnitude motion [4] to fully capture seismic activity [5]. Recent advancement and maturity of Micro Electro Mechanical Systems (MEMS) has opened up the possibilities of having smaller form-factor devices that can be deployed in denser arrays to increase sensing resolution [71]. Radar sensing by satellite can also be used to detect areas of concern for landslides in remote areas where traditional monitoring is difficult [72]. The choice of sensing technology to employ is dependent on the specific seismic monitoring application. Employing a diverse set of sensor types can provide a more robust solution, with capabilities from one type complementing another's limitations.

Due to the large volume of data that is collected and shared by seismic detection networks, continuous capturing is undesirable. To conserve resources, algorithms are used to identify changes from baseline activity [73]. One of the most well known is the Short Term Average/Long Term Average (STA/LTA) trigger. This combines the average of a shorter window to identify the start of a seismic event, and a longer window which terminates the event. Parameters such as trigger weight and pre-

and post- recording lengths are important to configure correctly in order to capture relevant information about seismic signals [74].

Given the expense and infrastructure needed to maintain and coordinate these networks, research has also been conducted into using lower cost systems that can be deployed to make a dense array of sensors, both for event detection as well as seismic activity analysis [75]. Raspberry Shake is a low-cost geophone built on a Raspberry Pi that has been shown to be an effective addition to ground motion sensing networks [76, 77]. Experiments with low-cost accelerometers, such as the ones used in smartphones, suggest that decentralized networks with limited capability sensors can be crowdsourced to detect seismic events [78] due to increased sensor density, but could suffer false alarms [79].

2.3.2 Seismic Sensing Applications in Metro Environments

City and metro locations provide a saturated sensing environment due to the large amount of anthropogenic noise that results from a large population. Recent studies have found ways to identify this as noise through machine learning applications to focus on earthquake events [80]. However, discarded noise is information-rich for the events and activities that are occurring in our cities. More than just detecting large-deformation seismic events, detecting subtle strains and vibrations provide the basis for imaging the near-surface and can inform us of local events in metro areas and infrastructure, such as crowd activity, explosions, or structural health monitoring. Natural gas and fuel explosions can be recorded in these sensing networks, and timing analysis from these networks can provide locality information on where these explosions occurred [9]. In 2011, a surprise play by the Seattle Seahawks caused such an uproar by the spectators that a strong-motion sensor was able to detect and monitor the event in such detail that specific portions of the play leading to the touchdown and extra point were able to be identified. [81]. Similarly, responses to encores and playlists in rock concerts can be pinpointed on these devices, as well as firework displays and more common events such as diurnal traffic cycles and subway traffic [82]. Sensors can be installed on buildings

and bridges to determine if there is damage to the structural integrity and can serve as an early warning sign to preserve life and prevent further damage to the infrastructure [6].

2.4 Fiber Optic Sensing

The use of fiber optic cables for environmental and physical sensing has been explored for several decades and has had significant impacts in many applications. Disturbances and environmental changes along a fiber route alter the strain imposed on the fiber optic cable and modify the cross section of the fiber causing measurable disturbances and changes to the output at the termination point of the fiber. Although many techniques and applications for fiber optic sensing have been published, we highlight three broad technological categories of particular importance for this thesis.

2.4.1 Integrated Sensors

As discussed in previous sections, external stresses and strains placed on the fiber, such as temperature or bending, ultimately reflect changes in the properties of light that is guided through the fiber. These sensors measure different characteristics at a termination point of a fiber and measure the integrated change of the route from an established baseline at a termination point [83]. The earliest fiber optic sensors measured the light that passed through a fiber. Reductions in intensity were observed when a pressure plate was activated, causing a strain that leaked light out of the fiber core [84, 35].

If fibers support multimodal transport, the projection of the interference between the light modes can be measured by Fiber Specklegram Sensing (FSS). The cost and complexity of equipment used in the construction of these devices is significantly less compared to more sophisticated methods of measurement [85]. FSS has been successfully demonstrated in several works over many years. Zhang et al. applied specklegram sensing in structural monitoring test and were able to measure minute

deformations in a concrete beam with an embedded test fiber [86]. Liu et al. were able to train a machine learning model to detect the amount of curvature in a suspended fiber [87]. Machine learning has also been used to determine the general locality of fiber displacement with specklegram sensing, with limited results [88].

Integrated sensors are relatively inexpensive and technically easy to use compared to other means of fiber optic sensing. However, the amount of information revealed from a route must be taken as a whole and are particularly sensitive to disturbances outside of the testing region and can suffer from reliable measurements [85]. Overall, they demonstrate significant potential for practical applications in monitoring structural integrity and environmental changes in otherwise undisturbed environments, and offer a cost-effective approach for measurement and analysis on fiber optic cable.

2.4.2 Modified Fiber Sensors

Fiber optic sensors can be especially effective by modifying the construction of the fiber optic cable to gain increased sensitivity. In particular, a Fiber Bragg Grating (FBG) has a modulated refracted index in a distinct pattern at specified locations. Depending on the configuration of the grating, these portions of the fiber cause reflection of a particular wavelength that varies with strain, which can be targeted for measurement. By using different grating periods, different wavelengths are affected. When combined with a broadband signal, this configuration can provide multiple readings at several points along a single strand of fiber that can be interrogated using filters or multiplexing receivers [89].

Comparative tests versus traditional strain gauges show that FBG fiber sensors have increased sensitivity and also offer resilience against undesirable environmental effects such as corrosion and electromagnetic interference [90]. These sensors have been used to monitor high-speed train traffic in real time by counting the pressure of the passing train wheels, and can also detect deceleration and acceleration as the train passes [91]. Other sensor applications involve measuring the axial strain of the spans of a bridge while load bearing trucks traversed the structure,

measuring the changes between the bridge piers and creating an overall vibration profile [7].

The use of a singlemode, multimode, singlemode (SMS) spliced fiber can also benefit fiber optic sensors. Using an SMS fiber as a filter for an FBG-based sensor, this configuration served to eliminate the wavelength variation of temperature and preserve changes in strain [92]. For FSS applications, this configuration reduces interference from disturbances outside of the testing area and can excite additional light modes, allowing higher-fidelity measurements [86, 93].

Modified fiber sensors are more expensive to deploy and maintain than point sensors, although they offer notable benefits, such as high-precision measurements, enabling various sensing responses, and limiting sensitivity to target-specific measurements. However, this type of sensing requires a separate installation for sensing purposes and cannot take advantage of existing fibers in optical network communications.

2.4.3 Distributed Acoustic Sensing

One of our main motivators for this research is the success of Distributed Acoustic Sensing (DAS) technology, which uses dedicated fiber optic cables as a sensing array for ground motion that results in acoustic signals. The sensing techniques used vary, but operate on similar principles as optical time-domain reflectometry (OTDR), which is used to evaluate the structure of the optical fiber used for communication [38]. DAS interrogator units send pulses of light down a dedicated fiber. Based on the light returned from Rayleigh backscatter, a profile of the fiber path is constructed. Small deviations from this profile indicate not just the magnitude and time of change but can also determine locality with resolution of as little as 1 m more than 40 km away. This capability serves as a linear array of sensors with one collection device [14].

DAS and fiber optic sensing have seen wide application in a variety of studies and applications, especially earthquake monitoring [94, 95]. These sensors have also been used to measure changes resulting from pipeline soil leakage over long

distances [96]. Due to their high sensitivity, DAS arrays have been deployed in order to characterize ambient noise signatures produced by cultural effects to further distinguish signals of interest [97]. DAS detects surface waves that are generated from high-speed railways [98] and can be deployed to serve as intrusion detection for border security over extended distances [99].

DAS is a versatile and powerful technology with broad applications in various fields, from geophysical monitoring to security. Although expensive, technically complex, and resource-intensive compared to other fiber optic sensing technologies, its ability to provide highly detailed and spatially resolved data over long distances makes a significant impact on detection techniques for subtle changes in an environment.

2.5 Fiber Optic Communications as an Environmental Sensor

Given the widespread presence of optical network communications infrastructure and the technological advances of fiber optic sensing, the integration of two distinct applications on the same infrastructure appears promising. However, it is essential to consider both the challenges and opportunities that arise from this combination. Given the technical and physical requirements that stem from these two domains, it presents unique technical and operational challenges that must be addressed to fully realize its potential.

2.5.1 Challenges

One of the primary challenges in combining optical networked communications with fiber optic sensing is the significantly different deployment strategies for each application. Fiber optic communication routes are engineered to shield them from environmental effects to maximize signal integrity, while sensing fibers are often exposed to these same conditions to effectively gather data. In addition, any disruption to the network can become a significant liability for organizations that

rely on the fiber optic infrastructure for high-bandwidth communications. These factors create a complex landscape where the incentive to implement such dual-purpose sensing must be balanced against the resource investment required to make the trade-off beneficial.

2.5.2 Opportunities

Despite these obstacles, there is a growing body of research focused on monitoring optical communication networks, which shows the wealth of data that can be observed. Wind galloping effects for aerial runs have been monitored through the use of polarimeters and optical transceivers [20, 100]. Similar measurement techniques have been used to detect high-speed train traffic on rail bridges with optical communication fiber routes [21, 101]. Although long-haul network monitoring presents an integrated response to changes throughout the monitored route, particularly quiet routes, such as on the ocean floor, can show a response to undersea earthquakes [16] and sea swells [19]. Changes in diurnal temperature along the fiber routes have been found to correlate with changes in PMD [102]. Measurement of fiber optic cable responses to tap testing can identify mismatches between historical route maps and reveal the locations of slack loops [103]. Recent research on combining distributed sensing with simpler communication schemes shows the possibility of integrating these two technologies [12, 104]. Initial research on the use of optical network performance metrics shows promise for future studies to incorporate sensors into the communications infrastructure [18].

Although these related studies highlight both the advantages and the intricacies of physical sensing on communications infrastructure, there is considerable potential available. Despite the significant challenges posed by varying deployment strategies and the risk of network disruptions, the extensive data and insights obtained from such a system can be extremely valuable. The possibilities of better monitoring and real-time data collection in various applications, ranging from infrastructure health monitoring to environmental surveillance, emphasize the need for ongoing research and innovation in this field. By addressing technical

and operational challenges by investigating pragmatic monitoring methods, we can utilize existing communication networks to develop a more robust and intelligent infrastructure, ultimately advancing both technological capabilities and societal benefits.

3 TRANSCEIVERS: EFFICACY OF USING COMMODITY OPTICAL EQUIPMENT FOR ENVIRONMENTAL SENSING

The challenge of adapting communication network optical fiber infrastructure for environmental sensing has two technical dimensions, (*i*) enabling sensing capabilities on optical fiber infrastructure, and (*ii*) the response of the infrastructure to environmental effects of interest. Capabilities can be achieved by deploying dedicated sensing equipment (*e.g,* DAS interrogators and polarimeters) on dark fiber that is available in network communication conduits [17, 20, 21], or by tapping into optical hardware that transmits the data signal [18, 10]. Although the former offers immediate deployment opportunities, longer-term challenges include scalability (limited to tens of kilometers of uninterrupted fiber section runs), management overhead (associated support needed for additional interrogators), and costs (each additional section of sensing fiber requires a new interrogator).

Our long-term goal is to create a highly sensitive global sensing system on top of existing network communication fiber optic infrastructure with no operational disturbance of its primary purpose of transporting data and with little to no additional cost.

Several recent studies show that optical transport equipment can be used to detect significant events that would impair network data in transit over the fiber [18, 105, 11] or to use coherent receivers as sensors in idealized environments [10, 19]. However, real-word urban deployments are engineered to protect against communication degradation and can be subject to a magnitude of smaller effects that mask responses of interest. *Our contribution is to explore the efficacy of using network communications infrastructure for environmental sensing in a general sense, both in practicality and sensitivity.*

We examine the current capabilities and limitations of using commodity network communication transport hardware by conducting a series of controlled laboratory tests to understand how the characteristics of light change as fiber is disturbed, as well as the level of sensitivity to disturbances of interest on fiber optic cable. We

then deploy our sensing system on fiber that more closely approximates a network communication installation in an urban environment. We characterize the specific geometry and coupling of the fiber run and determine what can be sensed with this system.

Through these experiments, we show that the use of optical communication equipment and infrastructure presents some limitations for ground motion sensing, but reveals important and previously unseen information about the environment around fiber optic cables that is useful in monitoring applications.

3.1 Overview of Research

A series of controlled laboratory and field-scale tests were conducted using an optical communications transceiver to assess the current capabilities and limitations of using commodity network communication transport equipment for ground motion sensing. The transceiver's capabilities were augmented with software that enables light signal data to be collected. A critical aspect of the design of an optical transceiver is its ability to recover data signals by detecting and compensating for linear transmission impairments that occur in the optical medium [3]. Over time, these adjustments can reveal polarization transience induced by fiber deformation, which we are interested in for sensing applications. It is important to note that typical transceivers are not designed to report this information directly and are thus typically unavailable for sensing applications. Our tests aimed to understand how the transceiver can report polarization transience as fiber deformation occurs due to vibrations and temperature changes, as well as the level of sensitivity to expected disturbances. Through these experiments, we were able to identify potential opportunities and limitations with the use of commodity network communication transport equipment for environmental sensing.

Despite these limitations, we were able to identify revealing information about the environment around fiber optic cables that is useful in monitoring applications. By tracking the polarization state and transient effects, we characterized how different impacts on the fiber were evident in polarization measurements and

determined what could be sensed with this system, providing effective coupling to areas of interest. We also provide a comprehensive report on our exploration of transceiver reporting metrics, the construction and improvements on our in situ fiber experiments, the characterization and analysis of the vibration signals of trains, and recommendations based on our results for selecting fiber-sensing routes.

Our findings advance the vision of harnessing network communications infrastructure for ground motion and environmental sensing. We highlight practical use cases for sensing via commodity optical transceivers, as well as the primary limitation of our test system which is the sampling frequency.

3.2 Transceiver Setup and Configuration

The commodity system used for these experiments is an Acacia AC1200 Dense Wavelength-Division Multiplexing (DWDM) Transponder Module, as seen in Figure 3.1. This device interfaces with up to 12 client network pluggable modules and transport data up to 1.2 Tbps via an optical link [106]. This module is commonly enclosed in larger rack-mountable equipment, and access to specific functions is constrained by the enclosure's vendor and system requirements. Our use of the AC1200 was through an evaluation enclosure that provides additional access to the registers beyond what is available through a standard management interface. Our experiments were performed in a homodyne configuration using a single lane for transmission and reception. This transceiver model was used in a previous study to correlate polarization transients from a submarine cable deployment to sub-sea earthquake activity [10].

The Peripheral Component Interconnect Express (PCIe) management interface allows reading and writing to hundreds of registers within the AC1200 that include device, vendor, customer, network, control, alarm, and monitoring information. Our initial investigation into the use of the device for a sensing system involved a subset of more than 30 network performance monitoring registers, represented in Table 3.1.

Register Purpose	Reporting Interval	Variants		
Polarization Dependent Loss	1 Hz*	Min	Max	Avg
Bit Error Rate	1 Hz*	Min	Max	Avg
Bit Error Rate	10 Hz	Current		
Optical Signal to Noise Ratio	1 Hz*	Min	Max	Avg
Q-Factor	1 Hz*	Min	Max	Avg
Chromatic Dispersion	1 Hz*	Min	Max	Avg
Differential Group Delay	1 Hz*	Min	Max	Avg
Signal to Noise Ratio by Modulation	1 Hz*	Min	Max	Avg
State Of Polarization Change Rate	1 Hz*	Min	Max	Avg
2nd Order Polarization Mode Dispersion	1 Hz*	Min	Max	Avg
OSNR by Polarization	1 Hz*	X-Pol	Y-Pol	
Received Total Optical Power	10 Hz	Current		
Received Total Optical Power	1 Hz*	Avg		
Received Signal Power	10 Hz	Current		
*Shortest performance monitoring interval configurable				

Table 3.1: Selected Performance Monitoring Registers for Evaluation.

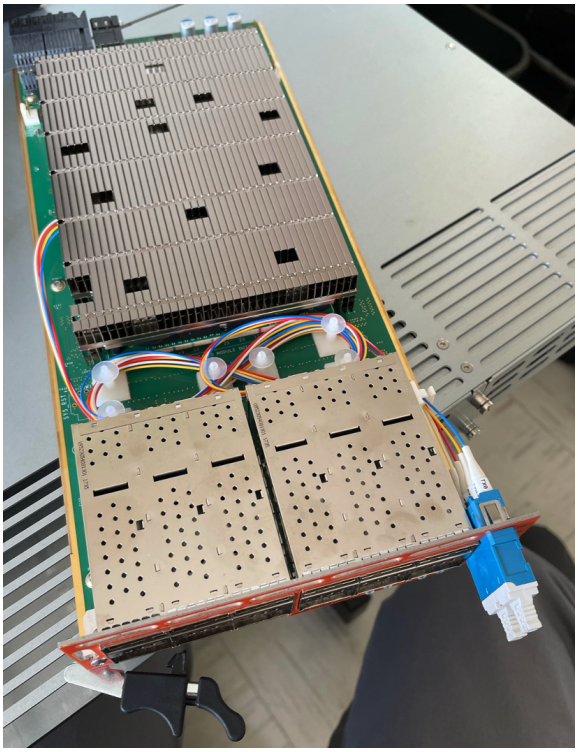

Figure 3.1: The Acacia AC1200 DWDM Transponder Module.

Several limitations became apparent after conducting initial calibration tests using the available network metrics: (*i*) The reporting interval was too long to retrieve our signals of interest. While metrics used the configurable Performance Monitoring (PM) value, with a minimum refresh rate of one second, almost all of our signals of interest for sensing applications would occur at 8-30 Hz (see Section 3.3.4). (*ii*) Reporting options such as minimum, maximum, and average values fundamentally obscure signals that could be used to detect oscillating patterns that can be generated by vibration. Furthermore, the reliability of the reported information was vague in terms of how the average values were calculated for a given metric. (*iii*) Network metrics that were available at faster reporting rates are produced after the initial reception of the signal. That is, signal processing effectively removes small disturbances that may have occurred due to environmental effects, and any effects that do not result in significant degradation of power or

signal cannot be captured. (*iv*) The granularity of the State of Polarization (SOP) change rate was designed to detect large disturbances, such as lightning strikes. Any effects that would cause small strains on the fiber would not register beyond the reported value. Although the information reported is sufficient for the intended operation of the transceiver, these metrics and their reporting method were not viable to capture our signals of interest. These issues highlight that adapting an optical communication transceiver for opportunistic environmental sensing is not straightforward.

During evaluation of the management interface, we also considered capturing the constellation information of the incoming signals. The device and management interface can sample data at high rates, but it only captures a single group of 4,000 to 6,000 adjacent symbols per request. Given the order of magnitude of symbol rates above 20 GBaud, this would not result in a meaningful sampling rate given the design of the AC1200 transponder.

We configured the transceiver to transmit and receive data modulated via Dual Polarization 64-ary Quadrature Modulation (DP-64QAM) format for the duration of our experiments. To extrapolate the polarization state for our measurements, the vendors provided additional firmware and software that collects and integrates information from the adaptive equalizer during signal recovery[1]. This results in a sufficiently accurate reconstruction of the polarization state from the receiver's perspective at a non-periodic reporting rate of 13 to 18 Hz.

This polarization state is stored in the device's registers as a partial Stokes vector (normalized parameters S1, S2, and S3). These values and any other requested PM registers are polled by the vendor software that resides on a client via the management port. The software retrieves and formats these values pairs each with a timestamp generated from the elapsed running time and stores the running output to disk for processing.

A significant issue we had to address was the calibration of the measurement timing. The AC1200 does not synchronize the internal oscillators with an external source, such as Network Time Protocol (NTP) servers, as it does not serve any

[1]Specific details on how these measurements are generated are proprietary to the device vendor.

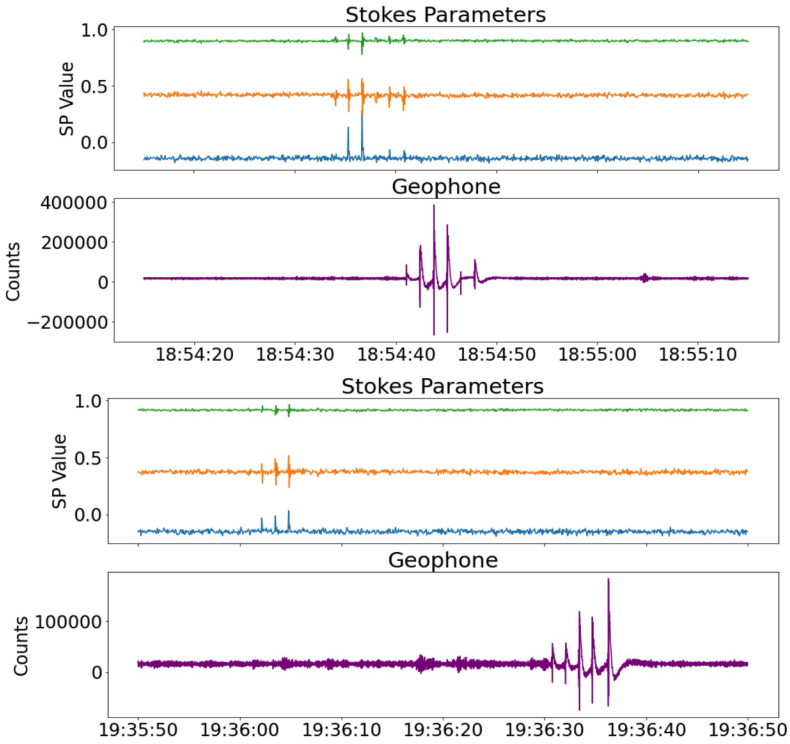

Figure 3.2: Timing analysis of AC1200 Stokes parameters and time-synchronized geophone readings. (top) shows 4 seconds of drift after 10 minutes of capture and (bottom) 31 seconds of drift after 50 minutes of capture.

purpose for normal data transmission. Furthermore, we discovered an error in the external timestamp generation function that caused a temporal drift in reporting. Figure 3.2 shows the results of a synchronization test between the AC1200 polarization reporting software and our geophone. To mitigate this effect, we created a wrapper around the vendor-provided software. We reset our capturing system every 59 minutes, with an average loss of about 15 seconds of recorded time every hour. After we implemented our clock patch, the timing was relatively stable. We adjusted the values reported during post-processing to align the recordings with measurements from the vertical axis geophone of a Raspberry Shake RS3D seismograph [76], which were time-synchronized using NTP.

Because the measurements focused on the polarization state, we sought additional parameters to enable the most accurate and sensitive reporting possible. The

AC1200 can be used for submarine transmission applications, where precise polarization state measurement is possible and beneficial. We conducted an extensive series of tests modifying relevant parameters, including fast-tracking polarization mode, modulation formats, cross-polarization gain settings, and power-level settings, to determine the optimal settings for our experiment. After evaluating the distribution and variation of the reported values, we conducted our laboratory and field experiments with the *fast polarization mode* (typically utilized for long-haul submarine links with disabled cross-polarization gain).

3.3 Methodology

After determining the optimal settings for our test system, we conducted a series of controlled laboratory tests and field experiments to measure the relationship between the displacement of a fiber optic cable and the polarization at the receiving endpoint of a fiber optic cable. Given that polarization transients occur due to bending, twisting, and applied pressure to a fiber optic cable, polarization measurements are an ideal candidate for environmental sensing [40].

3.3.1 Static Angle Tests

Our first objective was to characterize polarization transience due to repetitive fiber strain to correctly interpret environmental events. We used a setup shown in Figure 3.3 to measure the resulting polarization from several static positions to measure bending strain. In this experiment a bare fiber (10 m) is used. The fiber is looped four times around a 10 cm diameter transmit-side static anchor, bent around a middle static anchor, and then looped four times around a 10 cm diameter movable receive-side anchor. The fiber is kept under constant tension using a spring on the entry anchor to ensure relative consistency. The angle from the static anchor to the movable anchor is adjusted from 100 to 0 degrees in increments of 10 degrees, and the mean polarization is recorded for each step. Each test was repeated 4 times, with a middle anchor diameter of 7.5, 5.0, and 3.8 cm.

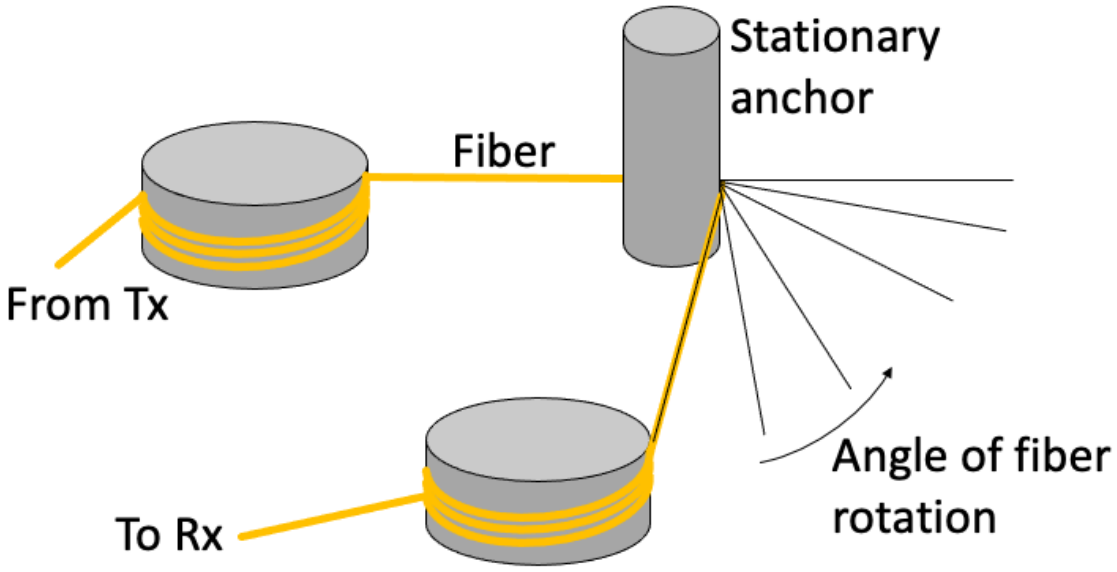

Figure 3.3: Static Angle Test Setup. Averaged Stokes parameters were recorded as the moveable anchor (bottom) was moved at 10-degree increments, from 100 to 0 degrees.

3.3.2 Vibration Plate Testing

Next, we conducted a series of experiments to determine the sensitivity of our measurement system to vibration, seen in Figure 3.4. A fiber optic jumper cable (10 m) was taped to a vibration plate (a VG-100 Vibration Generator from Vibration Test Systems [107]) that was 15 cm wide with adjustable frequency and amplitude. To ensure that an isolated portion of the fiber was subjected to the test, the fiber was adhered to a static frame 13.5 cm away from both sides of the vibrating plate with a small amount of slack to prevent damage. The transceiver and any fiber outside the vibration assembly was routed to a separate table 2 m away. The vibration frequency in our experiments ranged from 0.3 to 12 Hz (frequencies selected to align with the Nyquist limit of reporting by the AC1200), and the amplitude was measured using a displacement sensor and an accelerometer attached to the vibrating plate.

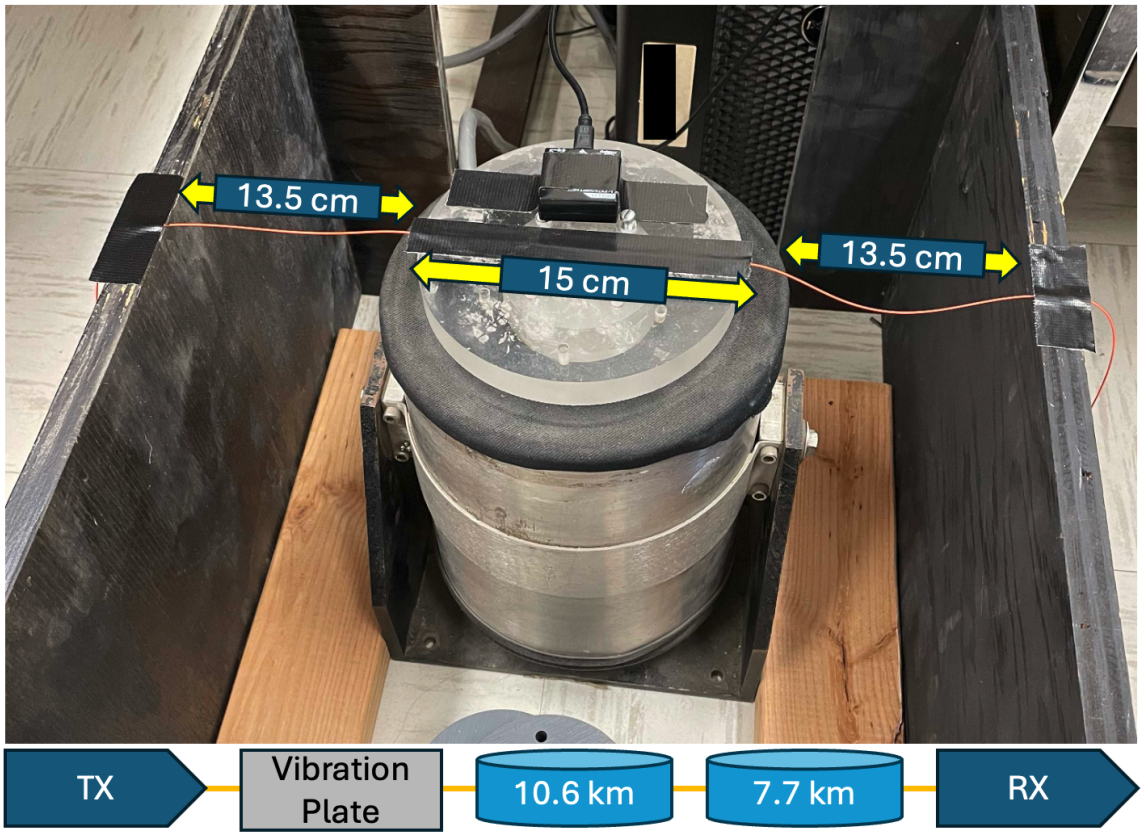

Figure 3.4: Vibration Plate Test Assembly. The fiber was vibrated on a 15 cm plate, and different fiber lengths were tested by adding two test spools (not shown) to determine the attenuation of the signal of interest.

We also assessed the effect of additional fiber lengths up to 17 km by inserting test spools into the fiber path after the vibrating assembly but before the receiving end to determine any signal attenuation.

3.3.3 Campus Route Monitoring

After completing laboratory experiments, we connected our system to a campus-scale fiber path consisting of an optical route of 4 km across the campus that included indoor and outdoor segments, shown in Figure seen in Figure 3.5 [103]. The indoor path was routed through several telecommunication rooms and between floors

of each building with a loopback adapter at the distant end. The outdoor path has an 80-m section that parallels and crosses underneath an active freight railway and traverses underneath several downtown streets. The fiber path beneath the railway was installed inside a steel conduit at a minimum depth of 5.5 feet below the surface according to state regulations [108].

To assess the sensitivity of different portions of the fiber run, we physically agitated armored cable and external fiber slack loops and subjected the fiber splice cases to physical shock. To detect the vibrational effects of nearby passing trains, we used geophone readings at the fiber egress point (located in the basement) approximately 20 m from the railway. We also used a truck-mounted weighted tap test device at more than a dozen locations along the outdoor fiber path. During initial monitoring, it was discovered that a main air-cooling outlet in the network test laboratory was positioned directly onto the rack where the AC1200 was installed and caused visible movement of the fiber under test. We created air baffles to reduce this unwanted effect and adhered the fiber patch cable to the floor-mounted equipment brackets to protect the fiber from the direct airflow path. We monitored this route for two weeks and correlated the results with the geophone data to determine polarization transience due to passing freight trains.

3.3.4 Train Signal Characterization

Train vibrations captured on the geophone have a distinct and pronounced signature. For every recorded passing train, the most significant vibration occurs as the engine passes, followed by the trailing cars. The predominant vibration frequency captured on the Raspberry Shake ranged from 8 to 30 Hz. Train events lasted from 30 seconds to several minutes, depending on the number of trailing cars. Due to the difference in the bandwidth of reported frequencies between our sensing system and the geophone, we also collected video recordings of passing train cars to analyze the average speed and determine the expected frequency of sub-Hz wheel noise when transiting over a rail segment gap. We estimate the train speed passing by the building to be 18.5 km/h and that a single 20-m train car would pass every 3.6

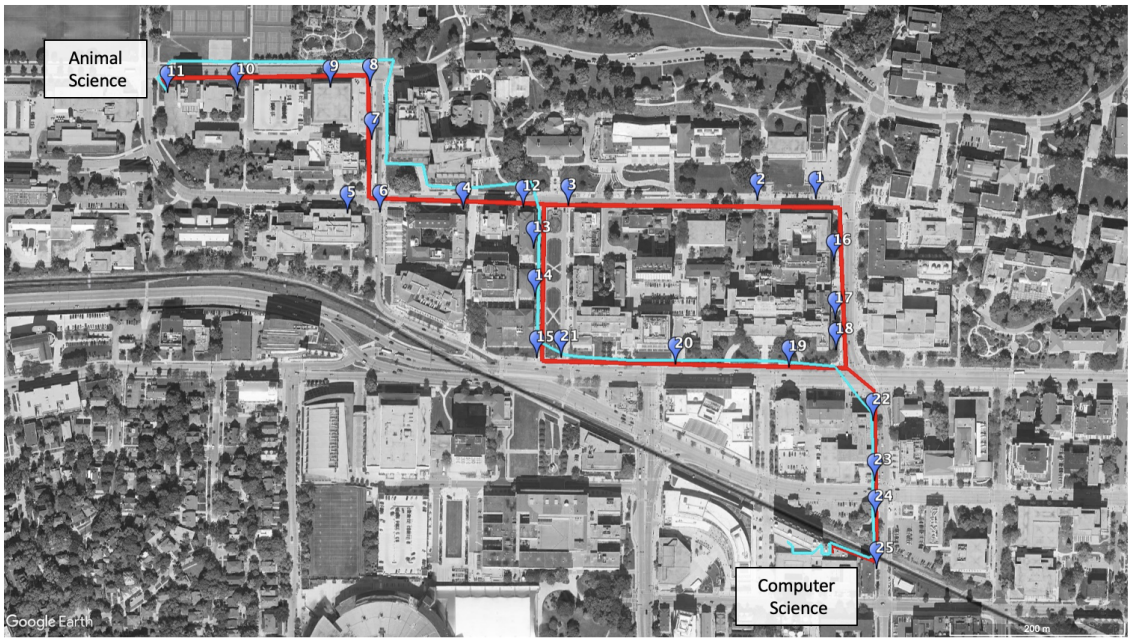

Figure 3.5: 4 km campus optical fiber route characterized for physical disturbances. Red line denotes historical map data, cyan line denotes fiber detected via DAS and tap testing.

seconds, on average. At this speed, the time between wheel assemblies in a single car traversing a rail segment gap is approximately 2.7 seconds (0.37 Hz).

3.3.5 Custom Fiber Installation

Although the previous experiment would give us an accurate understanding of environmental sensing on network communication fiber in a metro area setting, it would not explore what is possible given a route with a more advantageous location affected by environmental disturbances. To assess the sensitivity of our system in more detail, we installed a 9/125µm OS2 duplex fiber optic patch cable (100 m long) with a loop back adapter that ran parallel to the railway approximately 60 m in a drainage ditch adjacent to the rail ballast. The initial fiber was installed at approximately 1 cm depth along the railway. However, varying moisture in the soil of the drainage ditch reduced the coupling between the fiber and the

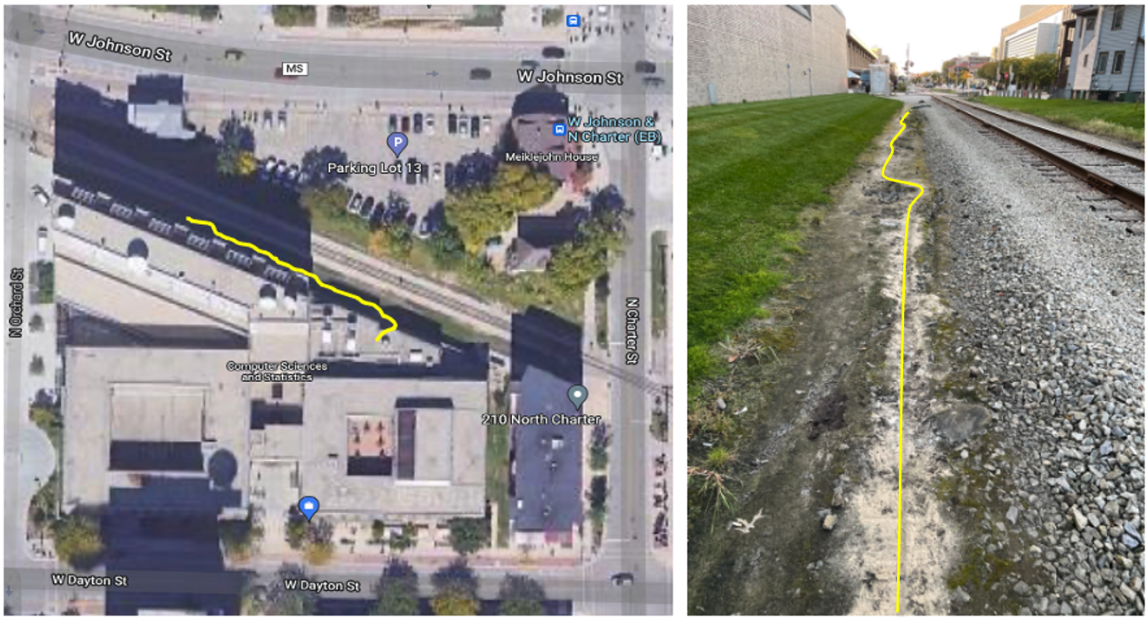

Figure 3.6: Satellite map of custom fiber run estimated in yellow installed next to freight railway (left). Ground-level picture of installed fiber location with burial location highlighted (right).

surrounding soil along the route. During several weeks, the installation was tested and temporarily improved by adding more than 225 kg of soil and sandbags to ensure a firm fiber coupling to the ground along the length of the railway-adjacent section. The fiber was partially uncovered to enter a signal pit connected to the building fiber egress. The approximate fiber route can be seen in Figure 3.6. This route was monitored for two weeks and correlated with data collected from the geophone.

3.4 Results

3.4.1 Static Angle Results

Figures 3.7 and 3.8 show the Stokes parameters during static testing. There are two types of transient signatures evident in the plots. As the movable anchor is repositioned at each step interval, there is a sharp change in the Stokes parameters.

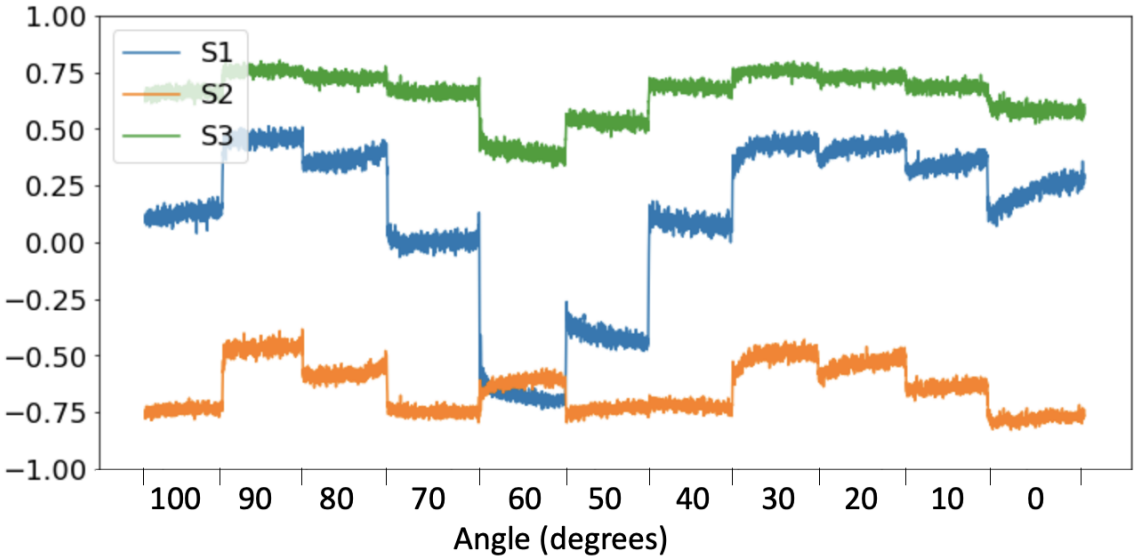

Figure 3.7: 2D plot of Stokes parameters during static testing shows two transient effects with a 3.8 cm diameter static anchor.

Additionally, gentle sloping of the parameters results from the fiber slack outside the experiment adjusting to a new resting position. Changes in the circumference of the middle anchor from 7.5 cm to 3.8 cm did not reveal substantial changes in polarization transience. Although not identical, the results of repeated tests show similar polarization change patterns as the movable anchor and fiber cable adjusted throughout each test. The polarization rotation rate (PRR) remained relatively small and constant during these experiments.

3.4.2 Vibration Plate Testing Results

Figure 3.9 shows a continuous wavelet transform (CWT) of the recorded response of a single Stokes parameter during vibration plate testing from 1 to 12 Hz. The CWT function provides a clear time and frequency localization of response signals, useful in our application for displaying responses that may be nonstationary and complex in nature, such as a passing train engine or train car sections. Lower frequency vibrations generate a stronger response versus higher frequency vibrations, with

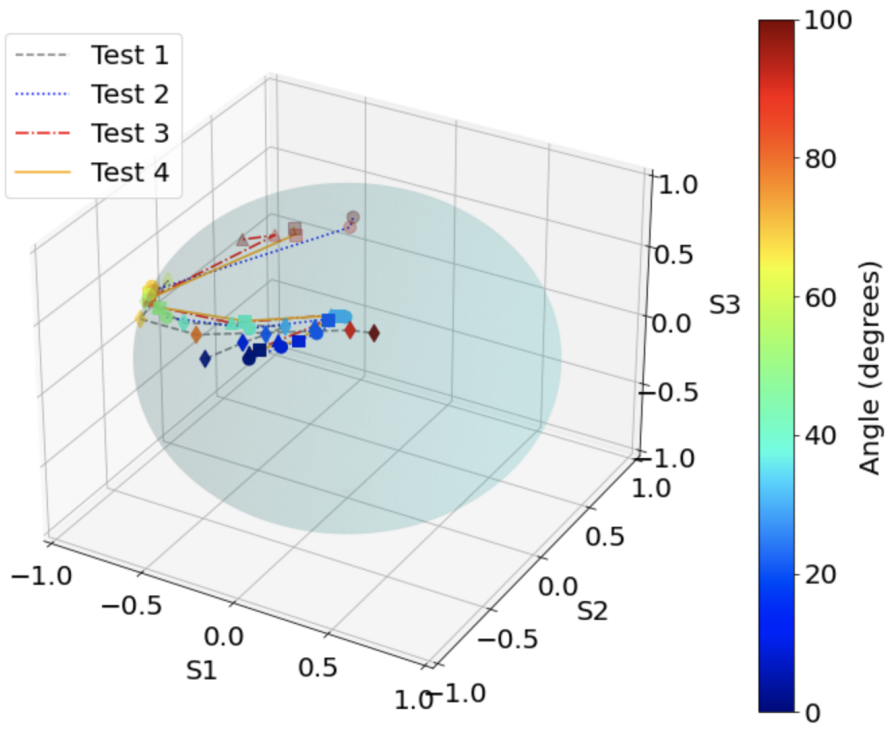

Figure 3.8: 3D plot of Stokes parameters across four tests with a 3.8 cm diameter static anchor shows repetitive polarization transience.

a significant reduction of response occurring approaching 7 Hz, although strong and consistent vibration at 9 Hz is perceptible. Second-harmonic frequencies were also detected during testing. Frequencies generated by the vibration plate as low as 0.3 Hz were detectable. Upon modification of the vibration amplitude and measurement of the displacement of the vibration plate, vibrations with movement as little as 2 mm were detected in at least one of the Stokes parameters. Regardless of the distance of the fiber cable from 100 m to 17 km, or the location of the vibration source on the fiber cable, *vibrations were detectable* provided that the entire fiber outside of the vibration plate assembly remained undisturbed.

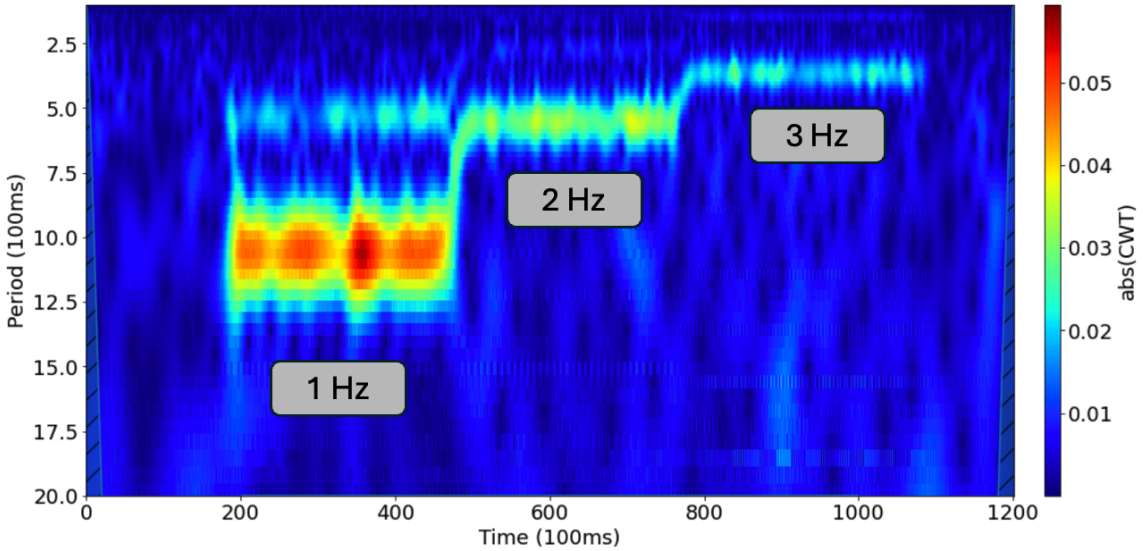

Figure 3.9: CWT of Stokes parameter S1 on a 17 km fiber length. Callout boxes indicate vibration plate test frequency.

3.4.3 Route Characterization

The results of physically manipulating the campus fiber inside the buildings show a distinct response to the change in polarization. The locations where the individual fiber could be manipulated with the least physical protection showed the highest response. Segments where the fiber was protected in an armored or buffered cable were less sensitive but showed a sloping response as the cable slowly returned to a resting position. Figure 3.10 shows the results of disturbing different fiber portions under test. Physical shock to the splice trays showed a sharp response (left) as the splice tray adjusted inside the housing but quickly returned to a new resting position. Fiber displacement in a slack roll of 5 cm (middle) showed rapid changes but gradually returned to a similar resting position. On the fiber routing racks, opening the routing tray that held the fiber under test (right) produced a sharp and flat change as the tray was opened and closed.

The results of the external fiber tests on campus were less revealing. Polarization measurements did not detect tap testing on the road surface above the external fiber route. Furthermore, the results of monitoring the campus fiber during eight

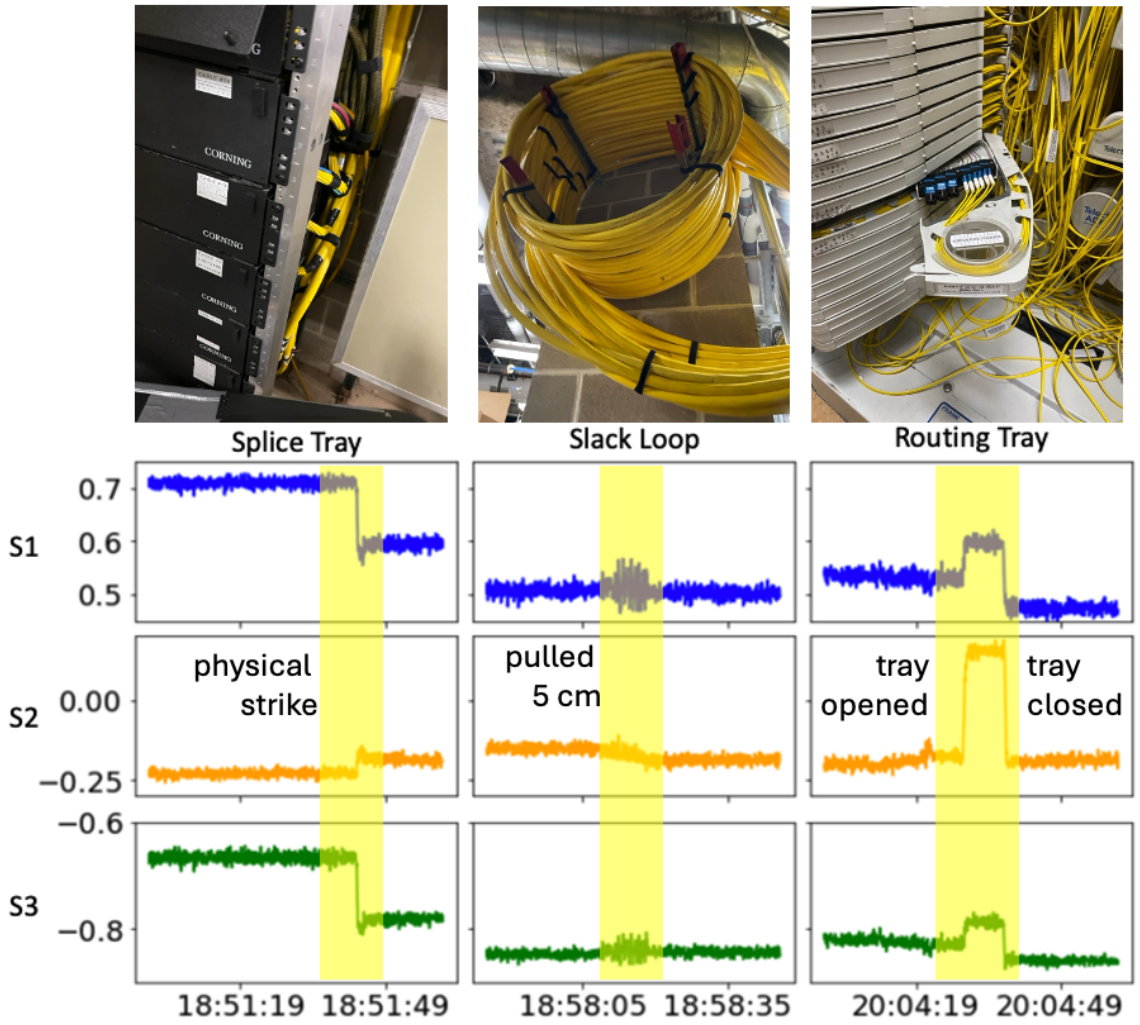

Figure 3.10: Results from route characterization. Plots of Stokes parameters during physically tapping a splice tray (left), agitating a slack loop about 5 cm (middle), and opening and closing a routing tray (right) show distinct signatures that can be characterized.

train events during the two-week span did not substantially impact the polarization state. The lack of response is attributed to high ambient building noise and significant shielding of the fiber route along and below the railway, reducing the coupling to vibrations of interest. This makes sense from a network communication perspective, where those deploying fiber would take precautions to limit exposure to environmental noise.

3.4.4 Route Monitoring

Using geophone data, we identified seven train events during the observation period. However, the custom fiber run did not show strong correlations with the vibration captured by the geophone as the trains passed by the cable. In five of the seven identified train events, the most significant polarization changes occur slightly before the train passes the fiber, but not during the event. The two other train events registered slight low-frequency polarization transience as the train passed by the cable. Figure 3.11 shows two sets of spectrograms from the continuous wavelet transform of geophone readings (above) and a continuous wavelet transform of Stokes parameter S1 recorded from the transceiver on the custom route (below). Stokes parameters were post-processed to adjust for timing and detrended by rotating to a 30-second mean vector, following methods introduced by Zhan *et al.*[10]. Increases in low-frequency vibration from 0.3 to 0.5 Hz were recorded around train events, but were not definitively correlated with the signals recorded by the geophone.

Figure 3.12 shows the Stokes parameters for one week on the custom fiber run next to the railway. The local temperature and precipitation were collected from monitors at a nearby airfield. Slower polarization transients show a strong correlation with changes in outdoor temperature. The diurnal cycle is observed in the recorded polarization, and there is a significant change during rainfall on the sixth day. Small spikes in polarization during daylight hours and one significant disturbance before the rain event that produced a minor but permanent displacement of the cable are attributed to pedestrian traffic across the buried portions of the

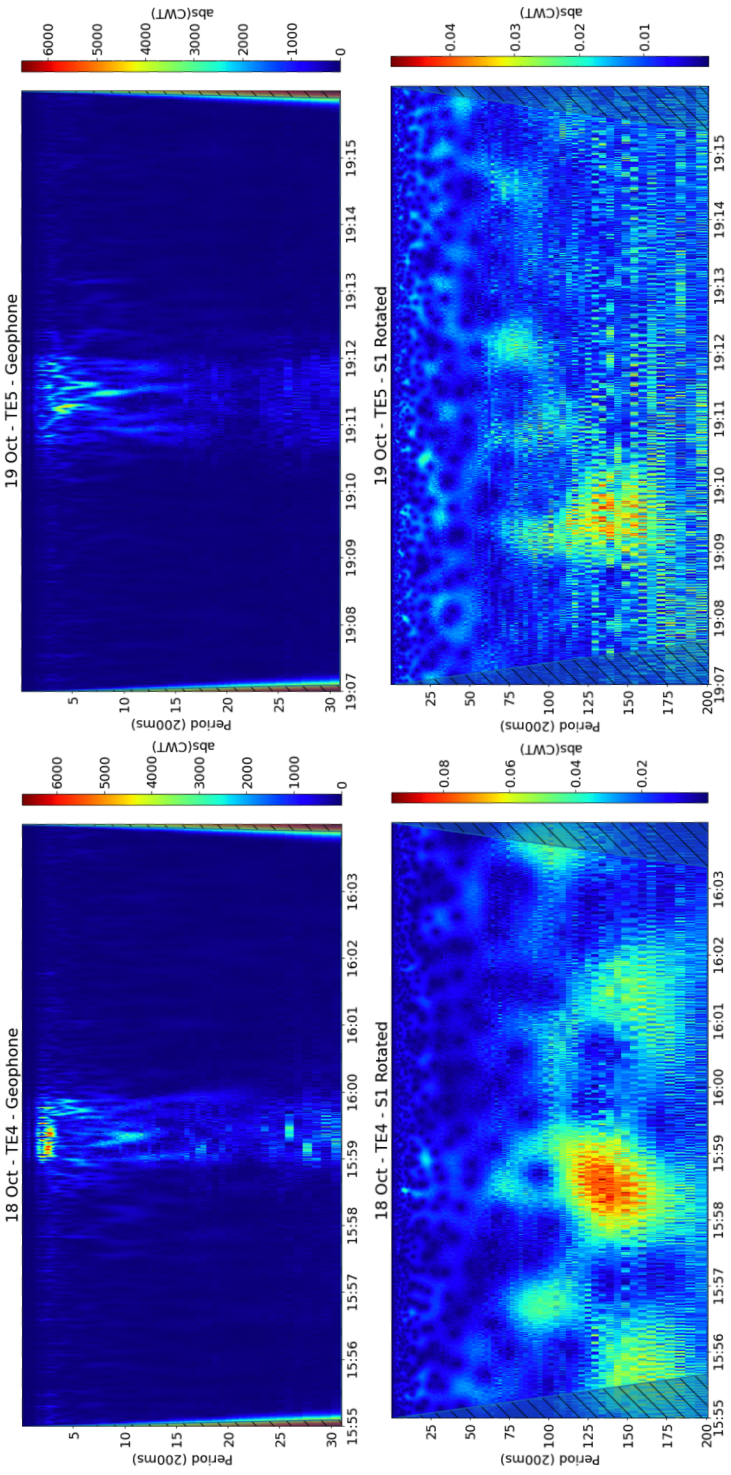

Figure 3.11: Continuous wavelet transform of two passing train events from data collected on a nearby geophone (top), and rotated and detrended Stokes parameter S1 measurements recorded on 100m fiber (bottom).

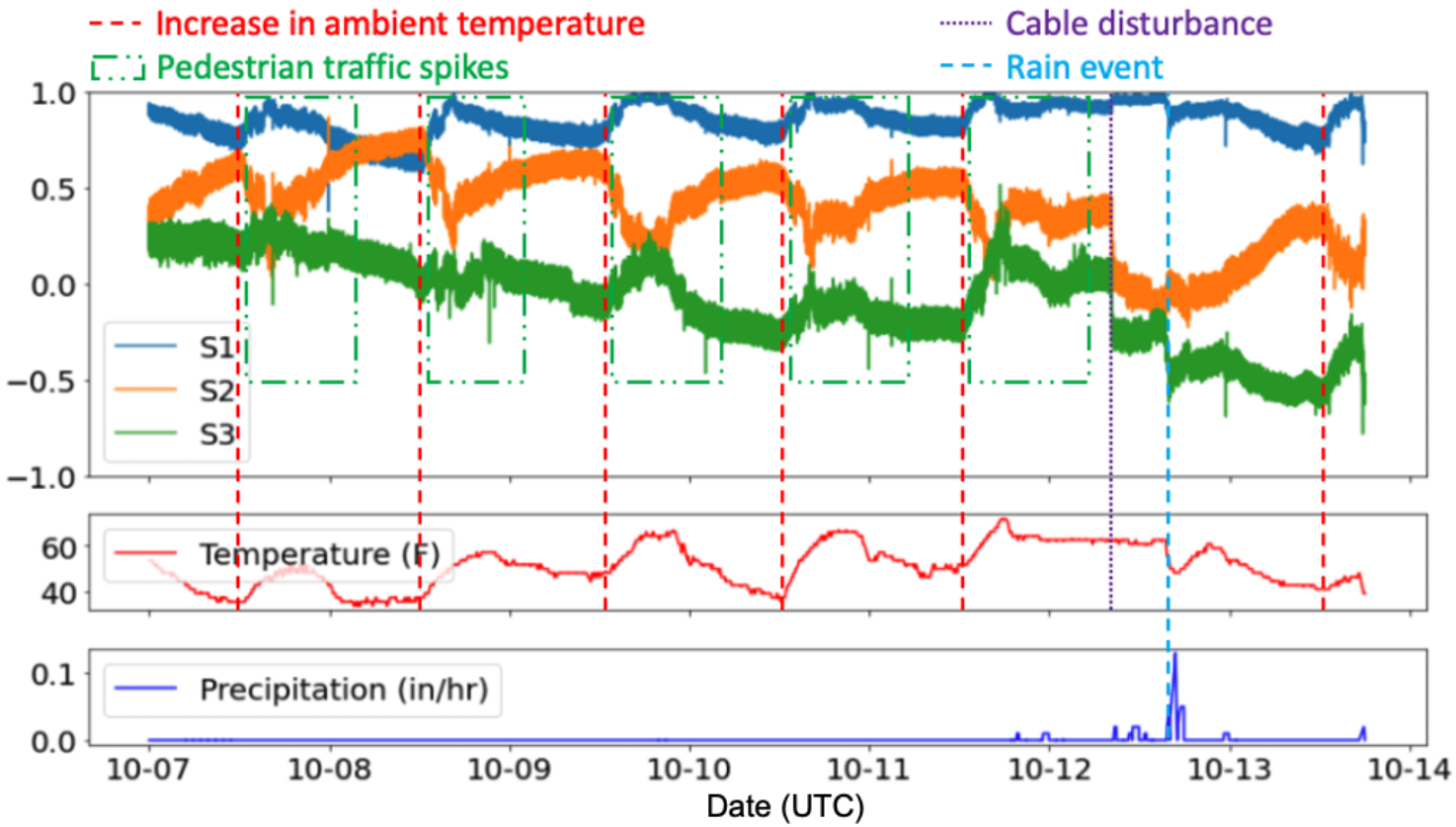

Figure 3.12: Recorded Stokes parameters (top) for one week on a 100 m fiber run. The polarization transient shows a strong correlation with the diurnal cycle, the local recorded temperature (middle), and precipitation (bottom).

cable, with the least amount of disturbance occurring during rainfall and on the third captured day, a Sunday. We observed that the drainage ditch adjacent to the railway formed a natural dirt path for pedestrians.

3.5 Discussion

Our findings indicate that network communication hardware that can produce polarization measurements has limited efficacy in a general ground sensing environment due to *sampling frequency* and fiber *coupling limitations*, but can still provide significant capabilities to offer insight on environmental changes on a fiber run.

3.5.1 Polarization Transient Signatures

During the experiments, we observed four distinct types of polarization transience. The first is the constant variation of polarization from one reading to the next, which we attribute to inherent vibration and electrical changes in the transport system and surrounding environment, which form our noise floor. The second is quick, discrete changes in polarization, which can be attributed to the physical displacement of the fiber route. The fiber is moved and finds a new resting position. The third signature is a sloping transient that occurs if the fiber relaxes as a result of displacement or a change in the physical environment in which the fiber lies. The fourth is an extremely slow change in polarization, which we attribute to the temperature of the cable as the fiber core and cladding expand and contract when heated or cooled.

3.5.2 Static and Vibration Laboratory Testing

Our static tests reveal that while an initial displacement of a fiber can unpredictably change the polarization, repeated changes closely correlated with a previous displacement without physical displacement of the fiber path will behave similarly. Vibration testing reveals a maximum frequency detection rate of about 7 Hz (consistent with the Nyquist limit for our system), with lower frequencies showing

more prominence in polarization change. There was no detectable floor for minimum vibration. Increasing the fiber length does not reduce the detection of fiber deformation, provided that the rest of the fiber remains static and does not undergo additional environmental changes.

3.5.3 Real-world Route Responses

Disturbing portions of the fiber in different ways shows distinct transient polarization patterns. Moderate and temporary changes to the geometry of the fiber by displacing the fiber show clear and identifiable changes, which are obvious and easy to detect, even at sub-Hz sampling rates. Larger displacements permanently change the resting geometry of the fiber once settled, which can be seen as both a positive for identifying disturbances along a fiber span and a negative for creating baselines for more subtle movements. This highlights the efficacy of cable security monitoring for sensitive areas as an application [109]. Longer environmental transients, such as temperature changes, can be detected effectively and may have useful applications for fiber deployed across areas sensitive to temperature changes. Ambient vibration sources from indoor equipment can cause additional polarization transience, which can obscure signals of interest.

3.5.4 Train Sensing

Although trains generate a considerable amount of energy that can be easily detected using standard seismic sensing equipment, it was challenging to distinguish train events in our data accurately. The recorded responses to train events during data collection did not exhibit the expected prominent characteristics. Although other studies have demonstrated the efficacy of fiber optic sensing for trains by training machine learning classifiers [101] or phase-based measurements [110], we focus on identifying the limitations of opportunistic environmental sensing. These limitations can be attributed to various factors: (i) freight trains generate a more pronounced frequency response within the 10-50 Hz range, exceeding the maximum frequency detection rate of our system, (ii) cancelation of the phase of

the vibration signal may occlude signals when the locomotive is positioned directly next to the fiber run section that runs parallel to the track, and (*iii*) our signals of interest were masked by disturbances from other noise sources along the route, such as ambient equipment vibration and pedestrian traffic.

3.5.5 Considerations of Optimal Fiber Placement for Environmental Sensing

Fiber coupling to vibration sources is critical for sensitivity, especially when integrated polarization measurements are collected at the end point. Communication fiber routes are intentionally engineered to stay out of reach from routine indoor activities, and outdoor cables and conduits are designed to reduce the impact of environmental effects. For train sensing applications, direct burial of the sensing is recommended at a maximum depth of 60 cm [111]. However, government and industry regulations for communication utility installations may require encasing conduits and significantly deeper burial depths [108], which will reduce the environmental effects of train vibrations, reducing sensitivity. Exposure to sources of noise from indoor buildings, such as power generators, air conditioning systems, and elevator machinery, will also introduce unwanted effects on minimally protected fibers. Fiber sensing applications should limit and shield indoor segments of fiber runs to avoid exposure to competing signals. Ideal routes for sensing should be in areas with low ambient noise and where fiber is strongly coupled to surfaces that are expected to produce signals to report clear polarization transience measurements.

There are several actions that can be taken to provide capabilities for both communications and sensing applications on the same fiber despite their competing requirements. First, optical transport equipment should provide an additional capability for reporting state-of-polarization information with a minimum of 50 Hz sampling rate to detect anthropogenic effects. Additionally, the fiber route should be strongly coupled to environmental effects that are desirable for measurement, such as a medium that propagates vibrations of interest or exposure to areas where

temperature may change. Care must be taken to ensure the cable is protected from physical damage and significant disruption of communications data that cannot be compensated by optical transport DSPs. Lastly, the cable should be shielded from ambient indoor effects than can occlude targeted polarization transients due to the nature of integrated responses. By implementing these strategies, optical fibers can be optimized for both communication and sensing, ensuring robust data transmission while effectively monitoring environmental changes.

4 HOMEBREW: LOW-COST POLARIMETRY BASED ENVIRONMENTAL SENSING ON OPTICAL FIBER

4.1 Introduction

Several recent studies have considered the efficacy of using polarization transient measurement in light transmission through fiber for ground motion and environmental sensing. Examples include identifying earthquake signatures in subsea cable infrastructure [10], detecting temperature changes and high-speed train crossings [21, 101] and detecting vibrations induced by adhering a portion of an optical fiber to speakers [112]. Although these studies have demonstrated the utility of polarization transience measurement for sensing, they have benefited from fiber optic cables placed in relatively low noise settings with strong coupling between cables and the environment, and where large dynamic disturbances are plainly visible. However, optical communication fibers in long-haul and especially metro environments are potentially noisier and mechanically uncoupled from the signals that we wish to detect.

4.2 Overview of Research

After assessing the capabilities and limitations of our previous research with commodity transport equipment, we focus on finding a solution that provides a broader range of sensing capability. Tracking polarization state and transience was effective at detecting changes in temperature and physical displacements in a deployed fiber optic cable but ultimately limited in its sensitivity by a low sampling rate.

Several other studies have shown that higher rates of polarization tracking are effective at detecting displacement events in fibers. Polarimeters have been used to study the long-term transience of PMD in a 128 km cable run [102]. They have also been used to investigate changes in the polarization of aerial fibers correlated to temperature variation and wind galloping effects [20, 100]. Another use of

polarimeters enabled the detection of trains passing along fiber sections and processing the output through a convolutional neural network [101]. Polarimeters have also been used in demonstrations that utilize polarization tracking as a means of detecting physical tampering and intrusion detection [113, 109]. Although these works show the efficacy of using polarization transience to detect external events, their research involves using fiber optic cables in idealized settings where large disturbances are plainly visible. A fiber optic run in a metro environment is both much more noisy and more protected from the signals that we wish to detect.

While commercial polarimeters can provide detailed information about polarization, they can also be prohibitively expensive for our purpose of creating an array of internet based sensors. Therefore, we aim to construct a low-cost polarimeter that can provide valuable insights into polarization states and transience by offering a sampling rate higher than our previous experiment using a commodity optical transciever. Other studies have also focused on developing low-cost polarimeters to monitor transience and correlating events. In particular, Simisarian *et al.* investigated detecting the effects of physical strikes on fiber optic cables by constructing a two-arm polarimeter that utilized a half-wave plate and a polarizing beam splitter [24]. This setup was replicated in other research to detect temperature changes and high-speed trains crossing rail bridges on a 40 km fiber route [21]. Furthermore, the two-arm polarimeter design was used to identify speaker-induced vibrations through K-means clustering [112].

Our study introduces a new 'homebrew' polarimeter for use in urban environments toward the goal of enabling the broad deployment of polarization-based sensors in Internet infrastructure. Specifically, we developed and examined a novel low-cost, four-arm system that can provide detailed polarization transience measurements at high sampling rates. We implemented this system in two different fiber cable configurations to assess its ability to capture events such as train traffic on nearby tracks. Our findings show that the polarization-based detection of train traffic in an urban environment is highly dependent on the coupling of fiber to infrastructure subjected to ground motion and that the use of optical fiber used in Internet communications may not be universally effective.

4.3 Two Arm Low-Cost Polarimeter Assessment

Although commercial polarimeters provide complete information on the polarization state, they can also be prohibitively expensive for the purpose of creating a network of Internet-based fiber optic sensors. Therefore, our goal was to construct a low-cost polarimeter that can sample the polarization state at a rate sufficient for measuring a wide range of ground-motion signals. Previous studies [23, 21, 24] have developed low-cost two-arm polarimeters to monitor transient events. In this system, the incident light is passed through a polarization beam splitter (PBS). The two resulting light paths are measured by a balanced amplified photodetector, and the Polarization Rotation Rate (PRR) is calculated from the outputs. However, the sensitivity of this system is a function of the polarization axes of the incoming light relative to the orientation of the PBS. Large areas of the Poincaré sphere can have a reduced sensitivity to polarization transients [21].

4.3.1 Two Arm Polarimeter Design

For our initial design of the two-arm polarimmeter, we chose to recreate this device using a free space optics design. The system was constructed with a 50 mW 1550 nm continuous-wave laser source that passes through a collimeter. A quarter wave plate polarizes the beam before entering a polarizing beam splitter cube, which is then intercepted by two photodetectors. A diagram of the free space setup is seen in Figure 4.1. The voltages of these photodetectors are then recorded by a Picoscope 3406D collecting at a sampling rate up to 200 KHz, and compared to each other in order to detect the polarization rotation rate using the following equation [24]:

$$PRR = 2\sin^{-1}\left(\frac{1}{2}\Delta|\frac{V_1 - V_2}{V_1 + V_2}|\right)\frac{1}{\Delta t} \tag{4.1}$$

where V_1 and V_2 are the output voltages reported by the photodetectors, and Δt is the sampling period. Initial testing of the design proved successful, but showed limited fidelity due to the small gradients between voltages recorded.

Our initial design showed successful results in initial vibration testing. Changes

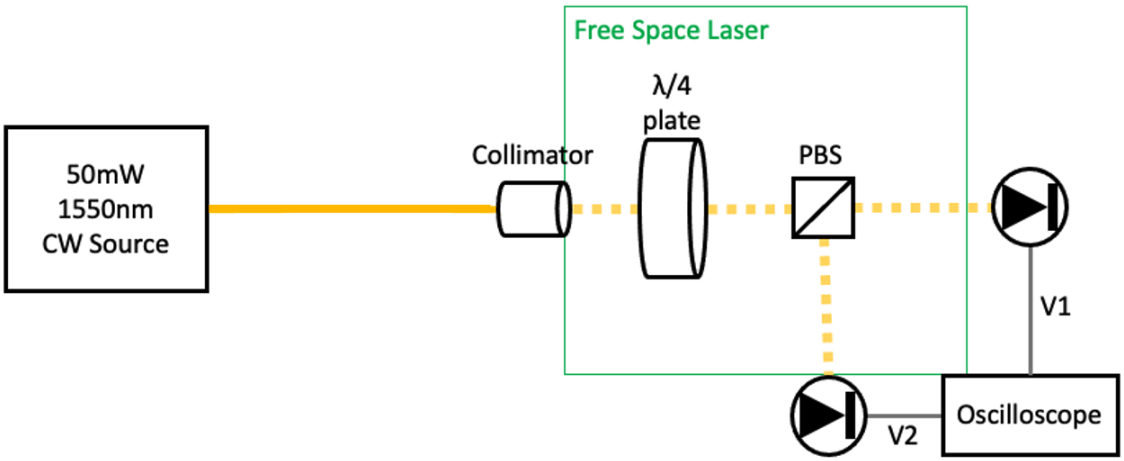

Figure 4.1: Free space configuration of a two-arm polarimeter.

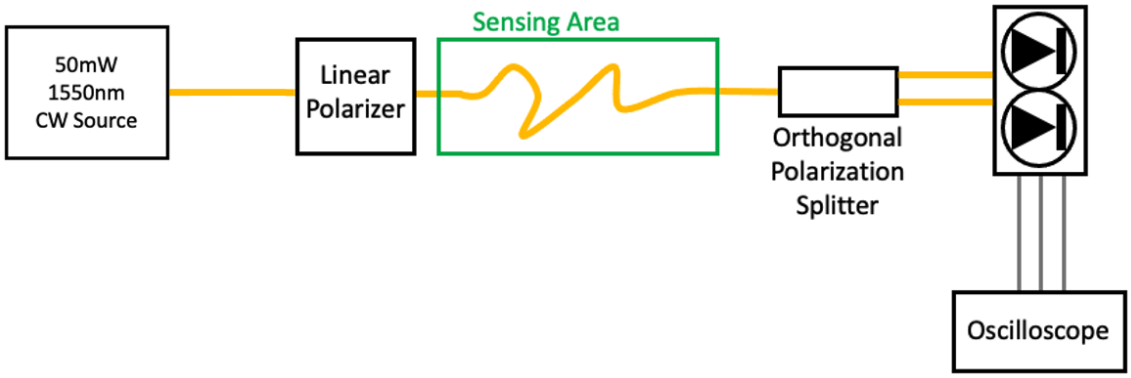

Figure 4.2: Initial inline configuration of the fiber-path 2-arm polarimeter.

in the fiber geometry across the vibrating plate were reflected in the changing voltages in our two photodetectors. In order to improve the portability of our sensing system, we included a linear polarizer before the sensing region of the fiber, replaced all free-space laser paths with fiber paths, and exchanged the PBS with an in-line orthogonal polarizing splitter. A diagram of our improved setup is shown in Figure 4.2.

Calibration testing of our inline design involved applying a 15 Hz vibration through a plate on the sensing area of the fiber. Our initial tests show a significant improvement over the free-space design with fewer reported outliers. We attribute

this to reduced attenuation and precision in keeping the light contained within the fiber. However, results from our calibration vibration test show a distributed range of polarization rate during vibration, as seen in Figure 4.3. During this test, we collected five seconds of the fiber at rest, then vibration at 15 Hz with three steps of increasing amplitude at ten seconds each, then five seconds at rest. The plot showed a continuous uniform distribution of polarization rates from zero to a maximum value dependent on the power of the induced vibration. We attribute this to the instantaneous capture of orthogonal polarization state transience, which is not constant during the fiber's movement.

4.4 Construction of Four-Arm Polarimeter

To improve sensitivity and expand the capability of polarization monitoring, we developed a polarimeter design that includes an optical tap to evenly split the incoming light into two independent two-arm measurements, as seen in Figure 4.4. We placed manual polarization controllers before the orthogonal splitters of each branch. The incoming polarization to each of our two-arm systems can be manipulated with these controllers that simulate a series of two quarter-wave plates (QWP) and one half-wave plate (HWP) in-between the QWPs. This configuration allows any incoming polarization to be adjusted to an arbitrary polarization [114]. To initialize our calibration, we manually configured the polarization controllers to send an even amount of energy (sum of balanced detector channels) through each of the four arms. We then induce a small test vibration on the fiber under test and ensure that the balanced output from each branch is near zero and tuned to maximum and minimum sensitivity to the test.

This procedure was validated by adding a ThorLabs PAX1000 commercial polarimeter [115] to monitor the incident light entering our polarimeter. The results of this test are shown in Figure 4.5. The recorded voltages show key similarities to the commercial polarimeter outputs, where the two incoming orientations (A-B and C-D channels, respectively) are observing different levels of transience, similar to the differences in the Stokes parameter outputs from the polarimeter. Although this

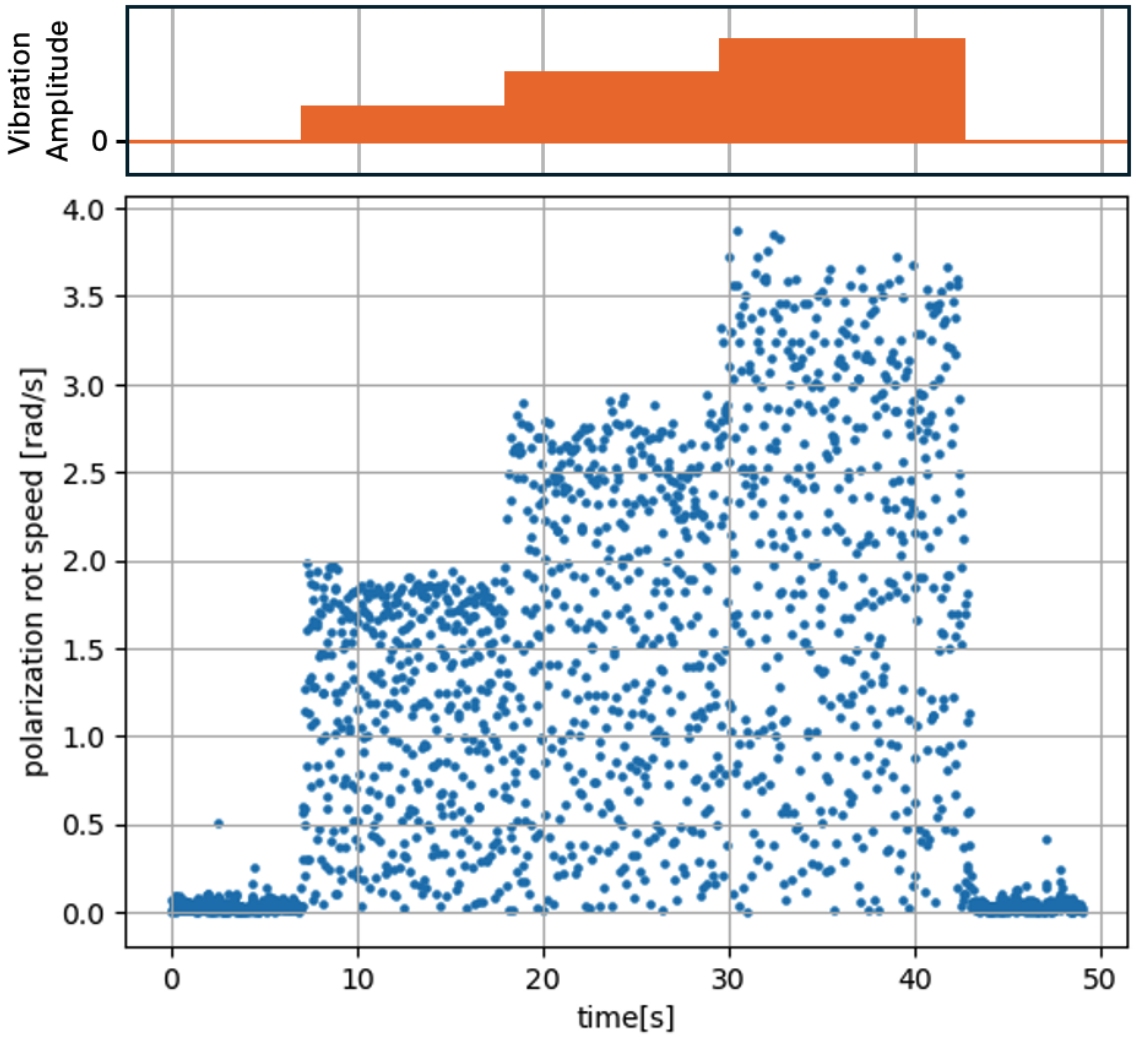

Figure 4.3: Polarization Rotation Rate of inline polarimeter design on a 15 Hz vibration plate with increasing amplitude steps.

configuration is adequate for our experiments, additional calculations to determine the optimal configuration follows in Section 4.7.2.

Our key innovation is that adding a second, two-arm system with a different axis orientation enabled us to maintain sensitivity when a single PBS might have missed a rotational change. The total cost of the components in our system was approximately $6,000, comparable to low-end polarimeters, and can achieve sampling rates

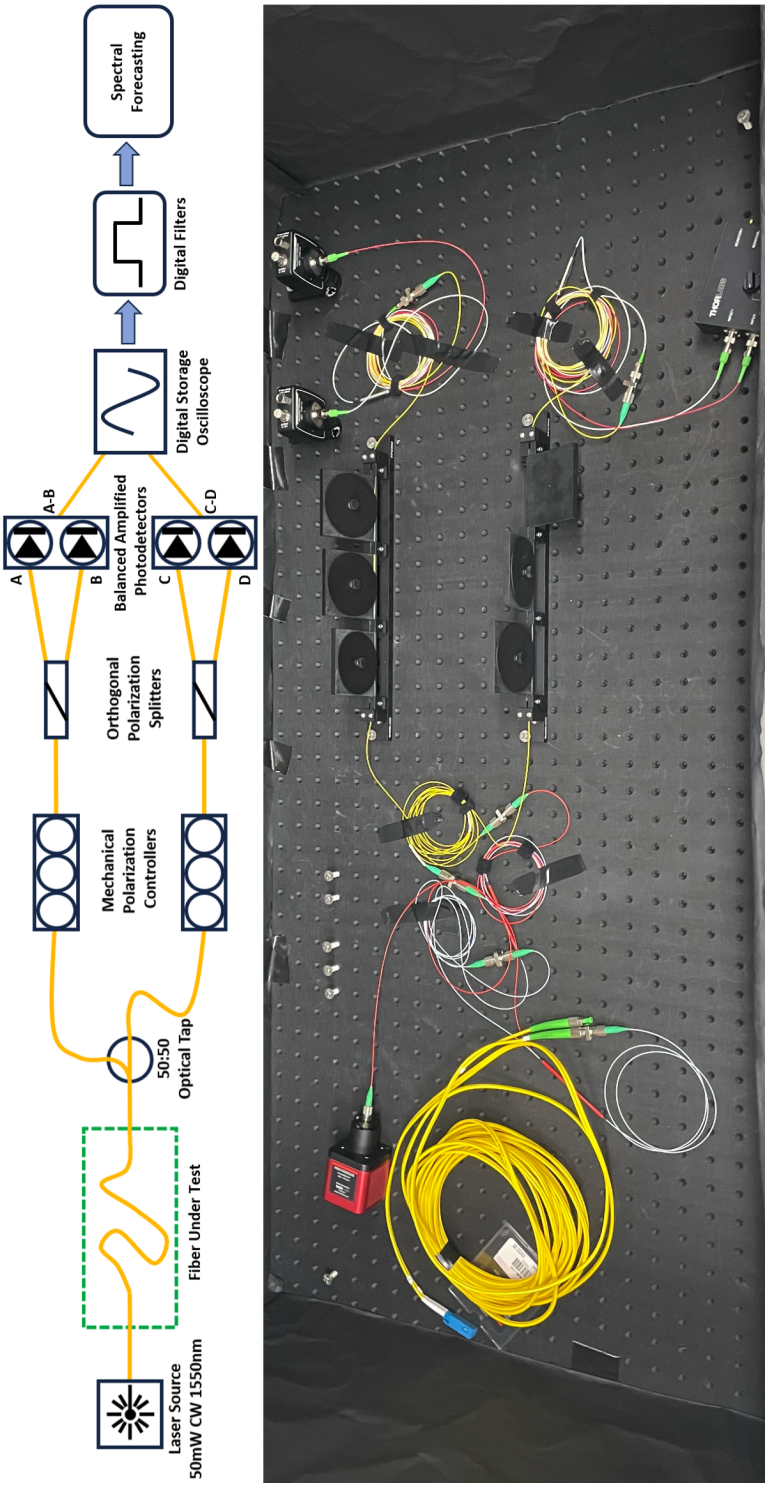

Figure 4.4: Diagram of the four-arm polarimeter (top), and picture of the physical setup with a Thor:abs PAX 1000 commercial polarimeter for validation (bottom).

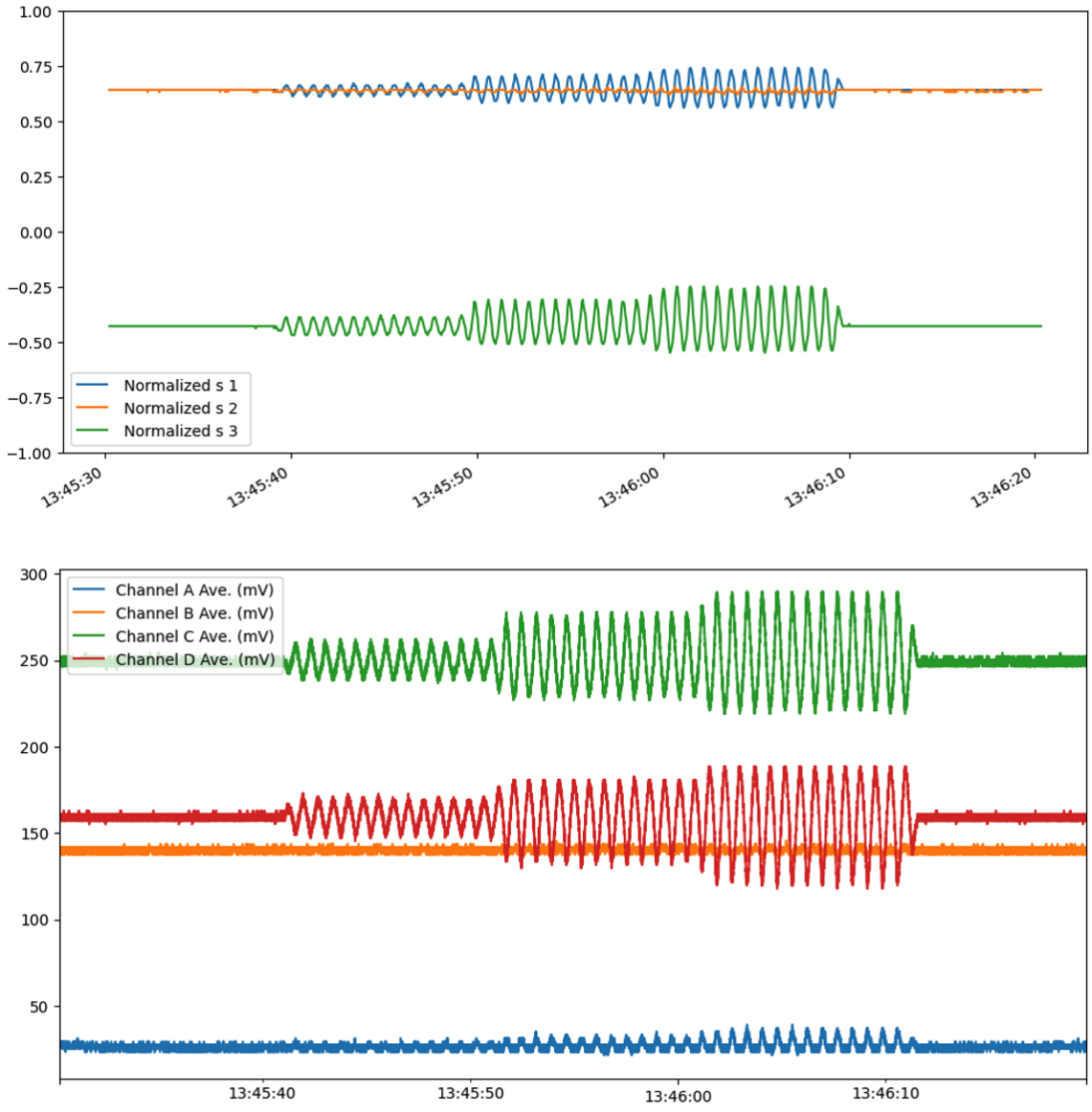

Figure 4.5: Results from a ThorLabs PAX 1000 commercial polarimeter (top) and our expanded four-arm polarimeter (bottom) from a 1 Hz validation test.

of 500 kHz in short-term measurements and 1 kHz for long-term measurements.

4.5 Experiment Methodology

We began by performing laboratory tests to assess and calibrate our system. In order to determine the impact of fiber coupling in polarization-based sensing, we then conducted a series of experiments by varying the cable coupling to a vibration source. First, we attached a section of 20-meter indoor fiber optic cable to the inside of a basement exterior wall with utility tape. The wall is approximately 15 meters from the freight rail and travels roughly parallel along the measured length. The fiber was attached to this wall in sections 1-, 2-, and 4-meters long. This room was not temperature controlled and ambient noise emitted from building cooling systems and equipment was present.

Second, we captured the polarization transients on a 4-kilometer urban campus fiber route, same as in Section 3. This route passes underneath and next to active freight railway tracks and under several campus and city roads through conduit and returns along the same path via a fiber loopback adapter at the distant end. Our homebrew polarimeter was placed at the fiber termination point in a temperature-controlled telecommunications room with large amounts of acoustic and airflow noise compared to the basement wall configurations.

During data collection, we used readings from a vertical-axis geophone[76] at the same basement location as the wall configurations to determine the amount of vibration produced by passing trains. Our system collected samples at 1 kHz from the balanced outputs of our homebrew polarimeter, as well as a single monitor reading from each balanced photodetector to calculate PRR [21]. By taking a weighted average of the two balanced filtered outputs based on a spectral forecasting algorithm [116], we found that the maximum of the band-filtered spectrogram clearly showed train events.

4.6 Results

Over a 35-day period, we captured 19 responses from passing freight trains on our polarimeter and geophone, with 14 responses on our basement wall configuration, and five on the 4-km campus route. Each collection was carried out continuously over several days with the same calibration and fiber configuration and contains between two and five train traffic events. The strongest responses to passing trains are recorded when the freight engine passes near the building, followed by the trailing freight cars. The responses recorded by the polarimeter contained occasional peaks associated with low-frequency vibrations when the fiber was disturbed so as to cause the fiber to set in a new position. During the passing of the freight engine, occasional peaks were seen at 60 to 70 Hz. However, the predominant and consistent responses were localized from 24 to 32 Hz during the train event. The results of the responses and the comparison of the mean spectral power maximum over 30 minutes after the start and end of a clear train response are shown in Figure 4.6.

Depending on the configuration of the optical fiber route, the spectral response of the passing train was more pronounced against the ambient polarization transience. To quantify the level of response, Pearson's correlation coefficients were calculated on the responses of the polarimeter from 22 to 38 Hz and the geophone two minutes after the start and end of the train vibration, as shown in Figure 4.7. We quantified any correlation greater than 0.4 to signify a positive response from our polarimeter. The tests recorded on the campus fiber route did not show a response to vibrations from train traffic on our polarimeter. However, our indoor basement installations show a distinct short-term transience during train events that correspond to the readings on our local geophone. The 4-m fiber route with the longest wall coupling length was more pronounced and consistent in each response to a passing train. Shorter-length couplings were less responsive and inconsistent in recording a response.

A slow polarization transience was observed for up to 24 hours after installation as the fiber cable settled to a new resting position after being disturbed. Our

four-arm design was able to capture train responses in one or both arms despite long-term changes in polarization. In some events, sensitivity banding of the train response can be seen when the vibration changes the polarization parallel to an arm's orthogonal split. PRR was calculated for every train event. However, PRR responses to train traffic events were not distinguishable above the ambient rotation rate and were not an effective metric to measure small fiber strain responses.

4.7 Discussion

The results of these experiments successfully demonstrated the potential of ground motion sensing through optical communications infrastructure in an urban environment, as well as the importance of strong coupling to vibration mediums for measuring environmental effects with polarization transience.

4.7.1 Results Analysis

Measurements taken from the 4 meter strongly wall-coupled fiber optic path show strong consistent responses to train events. Two responses were successfully recorded on the 1 meter coupled route, but incurred a low accuracy rate. Sometimes, responses were predominantly seen on one arm, indicating a more robust sensing range.

Campus route collections were unable to detect vibrations caused by train traffic. We believe this is due to two reasons; that the portion of the fiber run susceptible to vibrations from a passing train has been engineered to reduce the coupling to ground noise in order to allow minimum interference for optical communication, and building noise, such as other communications equipment or air conditioning systems along the route, introduce unwanted polarization transience, which raises our noise floor above the desired signal response. For optical communication routes to be useful for ground sensing, they must be tightly coupled to a vibrating medium where a response is expected. This level of coupling required for effective sensing

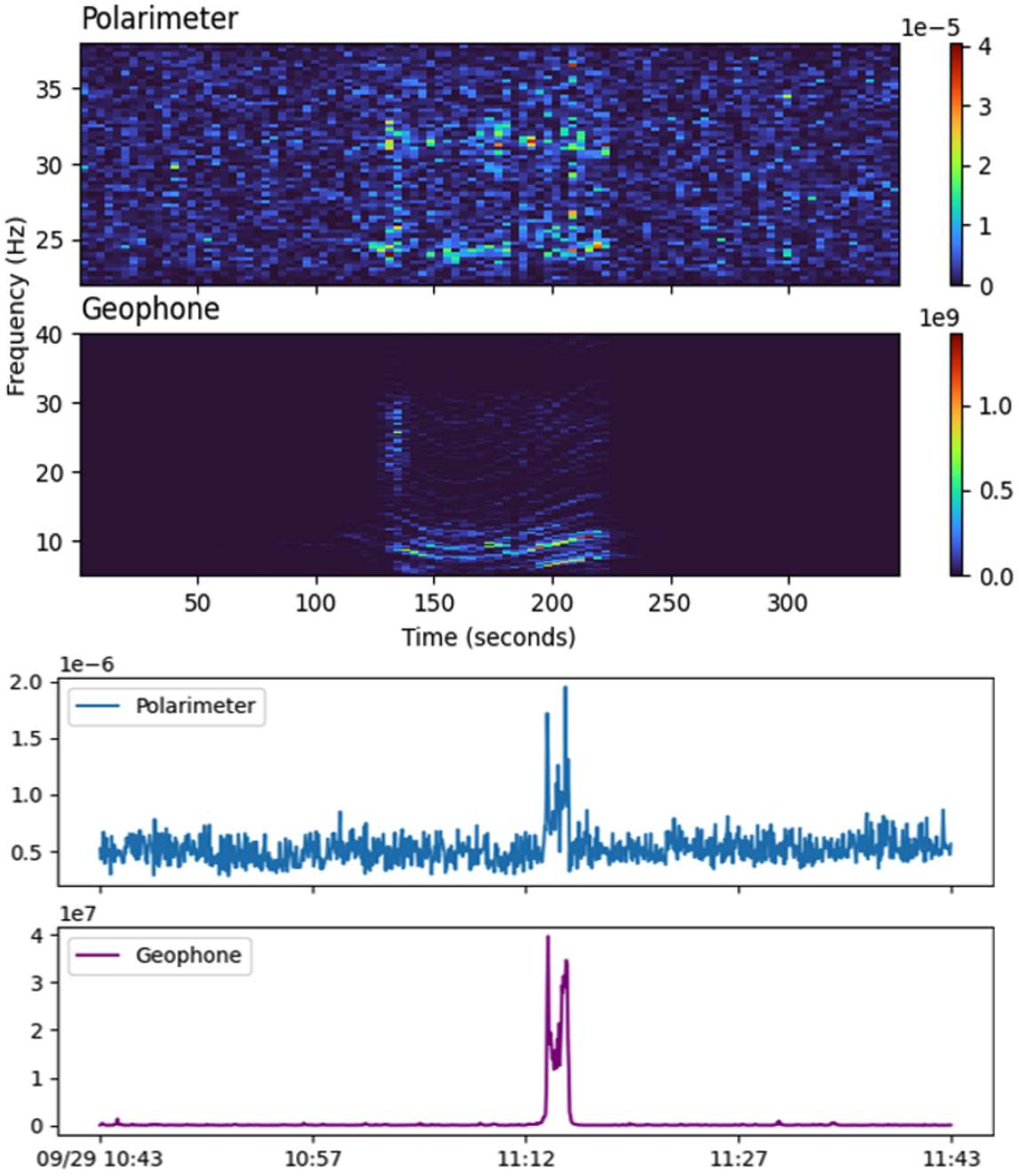

Figure 4.6: Spectrogram of signal responses during a train event (top) from the polarimeter combined output and the geophone. Plot of mean spectral power maximum for one hour with train event (bottom) from the polarimeter and the geophone.

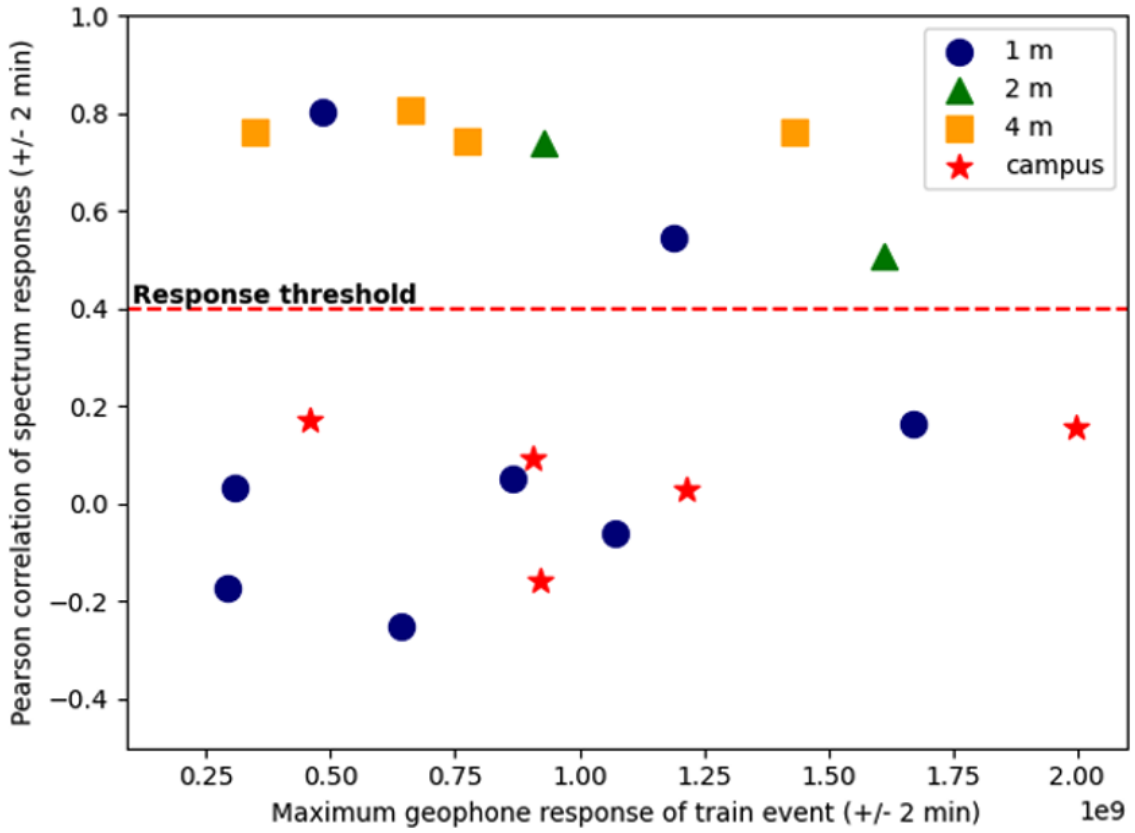

Figure 4.7: Plot of recorded train events by coupling length (color), maximum geophone response (x-axis), and Pearson correlation between geophone and polarimeter response for two minutes before and after train event (y-axis).

on urban fiber optic routes may need to be individually evaluated for sensing applications.

4.7.2 Calibration Optimization

Our four-arm polarimeter is designed to increase the observation range for polarization transience. For conducting our real-world experiments, we opted to conduct an efficient calibration sequence by tuning the two systems to measure the minimum and maximum sensitivity of a reference vibration, detailed in Section 4.4. We expect that optimally tuning the incoming polarization of both arms will

result in a significant increase in measurement performance. Previous literature concerning the effectiveness of the original two-arm polarimeter provides some insight on how to achieve this from a theoretical perspective.

The original publication of the two-arm polarimeter by Patterson notes that the basic operating principle of measurement relies on the function of the beamsplitter. If the incident light polarizaton is angled at a 45° to the beamsplitter axis, a balance of power is achieved between the outputs [23].

Simsarian and Winzer used the two-arm polarimeter design to illustrate fiber break detection. For their analysis, they conducted an empirical evaluation using repeated hammer strikes on a fiber under test. After 58 iterations, they compared the maximum PRR recorded from the two-arm polarimeter against a commercial polarization analyzer, reporting an approximate 40% loss of sensitivity of the two-arm design [24]. Maximum PRR can be useful for determining the levels of response to significant disturbances, such as hammer strikes. However, our initial evaluations discovered that the use of PRR to measure small vibrations can lead to inconsistent results.

Barcick and Munster used the two-arm polarimeter to measure transience resulting from vibrations of high-speed trains over a rail bridge. They report the normalized sensitivity of the polarimeter based on the incident polarization to the beam splitter as:

$$\varepsilon = \frac{1}{2}(\sin^2(2\psi) + \sin^2(2\chi - 2\psi)) \tag{4.2}$$

where ε represents the relative sensitivity from 0 to 1, and the incoming polarization parameters χ and ψ are the respective ellipticity and orientation angles. We record the corrected formula here, noting the published version originally transposed the two polarization angles [21]. A plot of their equation on the Poincaré sphere can be seen in Figure 4.8a. In contrast to Simsarian, this measure of relative sensitivity is not based on the rate of change. Compared to their evaluation, the average sensitivity of Barcick's equation is 0.497, significantly lower than Simsarian's empirical estimation.

Yao and Chen report on the use of polarization splitting for a different applica-

tion, polarization multiplexing of two incoherent data channels. For their purposes, the two channels use a power imbalance to recover the ellipticity and orientation angles through:

$$\Delta V = \cos 2\chi * \cos 2\psi \tag{4.3}$$

where ΔV is the power imbalance between the two signals [40]. While they find maximum efficiency in demultiplexing two signals when maximizing the difference in voltage, the two-arm polarimeter design finds maximum sensitivity when the balance is zero between the two outputs. For our application, we take the compliment of the absolute output of their equation in order to calculate sensitivity, which can be seen in Figure 4.8b. The average sensitivity of their modified equation is 0.596, which corresponds to Simsarian's results.

Both equations result in maximum sensitivity for measuring polarization transience when the incident polarization is rotated $\pi/4$ from the beamsplitting axis. The optimal setting for our four-arm polarimeter requires the second arm to be offset from the first by the same rotation to provide maximum coverage of the incident light. The theoretical optimal sensitivity for our four-arm polarimeter has been calculated both for Barcik and Munster's equation in Figure 4.8c, and for Yao's equation in Figure 4.8d. We believe that the modified Yao and Chen equation is more accurate for estimating the accuracy of the four-arm polarimeter, which reports a mean sensitivity of 0.767, and an improvement of the minimum sensitivity from zero to 0.298 across the Poincaré sphere.

Configuring the four-arm polarimeter to optimal angles can be accomplished by aligning the incident polarization to between three degenerate state pairs and ensuring that the four arm system is balanced on one pair, and the other pairs alternate between zero and the maximum difference [41, 117].

4.7.3 Processing Pipeline

Data from the outputs of our four-arm polarimeter was captured using long-term measurement settings and stored on the oscilloscope for post-processing. Due to the

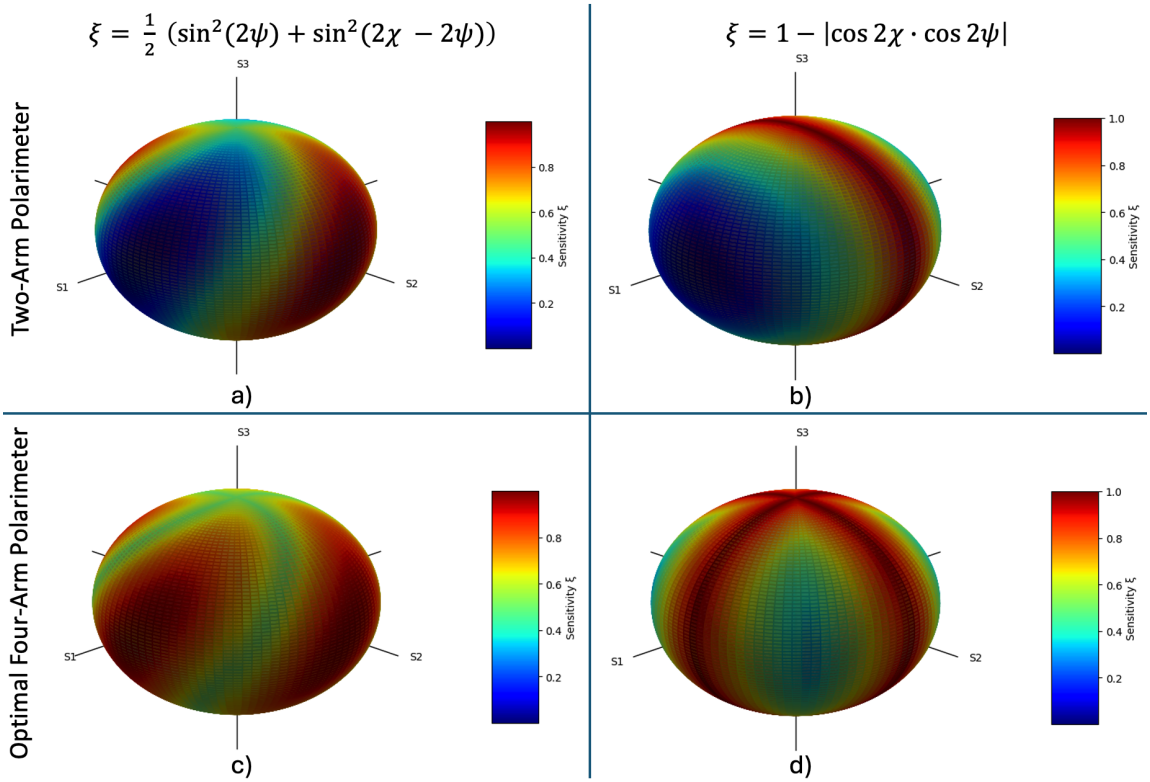

Figure 4.8: Relative sensitivity plots for incident polarizations for the original two-arm polarimeter (a) and (b), and the calibrated four-arm design (c) and (d). Left-hand plots (a) and (c) use Equation 4.2, and the right-hand plots (b) and (d) use the compliment of the absolute output of Equation 4.3.

amount of time required to export the data, changes to the processing pipeline are required in order to facilitate processing for near-real time detection of polarization transients resulting from ground motion. Provided the data can be streamed from an oscilloscope during collection, processing of the data to include frequency filters and spectral forecasting would incur a minimal computational delay and could then be sent to a monitoring platform for visualization and alerts. By constructing a data-processing pipeline in this fashion, multiple systems could report polarization transience from several sensing fibers which may or may not overlap along their length. These minor changes can lead to reporting localized incidents or more widespread ground motion events, thereby providing significantly more beneficial information about the environment.

4.7.4 Summary

Our polarimeter was effective in detecting small, fast vibrations emitted by passing freight trains on the highly coupled fiber path. Additionally, the two paths that split on different axes enabled detection over a wider range of polarization versus a two-arm system. Although our system shows increased sensitivity to polarization transience, it also highlights the importance of selecting fiber routes which are most attuned to signals of interest through strong coupling. Fiber installed for communication applications may not be universally sensitive among all routes, but the right conditions can reveal important information about environmental effects that occur on and around our communications infrastructure.

5 SEISMOSPECKLE: PRACTICAL SPECKLEGRAM SENSING ON OPTICAL COMMUNICATIONS FIBER

After exploring the use of polarimetry-based sensing on optical networked communications fiber, we conduct research on alternate methods of measurement. We introduce a novel, ultralow-cost specklegram sensing on communications fiber to evaluate its efficacy in monitoring changes in modal intensity caused by mechanical deformation along fibers. Our setup comprises various lengths of a single mode (SMF) OS2 optical fiber, a Visual Fault Locator Laser (650nm, 30mW), and a Blackfly S FLIR Camera with an 8mm lens and 150 fps to record projections of light into an enclosure. With this low-cost setup, we develop an efficient data processing pipeline to measure transient interference patterns resulting from fiber strain. We then measure the effect of attenuation caused by fiber length as a function of the location of the mechanical excitation and the accuracy of the measurements compared to geophone responses. We evaluated excitations caused by localized and distributed bending in different fiber sections at frequencies 50 Hz and below (to meet Nyquist frequency conditions). We then deployed our sensor to monitor vibrations on a basement wall near a freight railway for more than three weeks and measure the correlation between our sensor and a co-located geophone. Although the results are contaminated by different environmental noise levels, noise reduction and strong coupling of the fiber to a vibrating structure show positive correlations between mechanical excitations and speckle response. These results form a foundation for practical, low-cost, and minimally intrusive applications of deformation and vibration detection via optical network infrastructure.

5.1 Overview of Research

In this study, we investigate and assess the application of fiber specklegram sensing as a method for detecting alterations in a fiber's geometry to facilitate environmental sensing with optical internet fiber. Specklegram sensing involves using a laser

source to monitor small changes in a fiber's geometry by analyzing the changes in the interference pattern created by imperfections in the fiber. These changes can be caused by mechanical strain, temperature changes, or other environmental factors, and can be quantified to monitor the state of the fiber for the intended application. The technique has been successfully demonstrated in several works for structural monitoring [86], detecting fiber curvature [87], and determining fiber displacement locality [88].

We developed and tested a fiber specklegram sensor that can be deployed on shorter metro optical links to provide an enhancement to existing physical sensing systems at a reduced cost and minimal impact on communications infrastructure. We describe our exploration process during development and prototyping, and demonstrate a proof-of-concept system with low-cost parts showing the potential capabilities that specklegram sensing on communications infrastructure can add to deployed sensor networks.

5.2 Specklegram Sensing

Fiber specklegram sensing is a technique that uses a light source in an optical fiber to monitor small changes in strain and geometry. The laser light passed through a multimode fiber creates an interference pattern at the termination point. The relative intensity for different points of the pattern is a result of the combined intensity and phase correlation of the multiple modes of light traveling along the fiber path after reflecting off the fiber cladding. The speckle pattern will change as the length of the fiber experiences mechanical strain, temperature changes, or other environmental factors. The changes in mode paths cause small changes in the intensity of the speckles at the fiber termination point. By analyzing these variations over time, changes in geometry integrated along the entire length of the fiber can be detected and measured. These changes can quantify variations in the fiber for the intended application [118, 39, 85].

Specklegram sensing fundamentally relies on the modal dispersion of coherent light. Published literature involving this method uses the dispersion inherent in

step-index multimode fiber to increase the sensitivity of their instrumentation, as a higher number of modes will result in higher resolution measurements [85, 86, 88]. Due to the high volatility of the projected interference pattern, several methods involve splicing a singlemode-multimode-singlemode (SMS) configuration in order to confine sensitivity to the testing portion of the fiber, as well as increase the modality of the traversing light through the multimode portion of the fiber [93, 87].

A significant constraint for our application is that our sensing method must rely on existing optical communication fiber installations optimized for efficient long-distance communication wavelengths (such as 1550 nm), which is transmitted through single mode fiber. Given this strict requirement for the transport medium, it may first appear to preclude sensing that requires multi-modal propagation. However, opportunistic leveraging of the characteristics and performance of lower-wavelength light in this scenario leads to surprising results.

5.2.1 Specklegram Sensing on Single Mode Fiber

Step-index multimode fiber is characterized by an abrupt change of refractive index between the core and the cladding. Light modes reflect off the cladding and pass through the axial path, with higher-order modes traveling further than lower-order modes. The fiber core of graded index multimode fiber is constructed so the refractive index of the core gradually approaches the refractive index of the cladding moving away from the center. This reduces modal dispersion and has better performance for telecommunications. As opposed to multimode fiber, single mode fiber has a small core (typically 5 microns) that is designed to constrain the light to a single fundamental mode which minimizes attenuation and intermodal dispersion. Fibers are manufactured according to specifications that dictate optimal operational wavelengths. Any wavelengths that are below the baseline cutoff (1260nm for OS2 fiber) will experience intermodal dispersion, refraction, and dissipation [119]. Diagrams of each of these scenarios are shown in Figure 5.1.

Even if a fiber is not designed to transmit visible light, due to total internal reflection, the fiber still performs as an optical waveguide, just with limited efficiency.

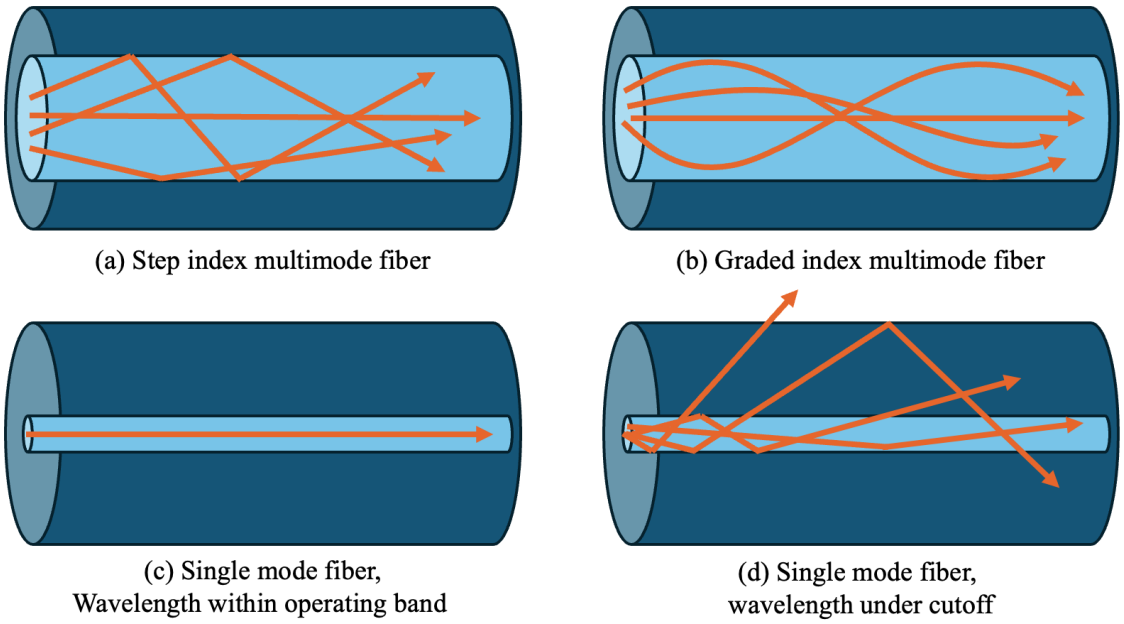

Figure 5.1: Propagation of light modes for different fiber types and scenarios.

This property allows technicians to employ Visual Fault Locators (VFLs) on spans of communication fibers for troubleshooting or repair. These devices are inexpensive battery-powered LEDs that couple to optical fiber connectors. If a fiber break is present, the damaged section of the fiber will illuminate through the thin plastic jacket, allowing the technician to identify and repair the existing fiber instead of requiring a new fiber installation.

For our purposes, the resulting dispersion from light below the fiber's cutoff wavelength can be used opportunistically on shorter spans to enable specklegram sensing with significantly lower cost compared to more sophisticated equipment.

5.3 Seismospeckle Sensor Construction

To detail the development process of our specklegram sensor, we organized our approach as follows. First, we explain the initial construction of our proof-of-concept sensor. We then describe our initial methods of using computer vision techniques, and note our discovered limitations. We then describe our improved designs for

our sensing system, using the knowledge gained through experimentation and specklegram sensing literature.

5.3.1 Proof-of-concept Sensor

Our sensor uses a VFL as a light source [120] which produces a 650 nm visible beam of light. As the visible wavelength is well below the wavelength cutoff designed for the OS-2 fiber, the light traveling along the fiber will leak into the fiber cladding and rapidly attenuate, with an anticipated maximum range of 3 km.

The VFL was coupled to a 10 m fiber optic cable. The cable was affixed to the experiment board and then routed across several different instruments to explore responses to different strain responses; tension was applied to the fiber using a tension adjuster, looped around a 12.7 cm pipe cross section was for bending strain, guided through a rotatable 2.5 cm pipe for torsion strain, and a solenoid motor was used to apply 0.5 cm displacement of various frequencies at four locations along the fiber. The fiber terminated at an FC connector with an 2.5 mm aperture, which was clamped to the experiment board to ensure consistent readings. The projected interference pattern was displayed on a target panel, placed perpendicular to the direction of the fiber termination point at a distance of 0.5 m away. A FLIR Blackfly camera with an 8mm lens is positioned directly above the termination point and captures the changing projection pattern [121]. Our proof-of-concept setup is shown in Figure 5.2.

The initial calibration results of our experiment revealed a detailed interference pattern projected from the end of the fiber. This pattern changed over time as a result of changes in strain placed on the fiber optic cable, with large variations in intensity throughout the image. Figure 5.3 shows the transience patterns of the image produced as the cable is disturbed and relaxes over time. These initial tests indicated the potential for monitoring environmental effects on optical communications infrastructure using visible light.

Figure 5.2: Initial experiment of visible light analysis through fiber. Left frame shows projection of visible light, right frame shows setup from light source through 10 m cable on evaluation board.

5.3.2 Initial Video Processing Pipeline

Modern cameras are designed to automatically process images in order to best display the intended outcome and compress the resulting file storage space. As our use case requires capturing rapid differences from an intense pattern of light, we established a custom configuration for our camera to ensure that we collected the intended data at a high frame rate by reducing the capture size, disabled automatic gain adjustment, and disabled variable shutter rate. After identifying the optimal setting for our camera, we were able to capture the projected speckle pattern at a minimum of 65 frames per second. After our preliminary testing, we first hypothesized that identifying light and dark ellipses in the speckle pattern would be an effective measurement for detecting environmental changes upon a fiber under test. To perform our analysis, we constructed a post-processing pipeline capable of evaluating settings using several computer vision techniques. Our inital pipeline was as follows:

- **Channel Reduction.** Our initial settings involved captures in red, blue, and green channels. Given our projection was from a single coherent light source

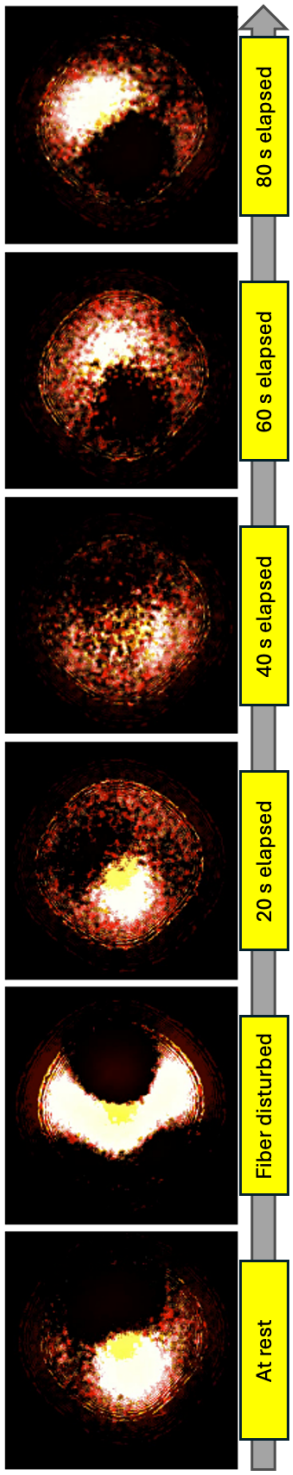

Figure 5.3: Speckle pattern captures using a heatmap filter from calibration testing of our initial processing pipeline, showing transience after fiber is disturbed. Times shown are approximate.

at 650 nm, each channel captured the intensity based on its relative quantum efficiency, so we converted the three-channel images to single-channel grayscale for further processing.

- **Image Scaling.** We set our overall image capture to 512 x 640 pixels to balance between framerate and definition of the projection. Images of this size were too large for timely processing, and further downsampling to 128 x 128 was implemented at the expense of reduced definition.

- **Shot Noise Reduction.** Shot noise describes random fluctuations of photons in low-light settings, resulting in rapid variation in pixel intensity for optical sensors in low-light. To focus on the larger shape patterns of the projection, we employed a 9 x 9 blurring kernel to reduce minor variations that did not contribute to broader patterns.

- **Comparison Filter.** To identify changing intensities of each pixel, we employed several techniques for creating a reference image that was subtracted from each individual frame. Establishing an initial baseline of the projection pattern at the start of a capture produced reliable results versus filters created from the entire capture set or a rolling average.

- **Contrast.** The resulting difference between an individual frame and the comparison filter resulted in pixels with low contrast. We increased contrast to increase the significance of the most pronounced changes between frames.

- **Edge Detection.** To identify the dark and light shapes in our image, we employed the use edge filters, including Sobel and Canny algorithms [122, 123]. These algorithms are designed to enhance sharp changes in pixel intensity and are used frequently for computer vision applications. These techniques, however, failed to produce reliable results in identifying intensity groups.

After evaluation, we concluded that shape detection would provide limited value for sensing due to the large amount of processing and unreliable results. We then looked to statistical methods that could more effectively describe changes in

intensity for our images. Our first method that we assessed involved identifying the brightest point of the full image. We utilized the formula presented by Rosin for identifying the location of the intensity centroid C [124],

$$m_{pq} = \sum_{x,y} x^p y^q I(x,y), C = \left(\frac{m_{01}}{m_{00}}, \frac{m_{10}}{m_{00}} \right) \tag{5.1}$$

where m_{pq} are the moments from the image, and $I(x,y)$ is the intensity value at a given coordinate. We evaluated measuring the distance between the intensity centriod between successive images to infer environmental changes. Our initial results could identify when the fiber was significantly displaced or strained, but failed to respond to smaller perturbations from vibration testing due to the ambient fluctuations in the centroid's location.

We then performed a best-fit plane over the difference of each individual frame, using each pixel's X and Y coordinates, combined with its intensity Z. Each coefficient can be determined by using a least-squares solution [125],

$$\begin{bmatrix} P \\ Q \\ R \end{bmatrix} = (A^T A)^{-1} A^T B \tag{5.2}$$

where A is the design matrix, and B is the intensity vector. While matrix multiplication is more computationally expensive than measuring centroid movement, the overall fluctuations of intensity across the entire image produced consistent measurements during testing. Given the success of this metric, we conducted a separate vibration test to determine levels of response depending on the distance of an excitation point from the termination point of the fiber. Figure 5.4 shows the results from vibration testing where a 15 Hz frequency can be identified by the best-fit plane method during this test. Given the clear results of this method, we moved to improve our prototype for our next phase of testing.

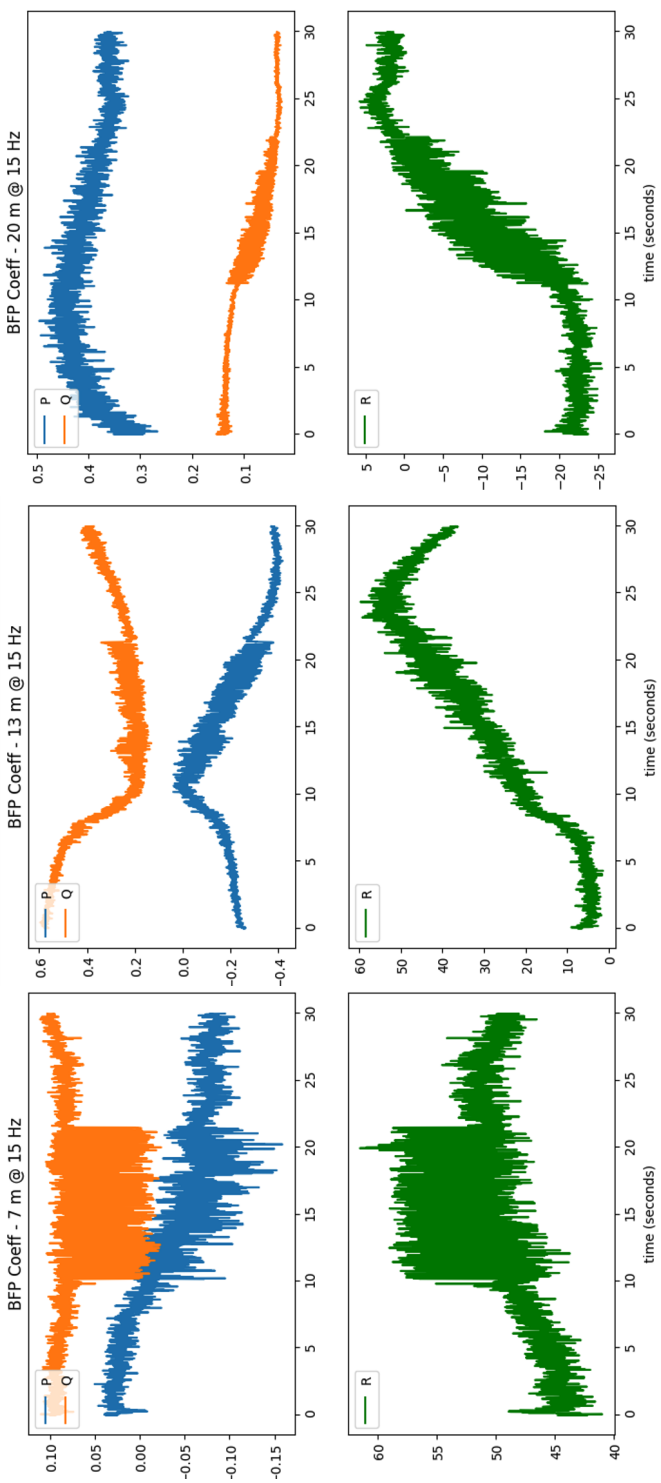

Figure 5.4: Best fit plane coefficient metrics during 15Hz vibration testing from a solenoid motor. Excitation point conducted at 7 m (left), 13 m (middle), and 20 m (right) from the fiber termination point.

5.3.3 Physical Design Improvements

Although our proof-of-concept design showed promise for speckle-based sensing on optical communications fiber, it was apparent several improvements were required to make a design that could be practical in a deployed environment. Our first improvement was to construct an enclosure on a metal baseboard. This ensured that ambient light from outside the experiment was reduced to a minimum. We also installed an adjustable angle bracket mount into the baseboard, on which we secured both the camera and a ring-mounted LC connector to serve as the termination point of the fiber optic cable. This provided maximum stability for our internal components of our sensor. We also installed an internal projection screen 20 cm from the camera and LC connector to complete the sensor. The internal components can be seen in Figure 5.5. As our light source was initially operated by 2 AA batteries, our expected operation time between battery changes was 8 hours. We modified the VFL by connecting to a 12 V deep-cell battery source, adjusted to the correct operational voltage for long-term captures.

5.3.4 Processing Design Improvements

Our method for generating and processing the received camera also required significant changes. Given our lessons learned from our prototype, we aimed to limit the host system processing as much as possible, and focused on making the camera hardware and software optimized to take images that would send the host machine images ready for processing. Our digital camera settings were changed to take 8-bit grayscale images, 200 x 200 image size, and the image was decimated by a factor of two to capture the complete projection image at 150 frames per second. This allowed continuous streaming of images from the camera to be stored on the device that were much closer to final processing. After a capture was completed, we performed post-processing to obtain the best-plane-fit coefficients for analysis. Our image baseline method was also modified to automatically take the average of the first thousand captures before measurement began. Although post-processing the coefficients was sufficient for our current analysis, we also implemented a reduced,

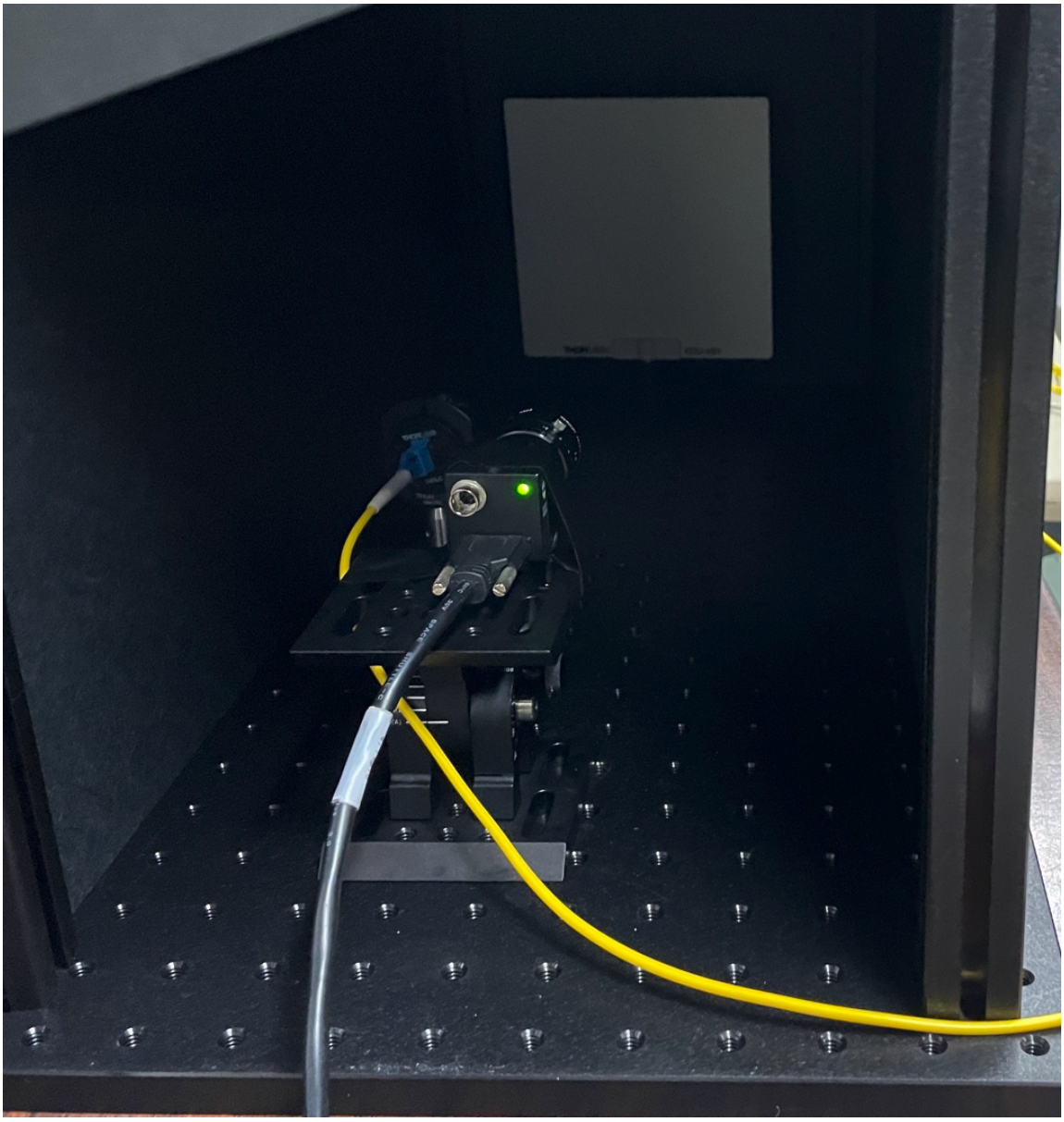

Figure 5.5: View of internal components for the Seismospeckle sensor.

online pipeline to generate best-fit plane coefficients concurrently during collection to give an indicator of possible events. While storing incoming images at full speed, our host system would opportunistically copy images for immediate processing on available CPU cores, down-sample the image by a factor of 2, and store the coefficient results. This process resulted in 100 samples per second on average, which can be suitable for sensing applications that require less precision, or could act as a triggering mechanism to identify capture periods of interest.

5.4 Methodology

After improving the design of our sensor, we devised a laboratory experiment to evaluate the sensing capabilities of our device. The configuration of our laboratory test system is shown in Figure 5.6. The sensing apparatus was attached to a 20-meter length of indoor OS2 fiber optic cable. The light source is connected to the distant end, followed by 3 meters of fiber secured to a flexible wooden beam of equivalent length. Both ends of the beam are clamped to a laboratory table and a vibration generator is positioned at the midpoint of the beam, with the excitation plate adhered to the beam with glue. The lowest point of travel for the excitation plate was in neutral contact with the wooden board. During operation, as the vibrating plate ascends, the beam flexes upward, stressing the cable along its length. This setup more accurately reflects vibrations that would occur along a fiber path than with a vibration generator alone. The fiber leaving the test section was secured to the ground with insulating foam pads to minimize any resultant vibrations from the test section. The 20-meter cable led to a LC/LC coupler, which interfaced with our sensing system located on a separate table. The coupler also facilitated the insertion of test spools to adjust the total fiber length.

Each test run comprised 50 seconds of data acquisition. Before starting data collection, the fiber was allowed to rest for 2 minutes with the light source active to allow the cable to stabilize in temperature and position after being disturbed. Upon the commencement of the test, the vibrating plate remained stationary for the initial ten seconds. Subsequently, at successive 10-second intervals, the vibrating

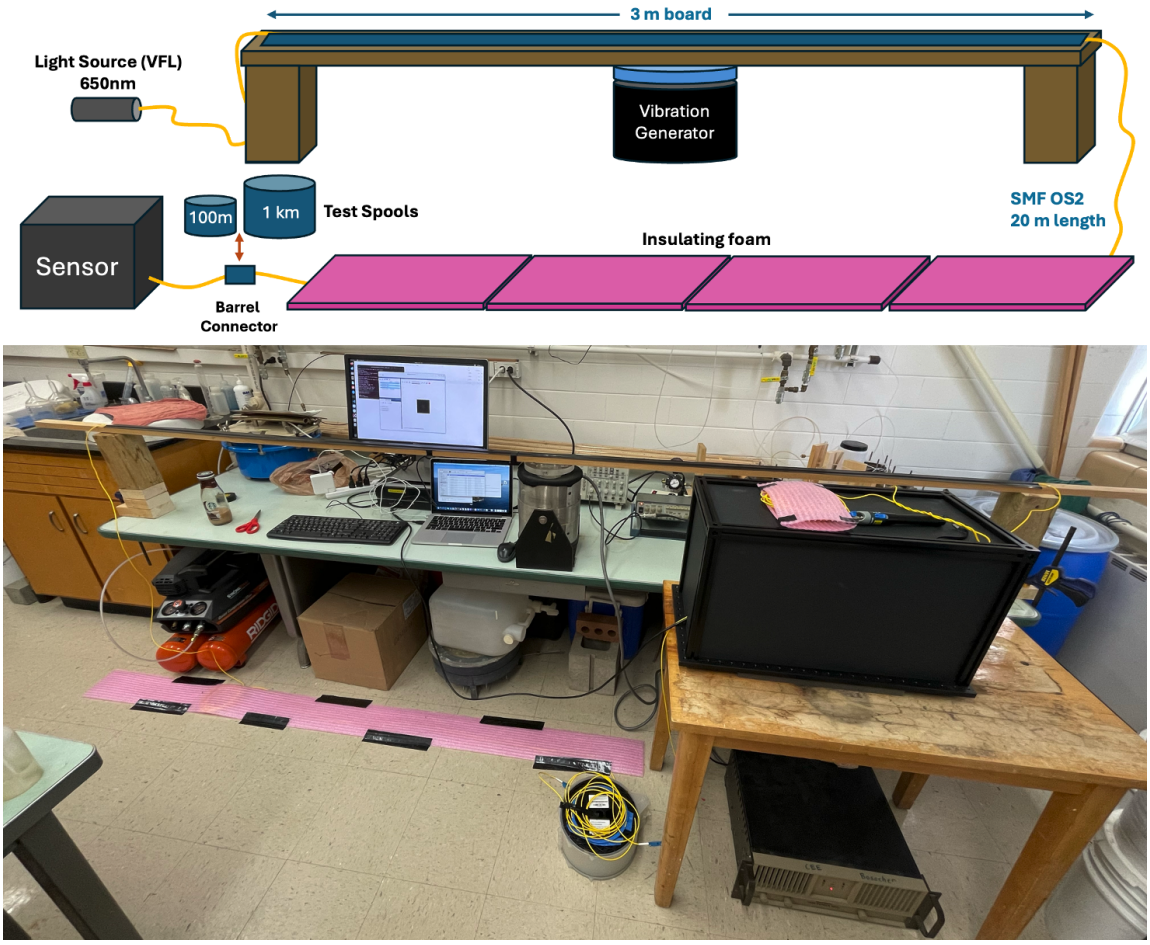

Figure 5.6: Diagram of the specklegram sensor laboratory test (top), and picture of setup (bottom).

plate power increased incrementally by one-third, reaching maximum vibration at 30 seconds. At the 40-second mark, the vibrating power was reduced to zero for the remainder of the data collection period. This test protocol was executed at various frequencies (10, 30, and 50 Hz) and at different distances by incorporating test spools, resulting in total fiber lengths of 20, 120, and 1020 meters. In addition, 50 second rest data was collected at each distance.

Following our laboratory-based evaluations, we sought to determine the device's capability for detecting real-world environmental effects. We implemented our

sensing system in the basement of a campus building adjacent to a freight railway, where our previous experiments were conducted [22, 25]. A 10-meter fiber was affixed to the basement wall using duct tape. The sensing system was stored on a cart nearby, with the enclosure protected from vibrations with insulating foam to limit ambient vibrations from directly affecting the sensor. The device was set to collect continuously for more than three weeks. Our measurements were correlated with seismic data from a geophone installed in the same location.

After collection, we analyzed the results to identify prominent features that correspond with passing train vibrations. We then implemented a basic trigger algorithm, conducted statistical analysis to tune parameters, and evaluated its effectiveness to detect passing trains.

5.5 Results

5.5.1 Laboratory Results

To evaluate the vibration tests, the results were analyzed by combining the output of the three best plane fit coefficients using spectral forecasting [116], with P and Q (X and Y coefficients, respectively) at equal weight, then R (intensity coefficient) at 30%. We then applied a band filter from 5 to 60 Hz and analyzed the combined spectral output. The vibrations from our tests were visible at all lengths of tested fiber, up to 1,020 meters. Figure 5.7 shows the spectral response of 50 Hz tests in different ranges. The tests carried out at the shortest distances (20 and 120 meters) were the most pronounced. The tests carried out at 1,020 meters were detectable but suffered significant attenuation.

All tested frequencies were visible, with the higher frequencies showing greater clarity and consistency. At 10 and 30 Hz, the harmonics of the vibration frequency were prominent, which we attribute to oscillations of the cable leading off the vibrating board. Figure 5.8 shows the test results for 10 and 30 Hz at different cable lengths.

We also observed captures without applied vibration when the fiber is at rest.

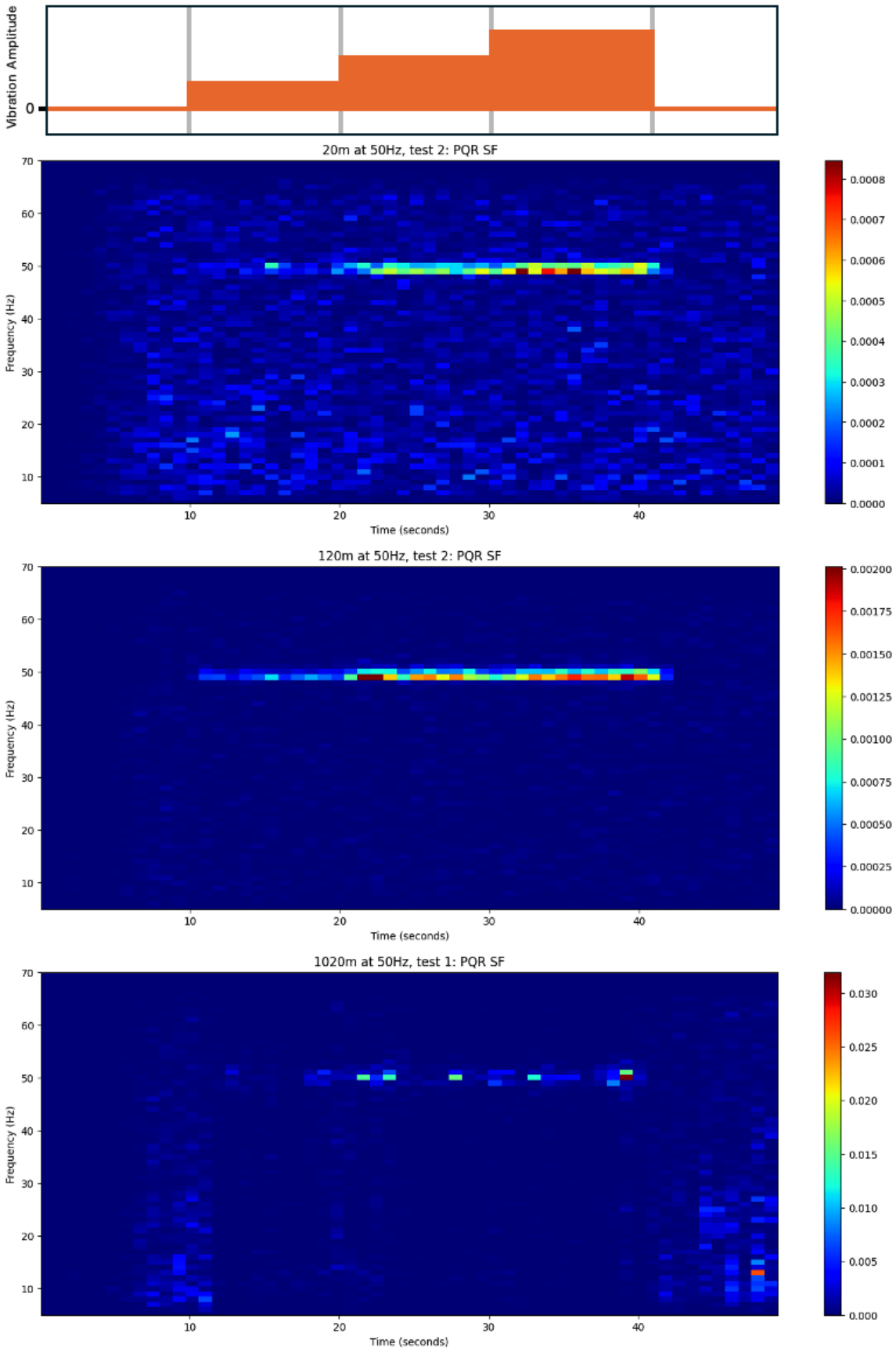

Figure 5.7: Spectrogram plots of combined output during 50 Hz tests at 20 m (top), 120 m (center), and 1,020 m (bottom).

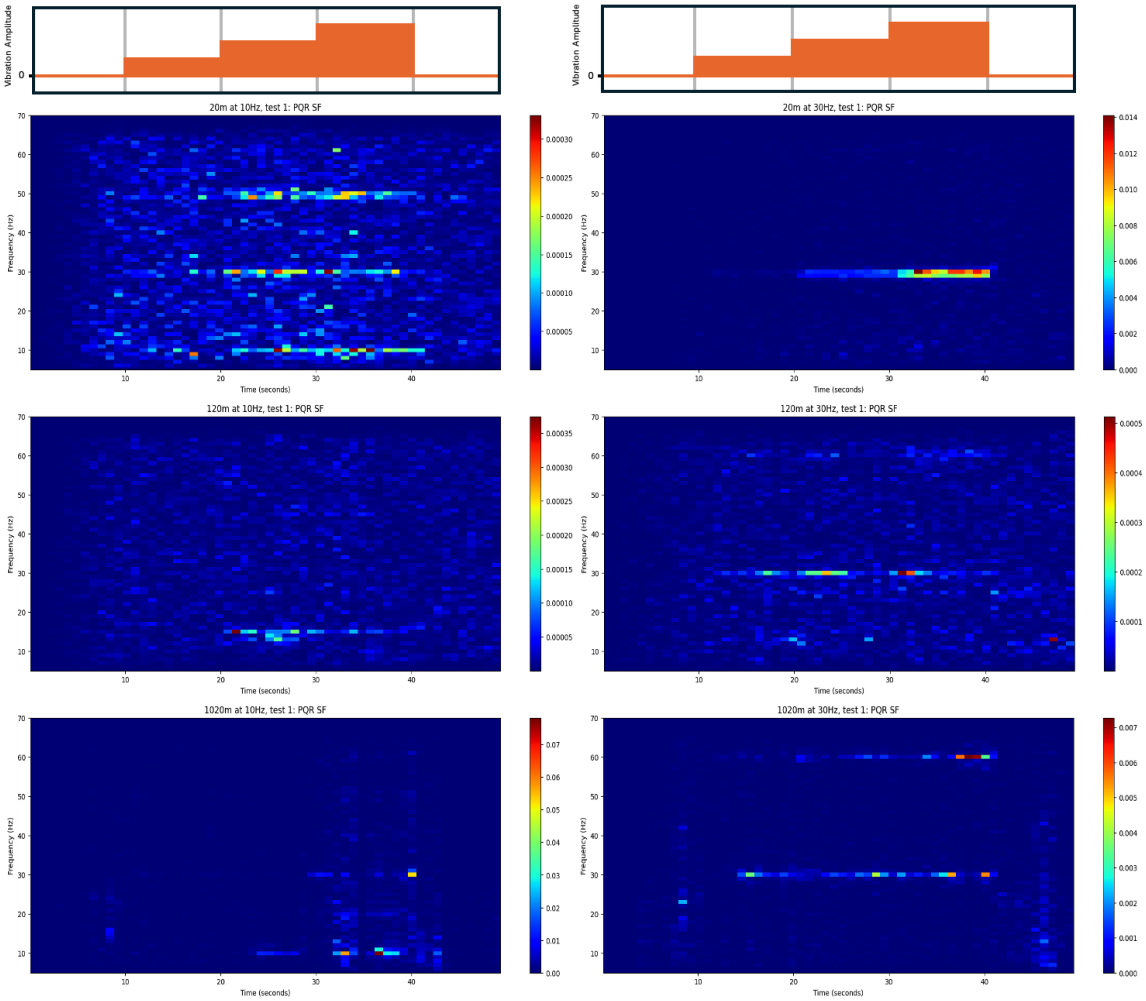

Figure 5.8: Spectrogram plots of combined output during 10 Hz (left) and 30 Hz (right) tests at 20 m (top), 120 m (center), and 1,020 m (bottom) fiber lengths.

Figure 5.9 shows the drift of the coefficients during three separate 50-second captures at different lengths. Even minute disturbances of the cable caused a significant change in the resulting speckle pattern. Regardless of the length of the test fiber, the speckle pattern perpetually changed as microscopic strains from ambient sources modified the path length of the light modes passing through the fiber.

5.5.2 Train Capture Results

During our three-week capture conducted on the basement wall, we were able to record 11 distinct train events, with the duration of passing trains ranging from less than a minute to more than four minutes. The sensor coefficient responses showed several different variations between the train events. Due to the significant variation between the coefficient responses, using spectral forecasting to combine the responses reduced the clarity of the responses overall. The most prominent responses showed a spike in frequencies from 25 to 35 Hz during the train passing. However, some train events show an overall increase in vibration around the train event but are obscured by larger fluctuations throughout the capture. Unlike a geophone which registers vibrations at a specific point, our sensor reports the integrated changes along the fiber path. Larger vibrations can affect portions of the sensing fiber differently along the basement wall. Fiber may have points of increased strain due to very small twists or bends which can amplify and distort responses, occluding an otherwise clear vibration response. These results suggest that there is a maximum sensing limit when detecting vibrations. Four coefficient spectrograms that record train events are shown in Figure 5.10.

5.5.3 Automated Trigger Algorithm.

In order to quantify the accuracy of detecting train events during collection, we decided to implement a trigger using Short Term Average / Long Term Average (STA / LTA), a historically proven algorithm used to generate alerts for seismic activity [74]. This algorithm collects two running averages over different timespans and will meet trigger conditions for activation and deactivation when a threshold

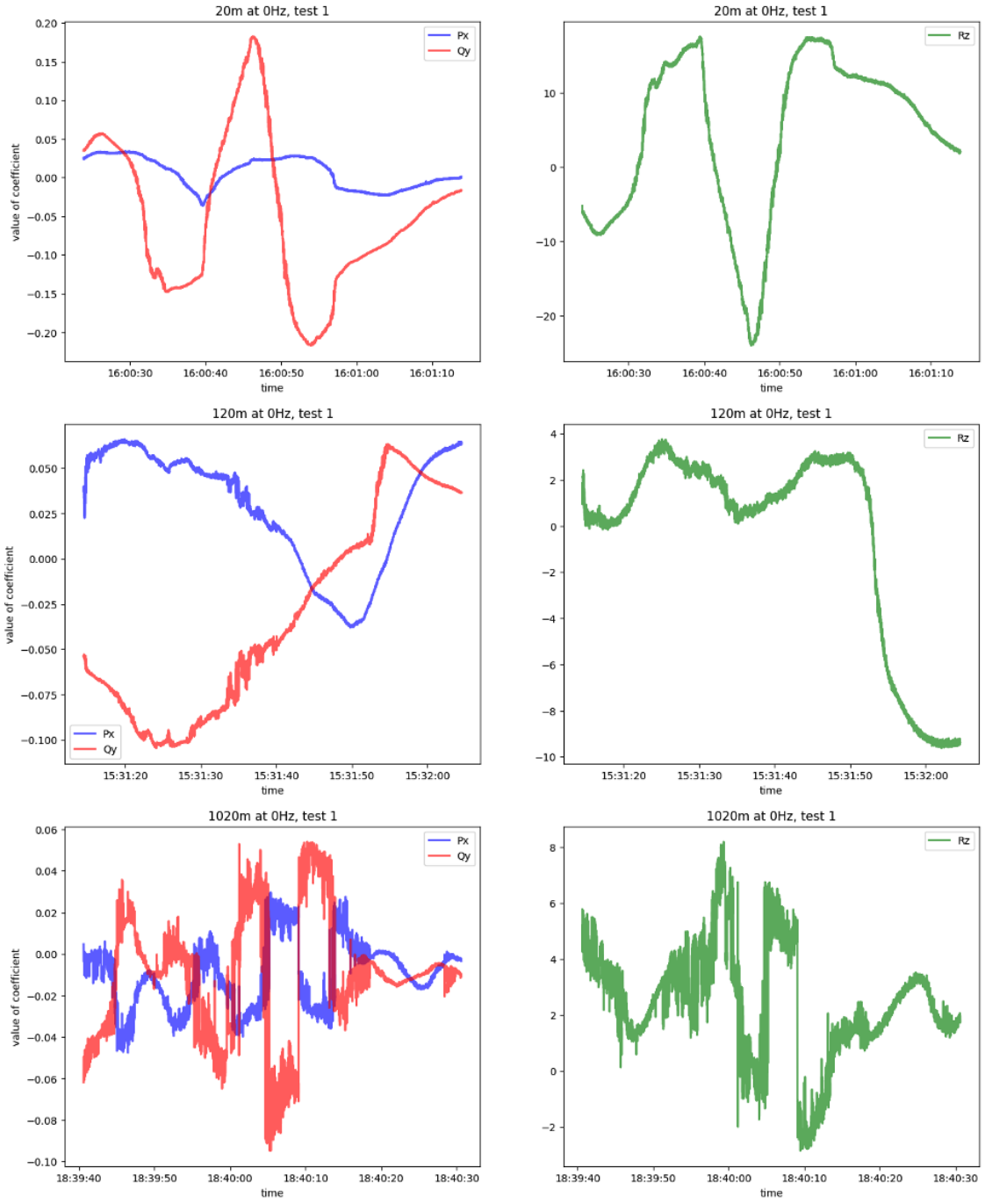

Figure 5.9: Plots of coefficient variance during rest captures at 20 m (top), 120 m (center), and 1,020 m (bottom).

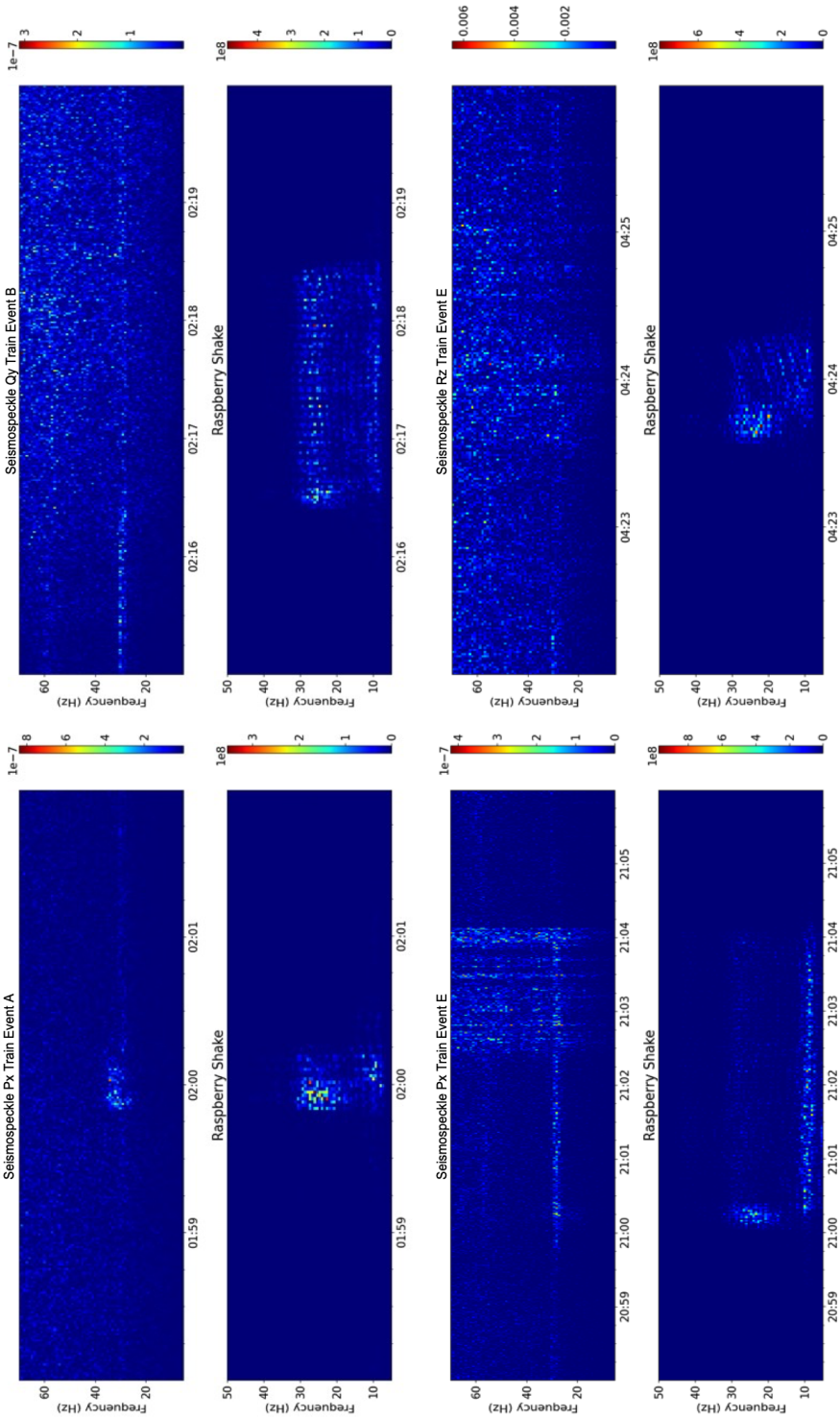

Figure 5.10: Spectrogram plots of four train events with sensor coefficient (top) and geophone (bottom).

ratio between the two is met. We selected this approach because of its compatibility with our sensing application and its lightweight processing requirements, which are suitable for remote sensor implementation.

Our trigger algorithm is applied independently to each coefficient response after using a 25 to 30 Hz bandpass filter. Each coefficient makes an independent trigger determination. Individual trigger activations are discarded if their duration is less than 30 seconds, less than the smallest recorded train duration. However, we only quantify a fully activated response if at least two of the three coefficients agree to an on/off trigger determination within a 60-second window.

In order to validate our sensor's overall accuracy, we included the processing of 20 randomly selected 12-minute intervals from a single 20-hour capture period. We ran a Monte Carlo simulation with a random selection of parameters for our trigger algorithm. The results for each configuration were scored per second compared to the recorded response from the geophone, with a positively weighted score applied for correct trigger activations during vibrations, and an inverted score when missing large vibrations or incorrect trigger activations during idle periods.

After running our simulation, we calculated the accuracy of our trigger responses using the best scoring parameters. For train events, our algorithm successfully identified a train event 8 out of 11 times. Some train event periods showed increased responses during passing trains, but were eclipsed by larger trends in the response data. Detailed train responses and trigger activations are shown in Figure 5.11. Given these results and observations from our laboratory testing, we attribute the sensor washout to earlier vibrations, where the fiber has yet to settle to a consistent baseline.

During idle measurements, the algorithm was triggered in 11 of the 20 time periods. Inspecting individual trigger responses revealed further nuance in the sampled data. During idle periods, 7 of the 11 trigger activations correlate with smaller vibrations recorded by the geophone. Applying the trigger agreement between the coefficient responses was effective in eliminating many, but not all, erroneous responses. This highlights how an integrated response across the basement wall from a vibration source can elicit a different response than a point sensor

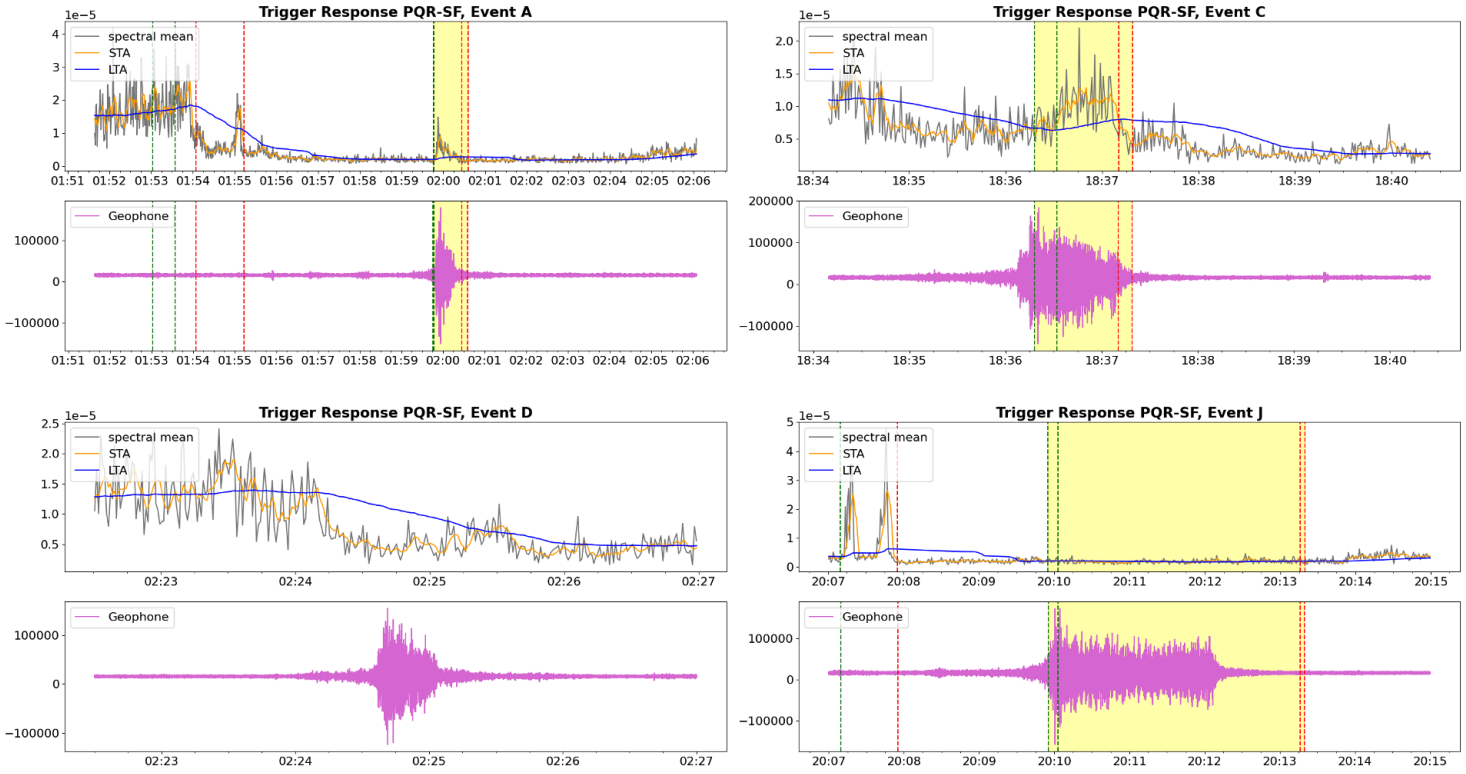

Figure 5.11: Four train events periods showing STA/LTA metrics (top) and the geophone response with recorded score (bottom). Individual trigger activations and deactivations are dashed vertical green and red lines respectively, and trigger agreements are shown in yellow.

on the basement floor. To illustrate these results, four samples from the idle period are shown in Figure 5.12.

5.6 Discussion

Our findings from our laboratory tests suggest compelling implications for the use of specklegram sensing for environmental effects on optical networked communications infrastructure. Although constructed with relatively inexpensive hardware and components, our sensor can detect environmental changes of interest along a short span of fiber. Although frequencies at or below 10 Hz show less response, frequencies between 30 to 50 Hz have shown the most sensitivity to external vibrations.

Although the results of specifically identifying passing trains are not as consistent as we had anticipated, the response patterns of our sensor show sensitivity to small and moderate vibrations, but lose effectiveness for larger, more complex vibration patters. Care must be taken to employ specklegram sensors on fibers that are both subject to vibrations of interest and are protected from unwanted signals. Although we implemented a lightweight detection algorithm, more advanced signal processing techniques may improve detectability for anthropogenic and ground motion events.

Our speckle-based measurement is able to detect integrated geometrical changes in a fiber span, similar to how polarimetry-based measurements are conducted: As polarization mode dispersion occurs to light above the cutoff wavelength, the degenerate fundamental mode will break symmetry in single mode fiber. For speckle-based measurements, the multimode fiber imperfections induce changes in phase unique to each mode resulting in a distinct interference pattern at the projection point. Both of these measurements indicate subtle physical changes of the lay of a fiber and can be analyzed to reveal the sources of these effects.

Given the reporting rate of 150 Hz for detailed measurements or 100 Hz for long-term online reporting, this sampling rate is suitable to detect cultural urban noise such as traffic. Further development and miniaturization of the projection, camera,

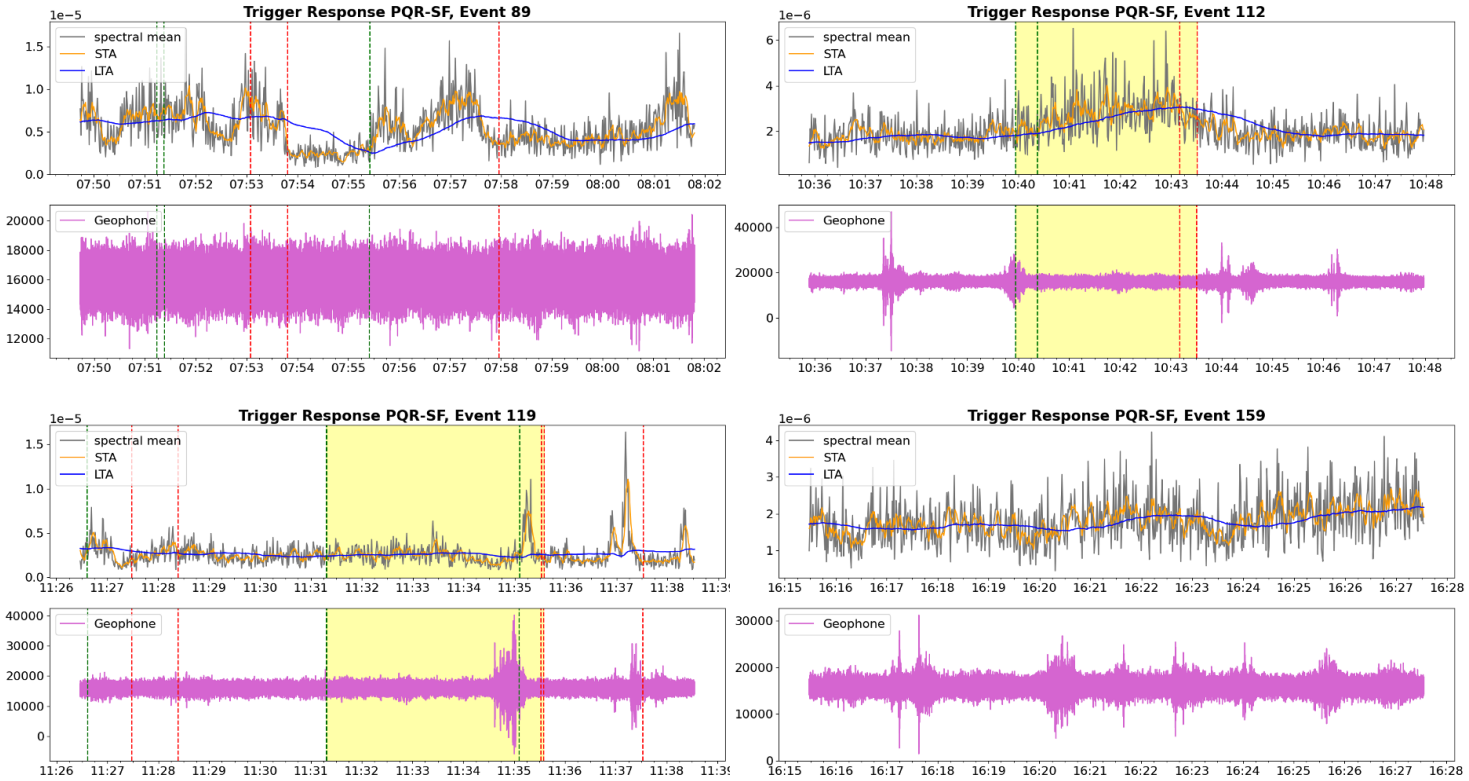

Figure 5.12: Four idle periods showing STA/LTA metrics (top) and the geophone response with recorded score (bottom). Individual trigger activations and deactivations are dashed vertical green and red lines respectively, and trigger agreements are shown in yellow.

and processing components can significantly reduce the footprint of the sensor, providing convenient deployments where larger and more expensive equipment would be prohibitive. Adding physical filters and taps along multiple spans of fiber can enable a group of these devices to report on environmental effects on optical communication cables, with the potential to infer spatial information about disturbances in a metro environment.

Our wavelength and camera decisions have been selected for low-cost price points, but lasers and cameras that are constructed for this purpose at an optimal wavelength may provide reduced attenuation while still operating underneath the wavelength cutoff can provide modal dispersion to provide sufficient granularity to detect environmental effects of interest.

However, the benefits of easy deployment and low cost are not without trade-off. Our lightweight trigger algorithm was moderately effective in discerning significant vibrations during our in situ test. Even in quiet conditions, subtle changes in temperature, air flow, building noise, or relaxing torsion strain will cause responses to the resulting projection. We are developing a processing pipeline that uses a modern image classifier to mitigate these effects, which we anticipate will provide improved accuracy beyond our initial methods. Despite the advantages of machine learning, our results confirm that a particular deployment of a fiber sensor must be characterized and assessed to determine the sensing fiber's suitability for detecting signals of interest.

6 CONCLUSION AND FUTURE WORK

Environmental sensing can inform us of critical events and help us understand imperceptible events around us. Conducting environmental sensing on the physical infrastructure of communication networks that run underneath and through our cities can supplement existing applications and provide additional and previously unrecorded data about these events. From security to public safety, monitoring the changing characteristics of light as a result of changing strains on fiber can provide significant benefit to the organizations and populations that inhabit our world's largest and most connected areas.

In this thesis, we explore the use of optical communication network infrastructure as an environmental sensor, provide an improved low-cost polarimeter design suitable for detecting polarization transience caused by cultural vibration, and develop and deploy an ultra-low-cost specklegram sensor for deployment on short spans of optical fiber. Each of these designs and studies was empirically evaluated by laboratory testing and real-world deployments to improve our understanding of the capabilities and limitations of sensing in optical communications networks and to improve the practicality of employing such sensors for monitoring applications.

6.1 Summary of Contributions

6.1.1 Contributions Related to Transceivers: Efficacy of Using Commodity Optical Transceivers for Environmental Sensing

We performed a detailed analysis of the use of an optical communications transceiver as an environmental sensor. We detail our assessment of the use of performance monitoring metrics commonly available to this type of equipment, as well as the advantages and shortcomings of opportunistically leveraging information extracted from standard DSP operations. We found that while polarization transience infor-

mation can reveal environmental effects, the reduced and nonperiodic sampling rate was a significant limiting factor in detecting sociocultural events, such as freight train traffic.

We also characterize polarization transience patterns found during our measurements, from significant changes to the fiber geometry, such as repetitive bending movements and vibrations and adjusting splice trays, to ambient changes in the environment from diurnal temperature changes and rainfall. Following our analysis from testing a 4 km inter-campus route and the installation and observation of a 100 m custom fiber route, we highlight the best practices for installation of fiber for sensing purposes that do not align with procedures for the installation of fiber for networked communication. However, opportunities are present where coupling of a fiber to a vibrating medium is considered.

6.1.2 Contributions Related to Homebrew: Low-Cost Polarimetry Based Environmental Sensing on Optical Fiber

After noting the capabilities and limitations of sensing with commodity communication equipment from our previous experiment, we aimed to measure the polarization transience at a higher sampling rate. We replicated the design of a low-cost polarimeter used in previous studies and evaluated its sensitivity in laboratory studies and rotation rate metrics. However, measurement dead zones and the loss of clarity led us to develop an improved design that incorporates the splitting of incoming light into four adjustable measurement arms with significant success.

After implementing a reliable calibration method, we tested our design in a series of measurements by coupling a fiber to a basement wall in the vicinity of an operating freight railway and comparing the measurements to the campus fiber route. Our results confirm that strong coupling to vibration sources is required to achieve high reliability in capturing environmental effects via polarimetry.

Our novel polarimeter design increases the average sensitivity range over the previous design and, when optimally calibrated, improves the theoretical sensitivity floor by at least 29%. It is also capable of achieving sampling rates of up to 1 kHz

for extended measurements, suitable for measuring environmental and cultural effects in metropolitan areas.

6.1.3 Contributions Related to Seismospeckle: Low Cost Specklegram Sensing on Optical Communications Fiber

Lastly, we looked to alternative methods of measurement beyond polarization transience. We designed, prototyped, and evaluated a specklegram sensor and related metrics for optical communication fiber. Our sensor is able to detect vibrations up to 75 Hz in short-distance optical fiber installations in at least a 1 km range. Although the sensor exhibits high sensitivity to ambient vibrations and movement, our sensor can be constructed from common components for a fraction of the cost of more sophisticated devices.

We also performed tests on a fiber adhered to a basement wall to detect passing freight trains. Our results show that these sensors may respond differently to external perturbations than point sensors and may also have a maximum sensitivity threshold where stronger vibrations can limit effective reporting. Although this sensor does not have an extended range compared to our previous polarization-based devices, its extremely low cost, portability, and online measurement capability give strong advantages for future applications in environmental sensing.

6.2 Summary of Findings for Research Questions

Three primary research questions guided our studies and evaluations, provided in Section 1.1.1. Each question focused on a specific dimension of our larger objective, the incorporation of environmental sensing applications on optical networked communications infrastructure in metro and urban areas. Our findings for each of these questions provide an understanding of both the present capabilities and the limitations that must be overcome toward this purpose:

6.2.1 What are the capabilities and limitations for using optical communications infrastructure for environmental sensing in metro and urban areas?

Although optical fiber is used for both sensing and communication applications, their installation requirements may have competing restrictions. Optical communication fiber installations are designed to protect the optical waveguide from external sources that may cause service degradation, such as stresses and strains that deform the fiber. This may distort the characteristics of light which are modulated to carry network data.

We observed that optical communication fiber installations are often heavily shielded in outdoor portions of the fiber run by burial depth, protective conduit, and shielded cables specifically designed to limit the influence of external effects. Indoor portions of fiber runs are also protected by cable trays and routing designs to ensure that the fibers are kept out of reach. However, indoor fiber optic cables are often more flexible for ease of installation and can be subject to a wide range of ambient building noise, such as heating and cooling systems, other telecommunication equipment, and airflow. When taking integrated measurements of light characteristics, signals of interest may be less pronounced and occluded by non-obvious sources of disturbance.

Physical displacement of even a few millimeters can create a significant polarization response. When measuring polarization transience, disturbances that temporarily adjust the lay of a fiber can be characterized. Permanent displacements should result in a change of resting polarization state, which can be easily detected, but may also require establishing a new baseline for more minute effects.

Additionally, the amount of coupling to a vibration medium is a significant factor for accurately detecting events. The lay of a fiber used for sensing should be evaluated and may need to be modified to increase the amount of desired vibrations transferred to the cable. Effects that permanently degrade the physical condition of the fiber, such as exceeding the recommended minimum bend radius or maximum strain guidance, should be avoided.

Lastly, integrated measurements from sensing on an optical fiber may produce a different response than what is recorded on a single-point sensor, such as a geophone. Particularly when using intensity-based measurements, intended and ambient vibration sources may result in large amounts of variation that can reduce clarity, masking specific frequency responses.

6.2.2 How can we integrate sensing capabilities onto optical communications infrastructure effectively?

Coherent communication DSPs transmit data through modulation of the carrier wave's polarization state. As the polarization state can be expected to change during transit, these devices routinely mitigate unwanted changes and continuously estimate the transmitted polarization to recover data. However, these devices are not designed primarily to report polarization information. Performance metrics that are available can give some insight into significant changes in the characteristics of light during transmission, but are oriented towards the quality of the communication link and lack sufficient detail to observe minor external events impacting a communications fiber.

Our study recorded polarization transients from an optical transceiver utilizing additional firmware and software. This provided detailed information on environmental effects that cause large polarization transients, such as opening a fiber tray, rising temperatures, or cable displacement. However, a limited sampling frequency may inhibit vibration monitoring.

Polarimeters are specifically designed to monitor the polarization state on an optical fiber with high precision. We were able to perform long-term polarization captures with our polarimeter design, which maintained a suitable sampling rate for observing vibrations from nearby freight trains on highly coupled fiber paths. Our four arm polarimeter design is able to detect a wider range of polarization transients than earlier designs, but also requires additional calibration steps of adjusting the incident polarization in each pair of sensing arms to perform optimally.

Intensity-based fiber specklegram sensing can be performed on an optical fiber

using a wavelength below the base cutoff because of modal dispersion. This method can provide detailed information about how short spans of 1 km of an optical fiber are perturbed but share characteristics common to this method of measurement. The device can be overly sensitive to both ambient events and large, complex disturbances. However, this provides a low-cost and easy to deploy alternative to polarization measurement if suitable for a specific sensing application.

6.2.3 How can we expand sensing through optical communications infrastructure with minimal impact to its primary function?

All three of our experiments sought to find sensing methods and devices that are inexpensive to install, operate, and maintain using optical communications fiber. Inherently, by using an optical fiber that is already installed, a separate fiber installation is not conducted. Additional modifications to increase coupling and reduce ambient noise, such as adhering to a vibrating surface or creating air baffles to direct air flow away from fibers, can be done inexpensively and can enhance the response from the targeted environmental effect. Due to the sophistication of modern DSPs, minor environmental disturbances can be expected to be mitigated with minimal impact to communications.

The use of existing optical transport hardware to perform environmental sensing is possible, especially if targeted effects produce large polarization transients, either quickly or gradually. Although our experiment used a modified device, it highlights what measurements can be conducted explicitly using optical communications equipment.

Our polarimeter design is relatively low cost compared to commercial polarimeters, constructed with components that cost approximately $6,000. It is able to conduct measurements using optical fiber designed for 1550 nm wavelengths, commonly employed in optical communications infrastructure. Although this design requires calibration to maintain sensitivity, this does not require additional equipment or services from a vendor. As this method measures polarization transients

to detect external effects, partitioning of sensing and communication carriers must be considered if the communication method modulates polarization as a means of transmitting data.

Our specklegram sensor provides a component price of approximately $500, using a low-cost power source and digital camera. Despite a reduced accuracy compared to polarization-based measurements, the small footprint of the device is easy to install and requires little maintenance to ensure proper camera settings. It senses changes in intensity of visible light and does not rely on monitoring wavelengths used for communication on the fiber.

We have provided detailed information on the setup and operation of these devices for detecting environmental effects in each respective chapter. These designs can be used as described to detect environmental effects, but they also provide avenues to continue maturation that enable higher-quality sensing on optical communications infrastructure.

6.3 Future Avenues of Study

Our research efforts in this thesis describe how we used empirical laboratory evaluation to develop practical fiber optic sensors, how these sensors detect changes in the strain placed on a fiber due to environmental effects, and how to best identify candidate fiber optic communication routes for sensing applications. Although all of these designs and findings provide significant insight into the use of optical communication networks for sensing, more research is required to further develop this concept.

6.3.1 Future Studies Related to Transceivers: Efficacy of Using Commodity Optical Transceivers for Environmental Sensing

Our study using an optical transceiver for sensing was only configured to test in a single-fiber homodyne arrangement. Given the limitations of what can be

detected on a single fiber strand, expanding the monitoring across several of these devices as part of a sensing network with multiple fibers can better demonstrate the capabilities of opportunistic environmental sensing on optical communication infrastructure. As each route may show different sensitivity to effects depending on the configuration of the particular fiber path, several sensors may provide spatial resolution to effects or can assist in reducing false detection rates for signals of interest.

Since the completion of our study, new models of optical transceivers have been released. Our study was focused on a single model from a single vendor, but different designs may offer advantages when it comes to environmental sensing. Devices that can offer more detailed polarization transience metrics or that can support higher sampling rates can further advance the field of sensing through communication networks. This also provides opportunities for vendors to respond to the growing interest in environmental measurements and incorporate metrics that allow monitoring with greater precision.

Additionally, our study focused on correlating polarization transience to external events on communications infrastructure but was not incorporated into a communications network. The communications community focuses primarily on the health and operation of the network. Further studies can investigate both the level of impact of sensing applications on data-transport networks and how advances in environmental sensing through communications networks may help provide insight for the physical security and of optical communications.

6.3.2 Future Studies Related to Homebrew: Low-Cost Polarimetry Based Environmental Sensing on Optical Fiber

Our novel polarimeter design was effective in detecting signals of interest, such as passing freight trains, when the fiber under test was strongly coupled to a vibration medium. It also provides an increased advantage over earlier designs by offering an extended sensitivity range across the Poincare Sphere when splitting on different polarization axes. However, our calibration methods were not designed to find the

true optimal setting for these axes. Including additional equipment and motorized polarization controllers, a system can be designed to automate optimal polarization settings to ensure maximum efficiency of the four-arm polarimeter.

Second, our system was tested on a dedicated fiber expressly for the purposes of sensing, and not on a shared fiber with communications equipment. Since coherent modulation utilizes the amplitude, phase, and polarization of light, our polarimeter must be able to operate separately when performing measurements on an active communications fiber. Further study of how to effectively separate these sensing and communication channels and a report of the impact to both applications would be highly instrumental.

Finally, our measurements required significant post-processing to recover the polarization information from the oscilloscope and to analyze and combine the separate channels. Our study also explicitly focused on understanding and characterizing polarization transience. By creating a processing pipeline to quickly ingest polarization measurements and then training a machine learning classifier, this device can be assessed for use in real-time alert applications, bringing a significant capability improvement to most sensing applications.

6.3.3 Future Studies Related to Seismospeckle: Ultra-Low-Cost Intensity Based Sensing on Optical Fiber

Our final study involved the use of visible light in an optical fiber designed to transmit C-Band wavelengths, and exploiting the distortion mechanism of modal dispersion to create a fiber specklegram sensor. Although our study focused on using low-cost components, the choice of 650 nm wavelength light may not be the optimal choice for sensing applications on this class of fiber. Longer wavelengths may propagate further along the waveguide before dispersing and increasing the effective range of sensing. Although this would incur a higher cost for more sophisticated laser and camera components, exploring the opportunity for increased range on long-distance communication networks would increase installation opportunities and research for our studies.

This research effort focused on exploring the potential capability for sensing on optical communications infrastructure. However, developing and researching a means to introduce the effects of this type of sensing on fibers used for communication can provide essential understanding of the further development of this type of sensing on optical networks. By incorporating fiber taps and physical muxes, specklegram sensing applications that share the same fiber as communication streams can be evaluated and developed for wider use.

We implemented a simple trigger algorithm to quantify responses to external events. Our results strongly suggest that more sophisticated processing can make more intelligent decisions when classifying events. With the use of modern image and video classifiers, we expect that our sensor can be deployed to a wider range of environments and may be able to reduce a significant amount of instability inherent to specklegram sensing.

Lastly, the limited range of this sensor may also be opportunistically leveraged when used as a series of sensors on a single long-distance path. The specklegram sensor can be further miniaturized using lenses and smaller cameras and local processors on smart phones [126], and can then be introduced at several access points along a fiber. Given the low cost and ease of deployment, this system may prove advantageous over more expensive equipment and can be tested for security-based applications along unmanned stretches, with pairs of emitters and receivers at the maximum effective range.

BIBLIOGRAPHY

[1] Kisaka, Y., Tomizawa, M. & Miyamoto, Y., Digital Signal Processor (DSP) for Beyond 100G Optical Transport, *NTT Technical Review*, **14**(9), 2016.

[2] Ip, E. & Kahn, J.M., Feedforward Carrier Recovery for Coherent Optical Communications, *Journal of Lightwave Technology*, **25**(9), pp. 2675–2692, 2007.

[3] Ip, E., Lau, A.P.T., Barros, D.J.F. & Kahn, J.M., Coherent detection in optical fiber systems, *Optics Express*, **16**(2), pp. 753–791, 2008.

[4] Kohler, M.D., Cochran, E.S., Given, D., Guiwits, S., Neuhauser, D., Henson, I., Hartog, R., Bodin, P., Kress, V., Thompson, S., Felizardo, C., Brody, J., Bhadha, R. & Schwarz, S., Earthquake Early Warning ShakeAlert System: West Coast Wide Production Prototype, *Seismological Research Letters*, **89**(1), pp. 99–107, 2017.

[5] Not all ground-motion sensors are created equal | Alaska Earthquake Center, `http://earthquake.alaska.edu/not-all-ground-motion-sensors-are-created-equal`, 2019.

[6] Das, S., Saha, P. & Patro, S.K., Vibration-based damage detection techniques used for health monitoring of structures: a review, *Journal of Civil Structural Health Monitoring*, **6**(3), pp. 477–507, 2016.

[7] Xiao, F., Meng, D., Yu, Y., Ding, Y., Zhang, L., Chen, G.S., Zatar, W. & Hulsey, J.L., Estimation of vehicle-induced bridge dynamic responses using fiber Bragg grating strain gages, *Science Progress*, **103**(1), 2020.

[8] Liu, T., Wei, Y., Song, G., Li, Y., Wang, J., Ning, Y. & Lu, Y., Advances of optical fiber sensors for coal mine safety monitoring applications, in *2013 International Conference on Microwave and Photonics (ICMAP)*, 2013, pp. 1–5.

[9] Explosion "Earthquakes", PNSN, `https://pnsn.org/blog/2016/03/10/explosion-earthquakes`, 2016.

[10] Zhan, Z., Cantono, M., Kamalov, V., Mecozzi, A., Müller, R., Yin, S. & Castellanos, J.C., Optical polarization–based seismic and water wave sensing on transoceanic cables, *Science*, **371**(6532), pp. 931–936, 2021.

[11] Wellbrock, G.A., Xia, T.J., Ip, E., Huang, Y.K., Huang, M.F., Wang, T. & Aono, Y., Field Trial of Vibration Detection and Localization using Coherent Telecom Transponders over 380-km Link, in *2021 Optical Fiber Communications Conference and Exhibition (OFC)*, 2021, pp. 1–3.

[12] Ip, E., Fang, J., Li, Y., Wang, Q., Huang, M.F., Salemi, M. & Huang, Y.K., Distributed fiber sensor network using telecom cables as sensing media: technology advancements and applications [Invited], *Journal of Optical Communications and Networking*, **14**(1), p. A61, 2022.

[13] Lu, P., Lalam, N., Badar, M., Liu, B., Chorpening, B.T., Buric, M.P. & Ohodnicki, P.R., Distributed optical fiber sensing: Review and perspective, *Applied Physics Reviews*, **6**(4), p. 041302, 2019.

[14] Parker, T., Shatalin, S. & Farhadiroushan, M., Distributed Acoustic Sensing – a new tool for seismic applications, **32**, 2014.

[15] Cartlidge, E., DAS: A Seismic Shift in Sensing, *Optica News*, (32), 2021.

[16] Zhan, Z., Distributed Acoustic Sensing Turns Fiber-Optic Cables into Sensitive Seismic Antennas, *Seismological Research Letters*, **91**(1), pp. 1–15, 2020.

[17] Ajo-Franklin, J.B., Dou, S., Lindsey, N.J., Monga, I., Tracy, C., Robertson, M., Rodriguez Tribaldos, V., Ulrich, C., Freifeld, B., Daley, T. & Li, X., Distributed Acoustic Sensing Using Dark Fiber for Near-Surface Characterization and Broadband Seismic Event Detection, *Scientific Reports*, **9**(1), p. 1328, 2019.

[18] Patnaik, S., Barford, P., Fratta, D., Jensen, B., Lord, N., Malloy, M. & Wang, H., Internet Photonic Sensing: Using Internet Fiber Optics for Vibration Measurement and Monitoring, 2020, arXiv:2009.13797.

[19] Mazur, M., Castellanos, J.C., Ryf, R., Börjeson, E., Chodkiewicz, T., Kamalov, V., Yin, S., Fontaine, N.K., Chen, H., Dallachiesa, L., Corteselli, S., Copping, P., Gripp, J., Mortelette, A., Kowalski, B., Dellinger, R., Neilson, D.T. & Larsson-Edefors, P., Transoceanic Phase and Polarization Fiber Sensing using Real-Time Coherent Transceiver, in *Optical Fiber Communication Conference (OFC) 2022 (2022), paper M2F.2*, Optica Publishing Group, 2022, p. M2F.2.

[20] Waddy, D.S., Chen, L. & Bao, X., Polarization effects in aerial fibers, *Optical Fiber Technology*, **11**(1), pp. 1–19, 2005.

[21] Barcik, P. & Munster, P., Measurement of slow and fast polarization transients on a fiber-optic testbed, 2020.

[22] Catudal, J., Dowsett, K., Barford, P., Fratta, D., Jensen, B., Lord, N. & Wang, H., On the Efficacy of Using Commodity Optical Transceivers for Environmental Sensing, in *28th International Conference on Optical Fiber Sensors (2023), paper W4.38*, Optica Publishing Group, 2023, p. W4.38.

[23] Patterson, L.H.C., Kihlstrom, K.E. & Everest, M.A., Balanced polarimeter: A cost-effective approach for measuring the polarization of light, *American Journal of Physics*, **83**(1), pp. 91–94, 2015.

[24] Simsarian, J.E. & Winzer, P.J., Shake before break: Per-span fiber sensing with in-line polarization monitoring, in *2017 Optical Fiber Communications Conference and Exhibition (OFC)*, 2017, pp. 1–3.

[25] Catudal, J., Zhou, Z., Pan, W., Barford, P., Fratta, D. & Wang, H., Homebrew: Optical Polarization Change Detection for Ground Motion Sensing, in *Optical Fiber Communication Conference (OFC) 2024 (2024), paper M2K.4*, Optica Publishing Group, 2024, p. M2K.4.

[26] AC1200 Product Family, `https://acacia-inc.com/product/ac1200/`, 2019.

[27] Agrawal, 1951-author, G.P.G.P., *Fiber-optic communication systems*, Wiley, [2010] ©2010, New York ; Chichester, 2010.

[28] Gholamzadeh, B. & Nabovati, H., Fiber Optic Sensors, **2**(6), 2008.

[29] Ling, S.J., Sanny, J. & Moebs, W., *University physics. Volume 1*, OpenStax College, Rice University, Houston, Texas, 2016, oCLC: 961352944.

[30] Lennie Lightwave's Guide To Fiber Optics - Home, `https://www.thefoa.org/Lennie/`, 2016.

[31] Lam, C.F. & Way, W.I., A system's view of metro and regional optical networks, in *Optical Metro Networks and Short-Haul Systems*, SPIE, 2009, volume 7235, pp. 9–17.

[32] Mardoyan, H., Jorge, F., Ozolins, O., Estaran, J.M., Udalcovs, A., Konczykowska, A., Riet, M., Duval, B., Nodjiadjim, V., Dupuy, J.Y., Pang, X., Westergren, U., Chen, J., Popov, S. & Bigo, S., 204-GBaud On-Off Keying Transmitter for Inter-Data Center Communications, in *2018 Optical Fiber Communications Conference and Exposition (OFC)*, 2018, pp. 1–3.

[33] Chhilar, R., Khurana, J. & Gandhi, S., MODULATION FORMATS IN OPTICAL COMMUNICATION SYSTEM, **13**, 2011.

[34] Udd, E., Fiber optic smart structures, *Proceedings of the IEEE*, **84**(6), pp. 884–894, 1996.

[35] Berthold, J., Historical review of microbend fiber-optic sensors, *Journal of Lightwave Technology*, **13**(7), pp. 1193–1199, 1995.

[36] Paschotta, R., Optical Fiber Communications, in *RP Photonics Encyclopedia*, RP Photonics AG, 2018.

[37] Roberts, K., O'Sullivan, M., Wu, K.T., Sun, H., Awadalla, A., Krause, D.J. & Laperle, C., Performance of Dual-Polarization QPSK for Optical Transport Systems, *Journal of Lightwave Technology*, **27**(16), pp. 3546–3559, 2009.

[38] Liu, X., Evolution of Fiber-Optic Transmission and Networking toward the 5G Era, *iScience*, **22**, pp. 489–506, 2019.

[39] Leal-Junior, A.G., Frizera, A., Marques, C. & Pontes, M.J., Optical Fiber Specklegram Sensors for Mechanical Measurements: A Review, *IEEE Sensors Journal*, **20**(2), pp. 569–576, 2020.

[40] Yao, X.S., *Polarization measurement and control in optical fiber communication and sensor systems*, John Wiley and Sons, Inc., 2023. ©2023, Hoboken, NJ, 2023.

[41] Collett, E., *Field guide to polarization*, SPIE, Bellingham, Wash., 2005.

[42] Kaminow, I., Li, T. & Willner, A.E., *Optical Fiber Telecommunications Volume VI, 6th Edition*, Acadenuc Press, 2013.

[43] Paschotta, R., Multiphonon Absorption - an encyclopedia article, in *RP Photonics Encyclopedia*, RP Photonics AG, 2016.

[44] Paschotta, R., Optical Fiber Communications - an encyclopedia article, in *RP Photonics Encyclopedia*, RP Photonics AG, 2005.

[45] The FOA Reference For Fiber Optics - Jargon, `https://www.thefoa.org/tech/ref/basic/SMbands.html`, 2020.

[46] Worton, ITU-T Standards for Various Optical Fibers | FS Community, `https://community.fs.com:7003/blog/itu-t-standards-for-various-optical-fibers.html`, 2021.

[47] G.709 : Interfaces for the optical transport network, `https://www.itu.int/rec/T-REC-G.709-202006-I/en`, 2020.

[48] G.694.1 : Spectral grids for WDM applications: DWDM frequency grid, `https://www.itu.int/rec/T-REC-G.694.1-202010-I/en`, 2020.

[49] Abdullah, M., Das, B. & Mohd Shah, N.S., DSP techniques for reducing chromatic dispersion in optical communication systems, in *2014 International Conference on Computer, Communications, and Control Technology (I4CT)*, 2014, pp. 305–309.

[50] Yurduseven, O., PMD fundamentals and a general review of PMD compensation techniques, in *2011 19thTelecommunications Forum (FOR) Proceedings of Papers*, 2011, pp. 1612–1615.

[51] Weng, Y., Wang, J. & Pan, Z., Recent Advances in DSP Techniques for Mode Division Multiplexing Optical Networks with MIMO Equalization: A Review, *Applied Sciences*, **9**(6), p. 1178, 2019.

[52] Alam, S.M.J., Alam, M.R., Hu, G. & Mehrab, M.Z., Bit Error Rate Optimization in Fiber OpticCommunications, *International Journal of Machine Learning and Computing*, pp. 435–440, 2011.

[53] Freude, W., Schmogrow, R., Nebendahl, B., Winter, M., Josten, A., Hillerkuss, D., Koenig, S., Meyer, J., Dreschmann, M., Huebner, M., Koos, C., Becker, J. & Leuthold, J., Quality metrics for optical signals: Eye diagram, Q-factor, OSNR, EVM and BER, in *2012 14th International Conference on Transparent Optical Networks (ICTON)*, 2012, pp. 1–4, iSSN: 2161-2064.

[54] Manghat, P., OSNR in Fiber Optic Communications, `https://vitextech.com/osnr-meaning/`, 2021.

[55] G.976 : Test methods applicable to optical fibre submarine cable systems, `https://www.itu.int/rec/T-REC-G.976-201405-I/en`, 2014.

[56] Tan, L., Su, W., Zhang, W., Lv, J., Zhang, Z., Miao, J., Liu, X. & Li, N., In-band Network Telemetry: A Survey, *Computer Networks*, **186**, p. 107763, 2021.

[57] Schulman, J., Building a Network Health Monitoring System, `https://storage.googleapis.com/site-media-prod/meetings/NANOG80/2235/20201020_Schulman_Building_A_Network_v1.pdf`, 2020.

[58] Gonzalez, A., Leigh, J., Peisert, S., Tierney, B., Balas, E., Radulovic, P. & Schopf, J.M., Big Data and Analysis of Data Transfers for International Research Networks Using NetSage, in *2017 IEEE International Congress on Big Data (BigData Congress)*, 2017, pp. 344–351.

[59] Grafana: The open observability platform, https://grafana.com/, 2021.

[60] Schulman, J., Netpaca - Optics Health Monitoring, https://github.com/netpaca/netpaca-optics, 2022.

[61] Miao, C., Chen, M., Gupta, A., Meng, Z., Ye, L., Xiao, J., Chen, J., He, Z., Luo, X., Wang, J. & Yu, H., Detecting Ephemeral Optical Events with {OpTel}, 2022, pp. 339–353.

[62] Clifford, J., Infrastructure Monitoring Basics with Telegraf, InfluxDB, and Grafana, https://www.influxdata.com/blog/infrastructure-monitoring-basics-telegraf-influxdb-grafana/, 2023.

[63] Catudal, J., Optimon, https://github.com/HodagJoe/optimon, 2022.

[64] Zoback, M.L., The 1906 earthquake and a century of progress in understanding earthquakes and their hazards, *Gsa Today*, **16**, 2006.

[65] Grundy, P., The Padang Earthquake 2009 – Lessons and Recovery, in *Australian Earthquake Engineering Society Conference*, 2010.

[66] How are earthquakes detected? British Geological Survey, https://www.bgs.ac.uk/discovering-geology/earth-hazards/earthquakes/how-are-earthquakes-detected/, 2021.

[67] How Do Earthquake Early Warning Systems Work? Caltech Science Exchange, http://scienceexchange.caltech.edu/topics/earthquakes/earthquake-early-warning-systems, 2020.

[68] Kennett, B., *Seismic Wave Propagation in Stratified Media*, ANU Press, 2009.

[69] Brady, A.G., Strong-motion accelerographs: Early history, *Earthquake Engineering & Structural Dynamics*, **38**(9), pp. 1121–1134, 2009.

[70] Broadband Sensors | EarthScope Instrument Center, https://www.passcal.nmt.edu/content/instrumentation/sensors/broadband-sensors, 2023.

[71] Hou, Y., Jiao, R. & Yu, H., MEMS based geophones and seismometers, *Sensors and Actuators A: Physical*, **318**, p. 112498, 2021.

[72] Grebby, S., Sowter, A., Gee, D., Athab, A., Barreda-Bautista, B.D.l., Girindran, R. & Marsh, S., Remote Monitoring of Ground Motion Hazards in High Mountain Terrain Using InSAR: A Case Study of the Lake Sarez Area, Tajikistan, *Applied Sciences*, **11**(18), p. 8738, 2021.

[73] Kumar, S., Vig, R. & Kapur, P., Development of Earthquake Event Detection Technique Based on STA/LTA Algorithm for Seismic Alert System, *Journal of the Geological Society of India*, **92**(6), pp. 679–686, 2018.

[74] Trnkoczy, A., Understanding and parameter setting of STA/LTA trigger algorithm, `https://gfzpublic.gfz-potsdam.de/rest/items/item_4097/component/file_4098/content`, 2021.

[75] Mellors, R.J., Pitarka, A., Matzel, E., Magana-Zook, S., Knapp, D., Walter, W.R., Chen, T., Snelson, C.M. & Abbott, R.E., The Source Physics Experiments Large N Array, *Seismological Research Letters*, **89**(5), pp. 1618–1628, 2018.

[76] Raspberry Shake, Earthquake and Infrasound Monitors-Seismograph, `https://shop.raspberryshake.org/`, 2020.

[77] Anthony, R.E., Ringler, A.T., Wilson, D.C. & Wolin, E., Do Low-Cost Seismographs Perform Well Enough for Your Network? An Overview of Laboratory Tests and Field Observations of the OSOP Raspberry Shake 4D, *Seismological Research Letters*, **90**(1), pp. 219–228, 2018.

[78] Faulkner, M., Olson, M., Chandy, R., Krause, J., Chandy, K.M. & Krause, A., The next big one: Detecting earthquakes and other rare events from community-based sensors, in *Proceedings of the 10th ACM/IEEE International Conference on Information Processing in Sensor Networks*, 2011, pp. 13–24.

[79] Chandrakumar, C., Prasanna, R., Stephens, M. & Tan, M.L., Earthquake early warning systems based on low-cost ground motion sensors: A systematic literature review, *Frontiers in Sensors*, **3**, 2022.

[80] Yang, L., Liu, X., Zhu, W., Zhao, L. & Beroza, G.C., Toward improved urban earthquake monitoring through deep-learning-based noise suppression, *Science Advances*, **8**(15), p. eabl3564.

[81] Vidale, J.E., Seattle "12th Man* Earthquake" Goes Viral, *Seismological Research Letters*, **82**(3), pp. 449–450, 2011.

[82] Díaz, J., Ruiz, M., Sánchez-Pastor, P.S. & Romero, P., Urban Seismology: on the origin of earth vibrations within a city, *Scientific Reports*, **7**(1), p. 15296, 2017.

[83] Villar, I.d., Matias, I.R. & Institute of Electrical and Electronics Engineers, eds., *Optical fiber sensors: fundamentals for development of optimized devices*, IEEE Press series on sensors, Wiley-IEEE Press, Hoboken, New Jersey, 2021.

[84] Fields, J.N. & Cole, J.H., Fiber microbend acoustic sensor, *Applied Optics*, **19**(19), p. 3265_1, 1980.

[85] Efendioglu, H.S., A Review of Fiber-Optic Modal Modulated Sensors: Specklegram and Modal Power Distribution Sensing, *IEEE Sensors Journal*, **17**(7), pp. 2055–2064, 2017.

[86] Zhang, Z. & Ansari, F., Fiber-optic laser speckle-intensity crack sensor for embedment in concrete, *Sensors and Actuators A: Physical*, **126**(1), pp. 107–111, 2006.

[87] Liu, Y., Li, G., Qin, Q., Tan, Z., Wang, M. & Yan, F., Bending recognition based on the analysis of fiber specklegrams using deep learning, *Optics & Laser Technology*, **131**, p. 106424, 2020.

[88] Cuevas, A.R., Fontana, M., Rodriguez-Cobo, L., Lomer, M. & López-Higuera, J.M., Machine Learning for Turning Optical Fiber Specklegram Sensor into

a Spatially-Resolved Sensing System. Proof of Concept, *Journal of Lightwave Technology*, **36**(17), pp. 3733–3738, 2018.

[89] Sahota, J.K., Gupta, N. & Dhawan, D., Fiber Bragg grating sensors for monitoring of physical parameters: a comprehensive review, *Optical Engineering*, **59**(6), p. 060901, 2020.

[90] Chen, Q., Zhang, X., Chen, Y. & Zhang, X., A method of strain measurement based on fiber Bragg grating sensors, *Vibroengineering Procedia*, **5**, pp. 140–144, 2015.

[91] Filograno, M.L., Corredera Guillen, P., Rodriguez-Barrios, A., Martin-Lopez, S., Rodriguez-Plaza, M., Andres-Alguacil, & Gonzalez-Herraez, M., Real-Time Monitoring of Railway Traffic Using Fiber Bragg Grating Sensors, *IEEE Sensors Journal*, **12**(1), pp. 85–92, 2012.

[92] Wu, Q., Muhammad Hatta, A., Semenova, Y. & Farrell, G., Use of a single-multiple-single-mode fiber filter for interrogating fiber Bragg grating strain sensors with dynamic temperature compensation, *Applied Optics*, **48**(29), p. 5451, 2009.

[93] Wang, J.J., Yan, S.C., Ruan, Y.P., Xu, F. & Lu, Y.Q., Fiber-Optic Point-Based Sensor Using Specklegram Measurement, *Sensors*, **17**(10), p. 2429, 2017.

[94] Li, Z. & Zhan, Z., Pushing the limit of earthquake detection with distributed acoustic sensing and template matching: a case study at the Brady geothermal field, *Geophysical Journal International*, **215**(3), pp. 1583–1593, 2018.

[95] Li, Z., Shen, Z., Yang, Y., Williams, E., Wang, X. & Zhan, Z., Rapid Response to the 2019 Ridgecrest Earthquake With Distributed Acoustic Sensing, *AGU Advances*, **2**(2), p. e2021AV000395, 2021.

[96] Ravet, F., Briffod, F. & Nikle's, M., Extended Distance Fiber Optic Monitoring for Pipeline Leak and Ground Movement Detection, American Society of Mechanical Engineers Digital Collection, 2009, pp. 689–697.

[97] Dou, S., Lindsey, N., Wagner, A.M., Daley, T.M., Freifeld, B., Robertson, M., Peterson, J., Ulrich, C., Martin, E.R. & Ajo-Franklin, J.B., Distributed Acoustic Sensing for Seismic Monitoring of The Near Surface: A Traffic-Noise Interferometry Case Study, *Scientific Reports*, **7**(1), p. 11620, 2017.

[98] Shao, J., Wang, Y. & Chen, L., Near-Surface Characterization Using High-Speed Train Seismic Data Recorded by a Distributed Acoustic Sensing Array, *IEEE Transactions on Geoscience and Remote Sensing*, **60**, pp. 1–11, 2022.

[99] Owen, A., Duckworth, G. & Worsley, J., OptaSense: Fibre Optic Distributed Acoustic Sensing for Border Monitoring, in *2012 European Intelligence and Security Informatics Conference*, IEEE, Odense, Denmark, 2012, pp. 362–364.

[100] Brugière, T., Crawford, T.H.R., Mortelette, A., Tanoh, M.J., Reimer, M., O'Sullivan, M., Doucet, D., Tremblay, C., Peterson, D.L., Xia, T.J., Wellbrock, G.A. & Bélanger, M.P., Polarization Activity Monitoring of an Aerial Fiber Link in a Live Network, in *Optical Fiber Communication Conference (2016), paper Tu3G.3*, Optica Publishing Group, 2016, p. Tu3G.3.

[101] Dejdar, P., Myska, V., Munster, P. & Burget, R., Trains Detection Using State of Polarization Changes Measurement and Convolutional Neural Networks, in *2021 IEEE International Symposium on Inertial Sensors and Systems (INERTIAL)*, 2021, pp. 1–4, iSSN: 2377-3480.

[102] Karlsson, M., Brentel, J. & Andrekson, P.A., Long-term measurement of PMD and polarization drift in installed fibers, *Journal of Lightwave Technology*, **18**(7), pp. 941–951, 2000.

[103] Cunningham, E., Neal, L., Fratta, D., Wang, H.F., Catudal, J. & Barford, P.R., Characterizing Dark Fiber Distributed Acoustic Sensing (DAS) along a University Campus Route, AGU, Chicago, 2022.

[104] He, H., Jiang, L., Pan, Y., Yi, A., Zou, X., Pan, W., Willner, A.E., Fan, X., He, Z. & Yan, L., Integrated sensing and communication in an optical fibre, *Light: Science & Applications*, **12**(1), p. 25, 2023.

[105] Boitier, F., Lemaire, V., Pesic, J., Chavarria, L., Layec, P., Bigo, S. & Dutisseuil, E., Proactive Fiber Damage Detection in Real-time Coherent Receiver, in *2017 European Conference on Optical Communication (ECOC)*, 2017, pp. 1–3.

[106] Cisco, AC1200 Product Family, `https://acacia-inc.com/product/ac1200/`, 2022.

[107] Vibration Test Systems VG-100-6 100 lbf Shaker Head/Vacuum, `https://www.atecorp.com/products/vibration-test-systems/vg-100-6`, 2017.

[108] Wisconsin Legislature, Utility Facilities on Department of Transportation Railroad Property, 2013.

[109] Hajj, R.E., MacDonald, G., Verma, P. & Huck, R., Implementing and testing a fiber-optic polarization-based intrusion detection system, *SPIE Optical Engineering*, **54**(9), p. 096107, 2015.

[110] Peng, F., Duan, N., Rao, Y.J. & Li, J., Real-Time Position and Speed Monitoring of Trains Using Phase-Sensitive OTDR, *IEEE Photonics Technology Letters*, **26**(20), pp. 2055–2057, 2014.

[111] Fiber Optic Sensing Association, Installation Considerations, `https://fiberopticsensing.org/installation-considerations/`, 2018.

[112] Šlapák, M., Vojtěch, J., Havliš, O. & Slavík, R., Monitoring of Fibre Optic Links With a Machine Learning-Assisted Low-Cost Polarimeter, *IEEE Access*, **8**, pp. 183965–183971, 2020.

[113] MacDonald, G., *Detecting eavesdropping activity in fiber optic networks*, Phd thesis, University of Oklahoma, 2012.

[114] Thorlabs, Inc., Manual Fiber Polarization Controllers, `https://www.thorlabs.com`, 2022.

[115] Thorlabs, Inc., Polarimeter Systems with High Dynamic Range, `https://www.thorlabs.com`, 2022.

[116] Gagniuc, P.A., Ionescu-Tirgoviste, C., Gagniuc, E., Militaru, M., Nwabudike, L.C., Pavaloiu, B.I., Vasilăţeanu, A., Goga, N., Drăgoi, G., Popescu, I. & Dima, S., Spectral forecast: A general purpose prediction model as an alternative to classical neural networks, *Chaos: An Interdisciplinary Journal of Nonlinear Science*, **30**(3), p. 033119, 2020.

[117] Temporao, G. & von der Weid, J., A simple low-cost broadband fiber optical polarimeter, in *Proceedings of the 2003 SBMO/IEEE MTT-S International Microwave and Optoelectronics Conference - IMOC 2003. (Cat. No.03TH8678)*, 2003, volume 2, pp. 627–631 vol.2.

[118] Briers, D., Duncan, D.D., Hirst, E.R., Kirkpatrick, S.J., Larsson, M., Steenbergen, W., Stromberg, T. & Thompson, O.B., Laser speckle contrast imaging: theoretical and practical limitations, *Journal of Biomedical Optics*, **18**(6), p. 066018, 2013.

[119] Large, D. & Farmer, J., Chapter 4 - Linear Fiber-Optic Signal Transportation, in D. Large & J. Farmer, eds., *Broadband Cable Access Networks*, Morgan Kaufmann, Boston, The Morgan Kaufmann Series in Networking, pp. 81–126, 2009.

[120] FS.COM INC, 1mW (5km) FVFL-204 Pen Shape Visual Fault Locator with Standard 2.5mm Universal Adapter - FS.com, `https://www.fs.com/products/35388.html`, 2024.

[121] Teledyne FLIR, Blackfly S USB3 | Teledyne FLIR, `https://www.flir.com/products/blackfly-s-usb3?vertical=machine+vision&segment=iis`, 2023.

[122] Kanopoulos, N., Vasanthavada, N. & Baker, R., Design of an image edge detection filter using the Sobel operator, *IEEE Journal of Solid-State Circuits*, **23**(2), pp. 358–367, 1988.

[123] Canny, J., A Computational Approach to Edge Detection, *IEEE Transactions on Pattern Analysis and Machine Intelligence*, **PAMI-8**(6), pp. 679–698, 1986,

conference Name: IEEE Transactions on Pattern Analysis and Machine Intelligence.

[124] Rosin, P.L., Measuring Corner Properties, *Computer Vision and Image Understanding*, **73**(2), pp. 291–307, 1999.

[125] Axelrod, B., Answer to "Best Fitting Plane given a Set of Points", `https://math.stackexchange.com/a/2306029`, 2017.

[126] Sultangazin, A., Kusmangaliyev, J., Aitkulov, A., Akilbekova, D., Olivero, M. & Tosi, D., Design of a Smartphone Plastic Optical Fiber Chemical Sensor for Hydrogen Sulfide Detection, *IEEE Sensors Journal*, **17**(21), pp. 6935–6940, 2017.